Mechanistically Driven Control over Cubane Oxocluster Catalysts

Fangyuan Song, Karrar Al-Ameed, Mauro Schilling, Thomas Fox, Sandra Luber, and Greta R. Patzke*

Supporting Information

Analytical characterizations.

Powder X-ray diffraction (PXRD) patterns were recorded on a STOE STADI P diffractometer (transmission mode, Ge monochromator) with Mo K_α radiation.

Attenuated total reflectance Fourier-transform infrared (ATR-FT-IR) spectra were recorded on a Bruker Vertex 70 spectrometer equipped with a Platinum ATR accessory containing a diamond crystal.

High-resolution electrospray mass spectra (HR-ESI-MS) were recorded on a Bruker maXis QTOFMS instrument. The samples were dissolved in MeOH and analyzed via continuous flow injection at 3 µL/min. The mass spectrometer was calibrated between *m/z* 50 and 3000 using a Fluka electrospray calibration solution (Sigma-Aldrich, Buchs, Switzerland) at a resolution of 20'000 and a mass accuracy below 2 ppm.

^{1}H NMR spectra were recorded on a BRUKER AV3-500 spectrometer (500.25 MHz ^{1}H frequency), and the longitudinal relaxation times (T_1) were determined with the inversion recovery method.

Raman spectra were recorded on an inVia Qontor applying a 785 nm excitation laser with 5 % intensity.

UV/vis spectra were recorded on a Lambda 650 S Perkin Elmer UV/visible spectrometer in the range of 300-800 nm using a Quartz SUPRASIL precision cuvette.

Experimental section.

Materials

All chemicals and solvents were purchased commercially: $Co(OAc)_2{\cdot}4H_2O$ (Sigma-Aldrich, ≥ 99.0 %), $Co(NO_3)_2{\cdot}6H_2O$ (Sigma-Aldrich, ≥ 98.0 %), $CoCl_2{\cdot}6H_2O$ (Sigma-Aldrich, ≥ 98.0 %), $CoSO_4{\cdot}7H_2O$ (Sigma-Aldrich, ≥ 99.0 %), $CoClO_4{\cdot}6H_2O$ (Sigma-Aldrich, ≥ 99.0 %), $Ni(OAc)_2{\cdot}4H_2O$ (Sigma-Aldrich, ≥ 99.0 %), $Ni(NO_3)_2{\cdot}6H_2O$ (Sigma-Aldrich, ≥ 98.5 %), $NiCl_2{\cdot}6H_2O$ (Sigma-Aldrich, ≥ 98.0 %), $CoSO_4{\cdot}7H_2O$ (Sigma-Aldrich, ≥ 99.0 %), di(2-pyridyl)ketone (Sigma-Aldrich, 99.0 %), $NaClO_4$ (Sigma-Aldrich, ≥ 98.0 %), $NaBF_4$ (Fluka, > 98 %), $NaPF_6$ (Sigma-Aldrich, 98 %), $NaNO_3$ (Merck, 99 %), $NaClO_3$ (Sigma-Aldrich, ≥ 99.0 %), NaCl (Fluka, ≥ 99.5 %), NaOAc (Sigma-Aldrich, ≥ 99.0 %), $NaClO_4$ (Sigma-Aldrich, ≥ 98.0 %), H_3BO_3 (Merck, ≥ 99.8 %), $Na_2B_4O_7{\cdot}10H_2O$ (Fluka, ≥ 99.5 %), triethylamine (Sigma-Aldrich, ≥ 99.0 %), CH_3OH (Merck, analytical pure), CD_3CN (Sigma-Aldrich, 99.8 atom % D).
Ultrapure water was produced with a Barnstead GenPure Pro Water Purification System with an electric conductivity of 0.55 µS/cm (Thermo Scientific).

Syntheses of type 1 {Co_4O_4} compounds

In order to align to synthetic conditions with those based on $Co(NO_3)_2$ as the starting material, all of the crystallizations were performed in a glovebox.
All **type 1** {Co_4O_4} compound syntheses were conducted through adding 3 mL dpk (0.4 mmol, aq.) dropwise into 3 mL $Co(OAc)_2{\cdot}4H_2O$ (0.8 mmol, aq.) containing the corresponding types and amounts of counteranions under stirring, and the reaction solutions were filtered to obtain the filtrates that were afterwards kept for crystallization at room temperature. The absence of counteranions and addition of 0.8-7 mmol NaCl afforded the pure **type 1** compounds [Co_4(dpy-C{OH}O)$_4$(OAc)$_4$] and [Co_4(dpy-C{OH}O)$_4$(Cl)$_4$], respectively. Addition of 0.8 mmol $NaClO_3$, $NaNO_3$, $NaBF_4$, or of 0.4 mmol $NaPF_6$ led to the pure **type 1** compounds [Co_4(dpy-C{OH}O)$_4$(OAc)$_3$(H_2O)]ClO_3, -NO_3, -BF_4, or -PF_6. The addition of a rather large amount of 7.0 mmol $NaBF_4$ resulted in the pure **type 1** compound [Co_4(dpy-C{OH}O)$_4$(OAc)$_2$(H_2O)$_2$](BF_4)$_2$. The violet hexagonal crystalline products of each compound were obtained in ~ 1 week, and single crystals for structure determination were selected from the corresponding products without further purification.

Syntheses of type 2-μ-OAc-Co_xNi_{4-x} compounds
All **2-μ-OAc-Co_xNi_{4-x}** compounds were obtained from the above synthetic procedure through replacing $Co(OAc)_2{\cdot}4H_2O$ with a mixture of $Co(OAc)_2{\cdot}4H_2O$ + $Ni(OAc)_2{\cdot}4H_2O$ with the corresponding Co:Ni ratios (0.64 mmol + 0.16 mmol, 0.6 mmol + 0.2 mmol, 0.4 mmol + 0.4 mmol, or 0.2 mmol + 0.6 mmol). The applied counteranions and their amounts for this series of syntheses are listed in Scheme 1. Prismatic product crystals in different colors with sufficient quality for single-crystal X-ray diffraction were obtained in ~ 1 week.

Syntheses of type 2-Co_xNi_{4-x} compounds
The corresponding **2-Co_xNi_{4-x}** compounds were synthesized via the procedure applied for **2-Co_xNi_{4-x}** with increasing additions of $NaClO_4$ (≥ 0.4 mmol for all the ratios of $Co(OAc)_2{\cdot}4H_2O$ + $Ni(OAc)_2{\cdot}4H_2O$), $NaClO_3$ and $NaBF_4$ (≥ 4 mmol for $Co(OAc)_2{\cdot}4H_2O$ + $Ni(OAc)_2{\cdot}4H_2O$ = 0.64 mmol + 0.16 mmol and 0.6 mmol + 0.2 mmol, ≥ 5 mmol for $Co(OAc)_2{\cdot}4H_2O$ + $Ni(OAc)_2{\cdot}4H_2O$ = 0.4 mmol + 0.4 mmol and 0.2 mmol + 0.6 mmol). Hexagonal product crystals in different colors with sufficient quality for single-crystal X-ray diffraction were obtained in ~ 1 week.

Syntheses of type 2-μ-OAc-Ni_4 compounds
2-μ-OAc-Ni_4 cubanes with all respective counteranions were synthesized through replacing the addition of a $Co(OAc)_2{\cdot}4H_2O$ + $Ni(OAc)_2{\cdot}4H_2O$ mixture with only 0.4 mmol $Ni(OAc)_2{\cdot}4H_2O$ in the corresponding synthetic procedure of **2-μ-OAc-Co_xNi_{4-x}**. The applied counteranions and their amounts for this series of syntheses are listed in Scheme 1. Light green prismatic crystals with sufficient quality for single-crystal X-ray diffraction were obtained in ~ 1 week.

Syntheses of type 2-(*gem*-aqua)-Co_4- and -Ni_4-NO_3 and [Co_5(dpy-C{OH}O)$_5$(dpy-C{O}$_2$)](NO_3)$_3$
A 3 mL aqueous solution with 0.4 mmol dpk and 0.05 mL TEA was added dropwise into 3 mL $Co(NO_3)_2{\cdot}6H_2O$ (0.4 mmol, aq.) containing 0.25 mL TEA and 3 mmol $NaNO_3$ under stirring. After filtering the above reaction mixture, the obtained filtrate was kept for crystallization by slowly evaporating the solvent at room temperature. A two-component crystalline product (unstable in air) of **2-(*gem*-aqua)-Co_4-NO_3** and [Co_5(dpy-C{OH}O)$_5$(dpy-C{O}$_2$)](NO_3)$_3$ with sufficient quality for single-crystal X-ray diffraction was obtained in ~ 3 weeks. The synthesis of pure light green crystalline **2-(*gem*-aqua)-Ni_4-NO_3** was modified based on the above procedure by using 0.4 mmol $Ni(NO_3)_2{\cdot}6H_2O$ instead of 0.4 mmol $Co(NO_3)_2{\cdot}6H_2O$. **2-(*gem*-aqua)-M_4-NO_3** can be crystallized into a different space group as an air-stable twinning crystal while applying ≥ 5 mmol $NaNO_3$.

Syntheses of type 2-Co_4-NO_3, -ClO_3, and -BF_4
2-Co_4-NO_3 was synthesized through modifying the synthetic procedure of **2-(*gem*-aqua)-Co_4-NO_3** by addition of 0.2 mmol NaOAc into TEA and $Co(NO_3)_2{\cdot}6H_2O$ (0.4 mmol, aq.) containing $NaNO_3$ (3 mmol). Based on the above synthesis, **2-Co_4-ClO_3** and **2-Co_4-BF_4** were synthesized replacing $Co(NO_3)_2{\cdot}6H_2O$ with $CoSO_4{\cdot}7H_2O$ and using $NaClO_3$ (4 mmol) and $NaBF_4$ (1 mmol) instead of $NaNO_3$, respectively. The filtrates of the above reaction mixtures were kept for crystallization by slowly evaporating the solvents. Violet hexagonal crystals with sufficient quality for single-crystal X-ray diffraction were obtained in ~ 1 week.

Syntheses of type 2-(half *gem*-aqua)-Ni_4-NO_3 and 2-Ni_4-NO_3
The syntheses of **2-(half *gem*-aqua)-Ni_4-NO_3** and **2-Ni_4-NO_3** were modified based the preparation of **2-(*gem*-aqua)-Ni_4-NO_3** through addition of 0.1 and 0.2 mmol NaOAc into TEA and $NaNO_3$ containing $Ni(NO_3)_2{\cdot}6H_2O$ (aq.), respectively. The light green prismatic (**2-(half *gem*-aqua)-Ni_4-NO_3**) and light green hexagonal (**2-Ni_4-NO_3**) crystalline products which were suitable for X-ray diffraction were obtained in ~ 1 week.

Synthesis of dpy-C{Ph}OH
In a 250 mL three-necked round bottom flask equipped with a reflux condenser, dry magnesium granulate (0.618 g, 25.4 mmol) was dispersed in 15 mL dry THF. One drop of Br_2 was added into to the

above-obtained colorless suspension. The mixture was heated to reflux and 30 mL of a solution of PhBr (2.7 mL, 28.7 mmol) in THF were added dropwise over 30 min. When the magnesium granulate was almost completely dissolved, the reaction was cooled down to room temperature. 30 mL of a solution of dpk in THF (2.580 g, 14.0 mmol) were added dropwise over 1 h into the above grey suspension at room temperature, and an instant color change to dark red and a precipitation were observed. 40 mL THF was further added and the resulting dark red suspension was heated to reflux for 2 h. The reaction was cooled to room temperature and quenched with adding 100 mL NH_4Cl (20 %) after the consumption of dpk was confirmed with TLC (EtOAc). The yellow mixture was extracted with Et_2O (3 × 100 mL), and the combined organic phases were washed with H_2O (2 × 50 mL) and brine (2 × 50 mL) and dried with $MgSO_4$. A pale brown solid was obtained after removing the solvent *in vacuo* without further purification.

^{1}H NMR (400 MHz, $CDCl_3$): 8.56 (*ddd*, *J* = 4.9, 1.8, 1.0, 2 × arom. CH); 7.82 (*td*, *J* = 8.0, 1.1, 2 × arom. CH); 7.71 (*ddd*, *J* = 8.0, 7.5, 1.8, 2 × arom. CH); 7.32-7.26 (*m*, 5 × arom. CH); 7.22 (*ddd*, *J* = 7.4, 4.9, 1.2, 2 × arom. CH); 6.92 (*br*. *S*, OH). **^{13}C NMR (100 MHz, $CDCl_3$):** 163.1 (*s*, arom. C); 147.2 (*d*, 2 × arom. CH); 146.4 (*s*, arom. C); 136.7 (*d*, 2 × arom. CH); 128.0 (*d*, 2 × arom. CH); 127.8 (*d*, 2 × arom. CH); 127.4 (*d*, arom. CH); 123.2 (*d*, 2 × arom. CH); 122.3 (*d*, 2 × arom. C); 80.8 (*s*, COH). **ESI-MS (MeOH):** 263.11 ($[C_{17}H_{15}N_2O]^+$, $[M+H]^+$); 245.11 ($[C_{17}H_{13}N_2]^+$, $[M-OH]^+$).

Synthesis of $[Co_2(dpy\text{-}C\{Ph\}O)_2(OAc)_2]$

A 40 mL MeCN solution of $Co(OAc)_2{\cdot}4H_2O$ (0.249 g, 1.0 mmol) and dpy-C{Ph}OH (0.260 g, 1.0 mmol) was heated in a 100 mL three-necked round bottom flask to reflux for 2 h. The resulting dark red reaction solution was filtered after cooling to room temperature. The filtrate was kept for crystallization while slowly evaporating the solvent, and the dark red crystalline product $[Co_2(dpy\text{-}C\{Ph\}O)_2(OAc)_2]$ with SC-XRD quality was formed within ~ 3 weeks.

Synthesis of the defect compound $[Co_4(dpy\text{-}C\{OH\}O\})_4(OAc)_4]$

A 3 mL ethanol solution of dpk (0.4 mmol) was added dropwise into 3 mL ethanolic solution of $Co(OAc)_2{\cdot}4H_2O$ (0.4 mmol) and $LiOH{\cdot}H_2O$ (0.4 mmol) under stirring. The obtained reaction solution was filtered and kept for crystallization while slowly evaporating the solvent. The violet crystalline product of the defect compound $[Co_4(dpy\text{-}C\{OH\}O\})_4(OAc)_4]$ was obtained as thin platelets in ~ 3 days, and crystals with SC-XRD quality were selected without further purification. The evolution of defect $[Co_4(dpy\text{-}C\{OH\}O\})_4(OAc)_4]$ to its cubane analogue was observed upon another ~ 2 weeks of storage of the above crystallized sample.

Elemental analyses

1-3OAc-BF_4 ($C_{50}H_{47}Co_4N_8O_{15}BF_4{\cdot}H_2O$): calc. (%) C, 44.80; H, 3.68; N, 8.36; F, 5.67; Co, 17.4; found (%) C, 44.51; H, 3.82; N, 8.32; F, 5.50; Co, 17.4.

1-3OAc-NO_3 ($C_{50}H_{47}Co_4N_9O_{18}{\cdot}3H_2O$): calc. (%) C, 44.43; H, 3.95; N, 9.33; Co, 17.4; found (%) C, 44.21; H, 3.86; N, 9.54; Co, 17.3.

1-3OAc-ClO_3 ($C_{50}H_{47}Co_4N_8O_{18}Cl{\cdot}2.5H_2O$): calc. (%) C, 43.83; H, 3.68; N, 8.18; Co, 17.3; found (%) C, 43.79; H, 3.81; N, 8.11; Co, 17.1.

1-3OAc-PF_6 ($C_{50}H_{47}Co_4N_8O_{15}PF_6{\cdot}H_2O{\cdot}0.5CH_3OH$): calc. (%) C, 42.88; H, 3.63; N, 7.92; F, 8.06; Co, 16.7; found (%) C, 42.59; H, 3.72; N, 7.84; F, 8.00; Co, 16.4.

1-4Cl ($C_{44}H_{36}Cl_4Co_4N_8O_8{\cdot}2H_2O$): calc. (%) C, 43.38; H, 3.31; N, 9.20; Cl, 11.64; Co, 19.4; found (%) C, 43.01; H, 3.48; N, 8.82; Cl, 10.90; Co, 19.0.

1-2OAc-2BF_4 ($C_{48}H_{46}Co_4N_8O_{14}B_2F_8{\cdot}6H_2O$): calc. (%) C, 39.05; H, 3.96; N, 7.59; F, 10.29; Co, 16.0; found (%) C, 39.12; H, 3.90; N, 7.55; F, 10.30; Co, 15.7.

2-Co_xNi_{4-x}-BF_4 ($C_{48}H_{46}Co_xNi_{4-x}N_8O_{14}B_2F_8$): calc. (%) C, 42.09; H, 3.36; N, 8.18; found (%) C, 41.43; H, 3.46; N, 8.03. (Co = Ni = 59)

2-Co_xNi_{4-x}-ClO_3 ($C_{48}H_{46}Co_xNi_{4-x}N_8O_{20}Cl_2$): calc. (%) C, 42.34; H, 3.40; N, 8.23; found (%) C, 42.72; H, 3.32; N, 8.30. (Co = Ni =59)

2-Co_xNi_{4-x}-PF_6 ($C_{48}H_{46}Co_xNi_{4-x}N_8O_{14}P_2F_{12}$): calc. (%) C, 38.83; H, 3.12; N, 7.55; found (%) C, 39.17; H, 2.96; N, 7.76. (Co = Ni =59)

Visible-light-driven water oxidation

The deaerated reaction solutions were prepared in a 10 mL glass vial as follows: 9.5 mg $Na_2S_2O_8$ (5 mM) was added to a 8 mL borate buffer (80 mM, pH 8.5) containing completely dissoved 6 mg $[Ru(bpy)_3]Cl_2 \cdot 6H_2O$ (1 mM) and catalyst (desired concentration). Glass vials with the above solutions were sealed with a combination of a rubber septum (PTFE) and an aluminum crimp cap, followed by deaeration through purging with helium (purity 6.0) for 12 min.

O_2 evolution of the above catalytic solutions was measured independently by Clark electrode techniques and gas chromatography. For Clark electrode measurements, an oxygen sensor (OX-N) Clark electrode (Unisense) was inserted into the deaerated solution through the rubber septum, followed by irradiation with a 470 nm high flux LED light (26.1 mW/cm^2, Rhopoint Components LTD) after a constant signal of the Clark electrode was obtained under a stirring rate of 1000 rpm. O_2 evolution was monitored with the SensorTrace software (Unisense) applying a frequency of 1 data point per sec. The calibration of the Clark electrode was done according to the procedure provided by the Unisense user manual with a sodium ascorbate solution (2 g sodium ascorbate in 100 mL 0.1 M NaOH solution) as the zero calibration solution and aerated water as the aerated calibration solution (for details cf. Unisense user manual).

For GC measurements, the deaerated solution was irradiated with the above LED light source for 30 min under a stirring rate of 1000 rpm, and a 200 μL gas sample was taken with a gas-tight micro-liter syringe (Hamilton-1825RN) and transferred to the GC injection port. After pushing the syringe bar to the 100 μL mark, 100 μL of the gas sample was quickly injected into the GC (Agilent Technologies 7820A) equipped with a thermal conductivity detector (Varian). O_2 and N_2 were separated by passing the sample through a 3 m * 2 mm packed 5 Å molecular sieve 13X 80-100 column with a helium carrier gas (purity 6.0). Quantification of O_2 evolution was carried out with a good linear GC calibration curve obtained from measuring a series of volumes (50-500 μL) of pure O_2 vs. the peak area of each O_2 signal. Contamination of air was corrected by subtracting the half peak area of N_2 from the peak area of O_2 (due to the similar GC response to O_2 and N_2, the peak area of the contaminating O_2 basically equals 1/3 of the N_2 peak area). The pH value of the post-catalytic solution was measured with a METTLER TOLEDO SevenCompact pH meter.

Filtration-recycling tests

Standard activity tests were completed according to the above procedure for visible-light-driven water oxidation, and the as-obtained post reaction solution was filtered through a 200 nm filter. The pH value of such filtered solutions was readjusted to 8.5 by adding solid $Na_2B_4O_7 \cdot 10H_2O$. After adding 9.5 mg of $Na_2S_2O_8$, the activity recycling test was started applying the standard procedure. O_2 evolution during each test was monitored with a Clark electrode.

Single-crystal X-ray diffraction

Suitable single-crystals were selected on the polarizing microscope, mounted on a glass fiber loop with Infineum oil and measured on an Oxford Xcalibur Ruby CCD diffractometer equipped with a fine-foucs sealed X-ray tube (Mo K_α, λ = 0.71073 Å) and a graphite monochromator (cooled N_2 stream at 183 K) or on an XtaLAB Synergy, Dualflex, Pilatus 200K diffractometer (Rigaku Oxford) equipped with a Photonjet (Mo and Cu) X-ray source (Mo K_α, λ = 0.71073 Å; Cu K_α, λ =1.54184 Å) and a mirror monochromator (cooled N_2 stream at 160 K). The data processing and absorption correction (Analytical, Gaussian, or Multi-scan) were carried out using the program CrysAlisPro 1.179.39.9b (Rigaku Oxford Diffraction, 2015) or 1.179.39.46 (Rigaku Oxford Diffraction, 2018). Structure solutions and refinements were performed using Olex2 1.2.10 package.[1] The initial structures were obtained with intrinsic phasing method using SHELXT (2018/2),[2] and refined with full-matrix least-square methods on F^2 using SHELXL (2018/3).[3] The H atoms of all hydroxyl groups, all aqua ligands, and a part of solvent water were found according to the difference Fourier map and their positions were refined freely along with individual isotropic displacement parameters. The solvent water O atoms without reliable difference Fourier maps positioning their H atoms were only anisotropically refined without adding H. Nevertheless, such corresponding H numbers were still included in UNIT to obtain the correct formulas. All other H atoms were placed in geometrically idealized positions and were constrained to ride on their parent atoms with C─H = 0.95 Å (aryl) or 0.98 Å (methyl) and U_{iso}(H) = 1.2 U_{eq}(C) (aryl) or 1.5 U_{eq}(C) (methyl).

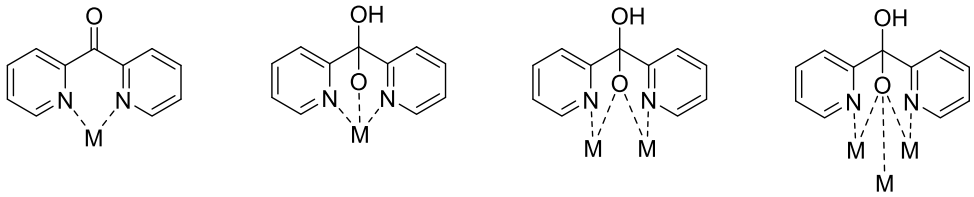

η^1:η^1 η^1:η^1:η^1 η^1:η^2:η^1 η^1:η^3:η^1

Figure S1. Different coordination models of dpk and dpy-C{OH}O^-.[4]

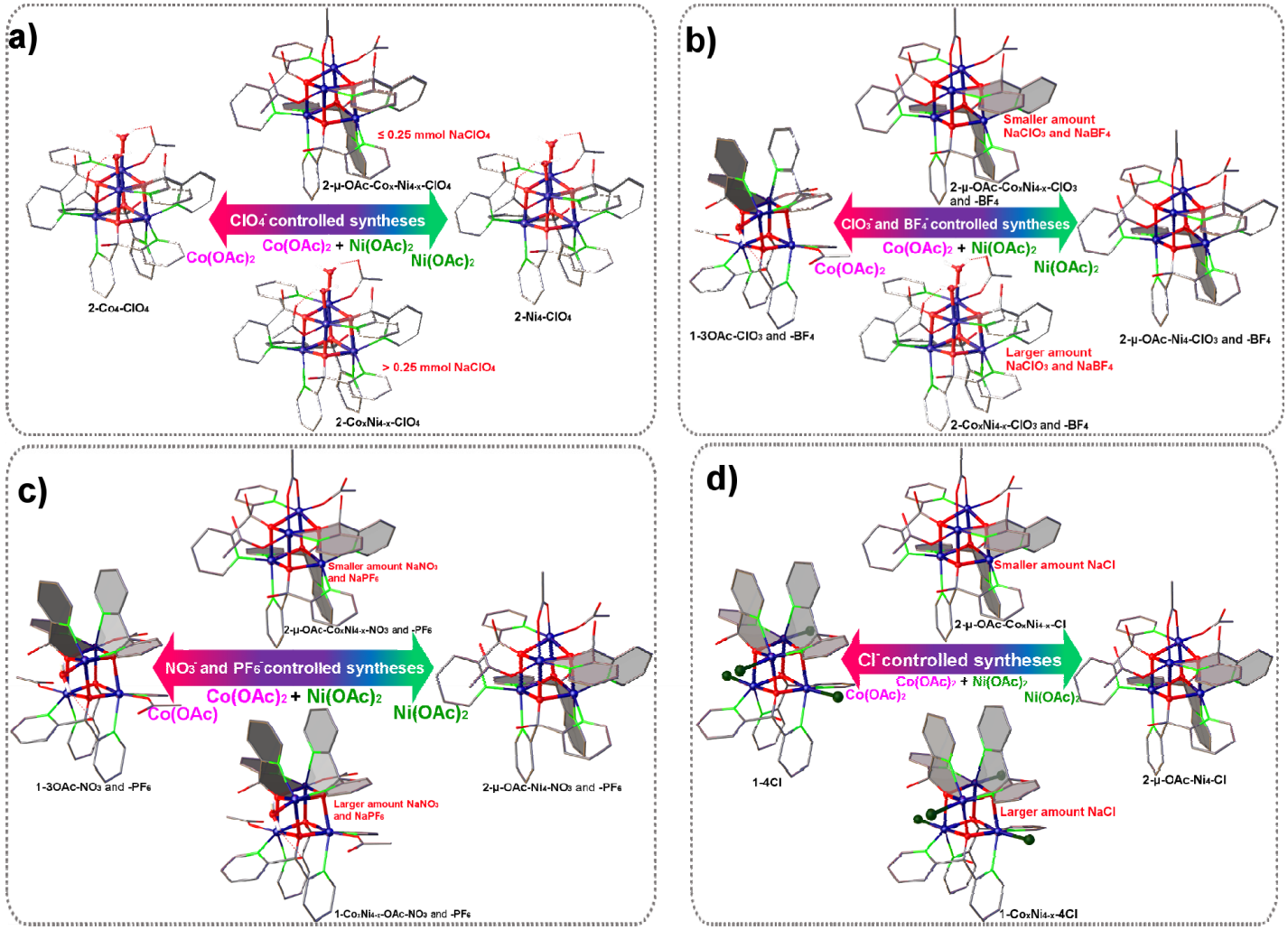

Figure S2. Survey of structure-directing counteranion effects in $\{Co_4O_4\}$, $\{Co_xNi_{4-x}O_4\}$, and $\{Ni_4O_4\}$ cubane syntheses (cf. Scheme 1 for the respective concentration ranges of additional counteranions).

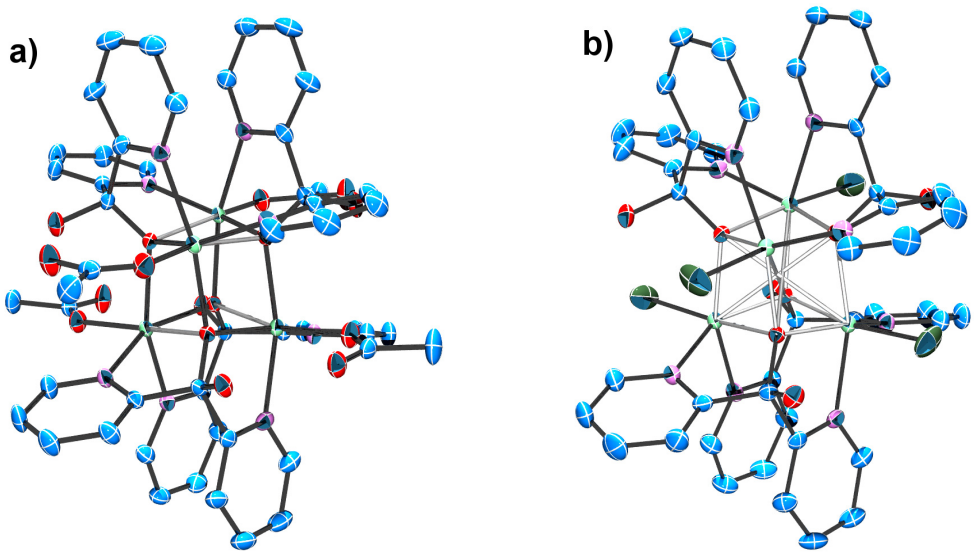

Figure S3. Thermal ellipsoid representations of **1-4OAc** (**a**) and **1-4Cl** (**b**) at the 50 % probability level (solvent water molecules, counteranions, and ligand hydrogen atoms are omitted for clarity); (**b**) also represents the Co/Ni heterometallic analogue.

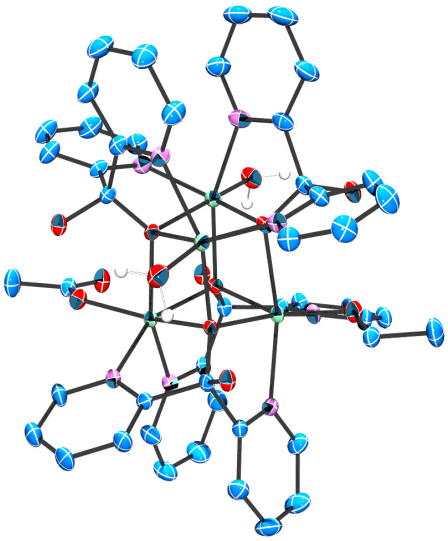

Figure S4. Thermal ellipsoid representation of cationic **1-2OAc-2BF$_4$** at the 50 % probability level (solvent water molecules, counteranions, and ligand hydrogen atoms are omitted for clarity).

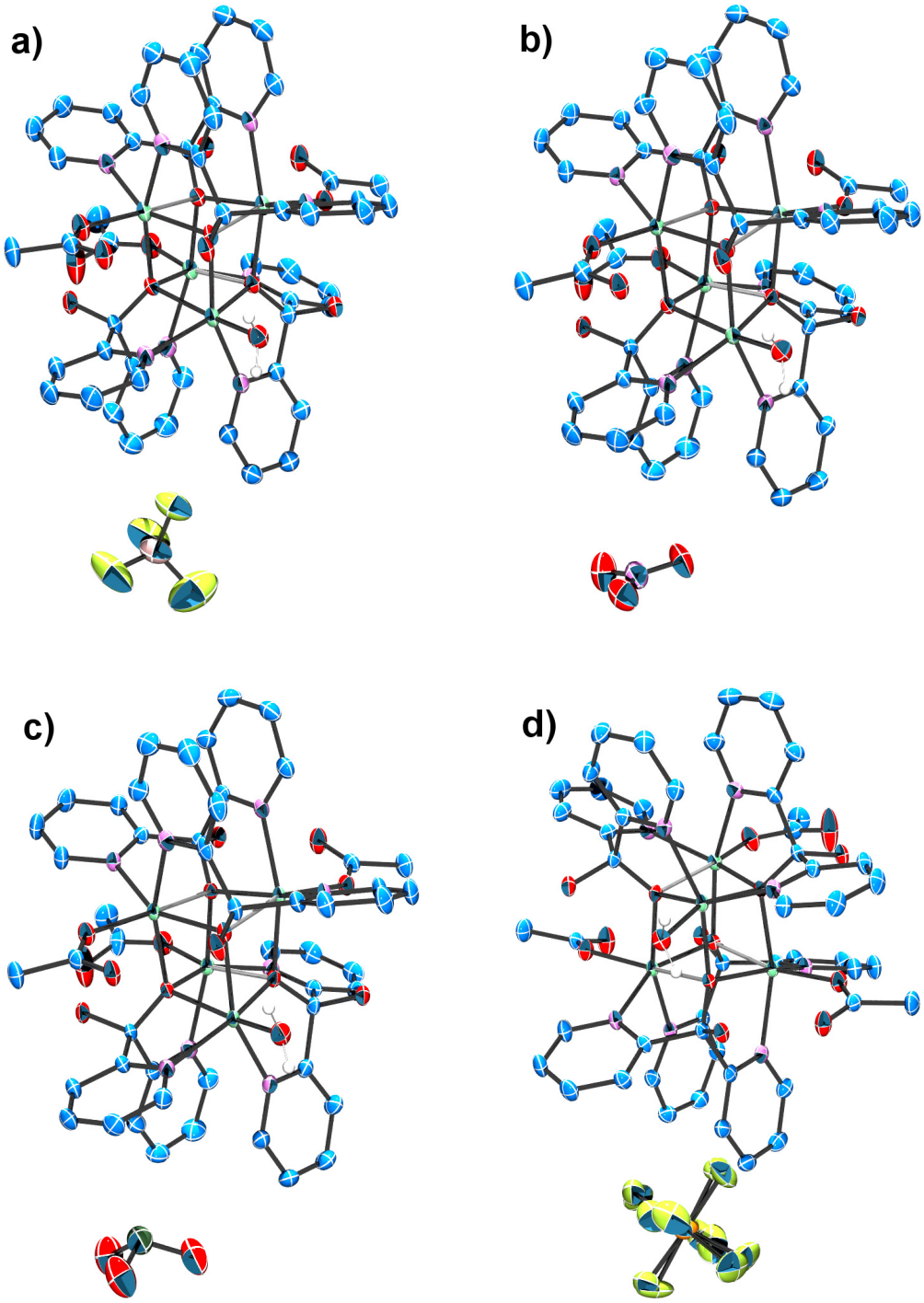

Figure S5. Thermal ellipsoid representations of **1-3OAc-BF$_4$** (**a**), **-NO$_3$** (**b**), **-ClO$_3$** (**c**), and **-PF$_6$** (**d**) at the 50 % probability level (solvent water molecules and ligand hydrogen atoms are omitted for clarity); (**a**), (**b**), (**c**), and (**d**) represent their Co/Ni heterometallic analogues as well.

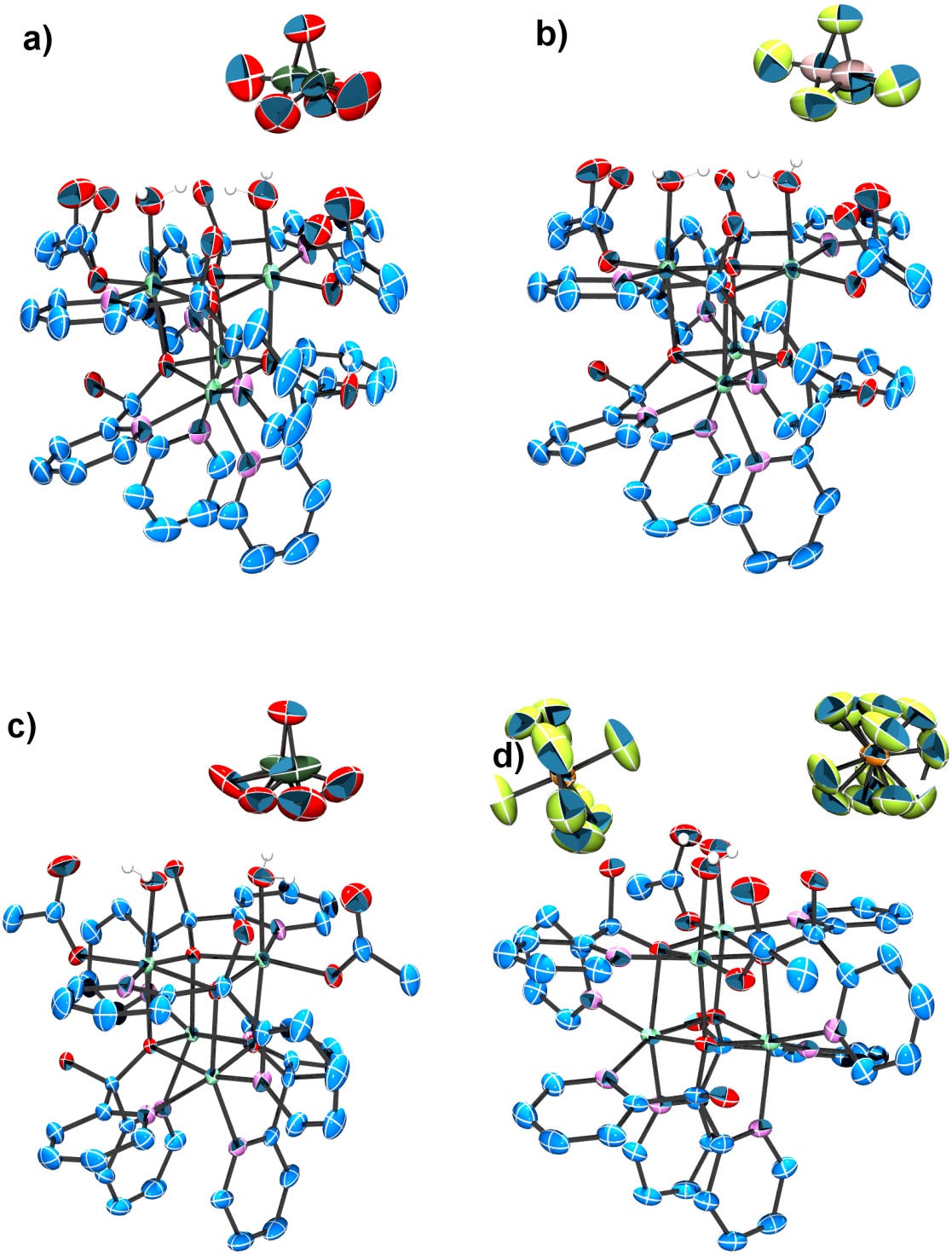

Figure S6. Thermal ellipsoid representations of **2-Co_xNi_{4-x}-ClO_4** (**a**), **-BF_4** (**b**), **-ClO_3** (**c**), and **-PF_6** (**d**) at the 50 % probability level (solvent water molecules and ligand hydrogen atoms are omitted for clarity).

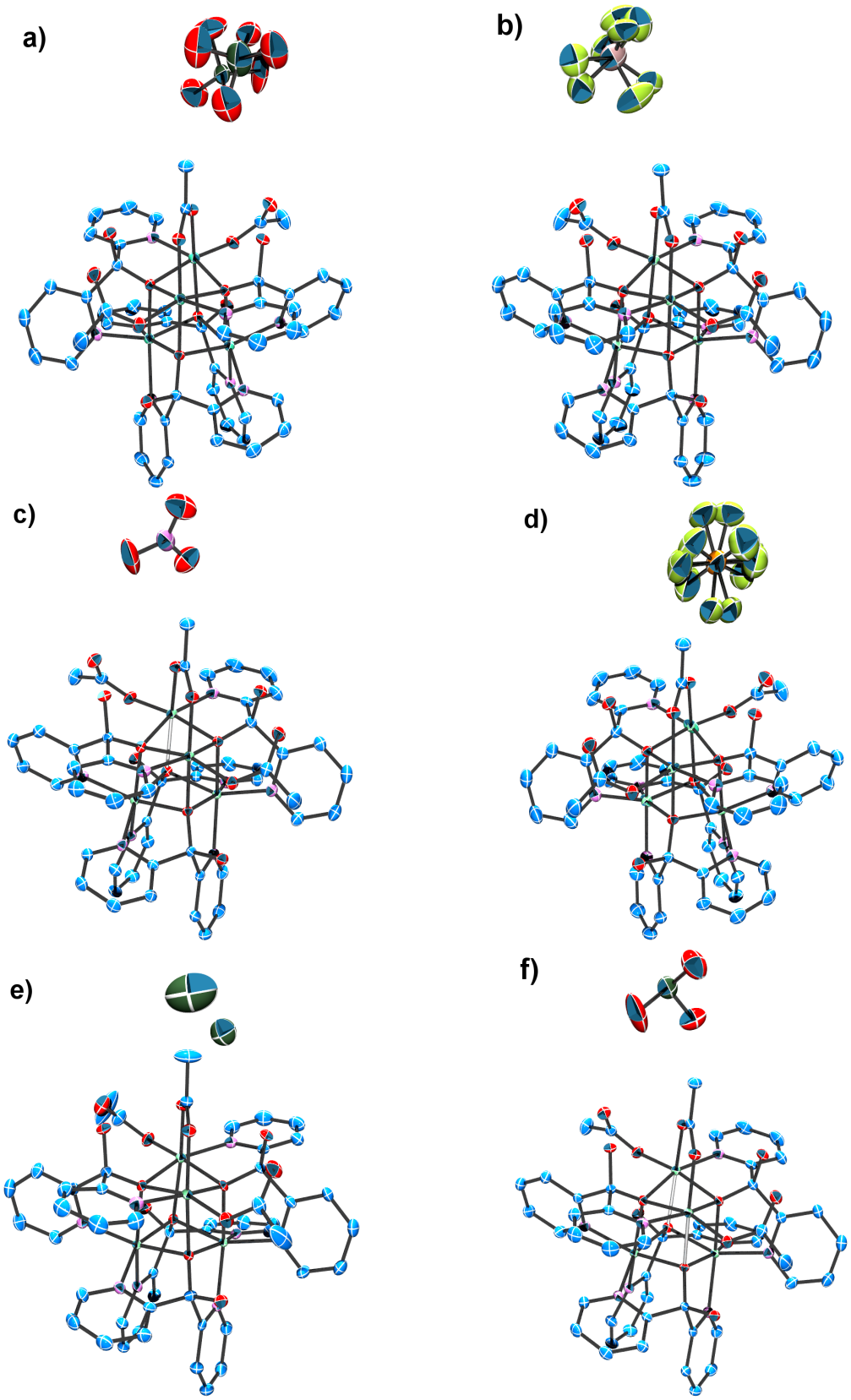

Figure S7. Thermal ellipsoid representations of **2-μ-OAc-Co$_x$Ni$_{4-x}$-ClO$_4$** (**a**), **-BF$_4$** (**b**), **-NO$_3$** (**c**), **-PF$_6$** (**d**), **-Cl** (**e**), and **-ClO$_3$** (**f**) at the 50 % probability level (solvent water molecules and ligand hydrogen atoms are omitted for clarity); (**a**), (**b**), (**c**), (**d**), (**e**), and (**f**) also represent their pure Ni analogues.

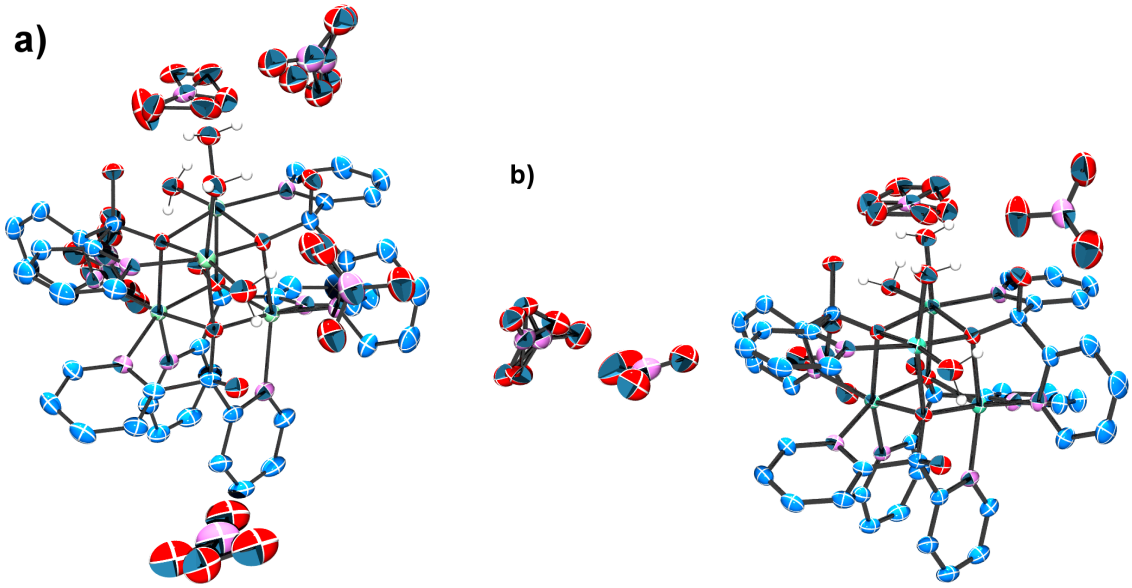

Figure S8. Thermal ellipsoid representations of **2-(*gem*-aqua)-Co_4-NO_3** (**a**) and **2-(*gem*-aqua)-Ni_4-NO_3** (**b**) at the 50 % probability level (solvent water molecules and ligand hydrogen atoms are omitted for clarity).

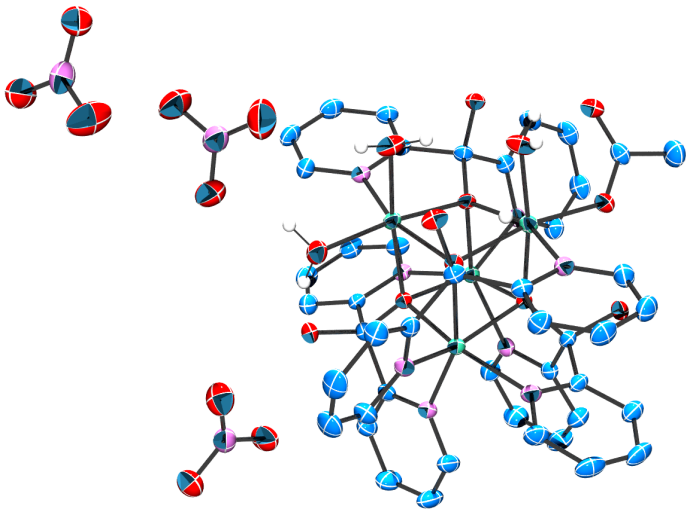

Figure S9. Thermal ellipsoid representation of **2-(half *gem*-aqua)-Ni_4-NO_3** at the 50 % probability level (solvent water molecules and ligand hydrogen atoms are omitted for clarity).

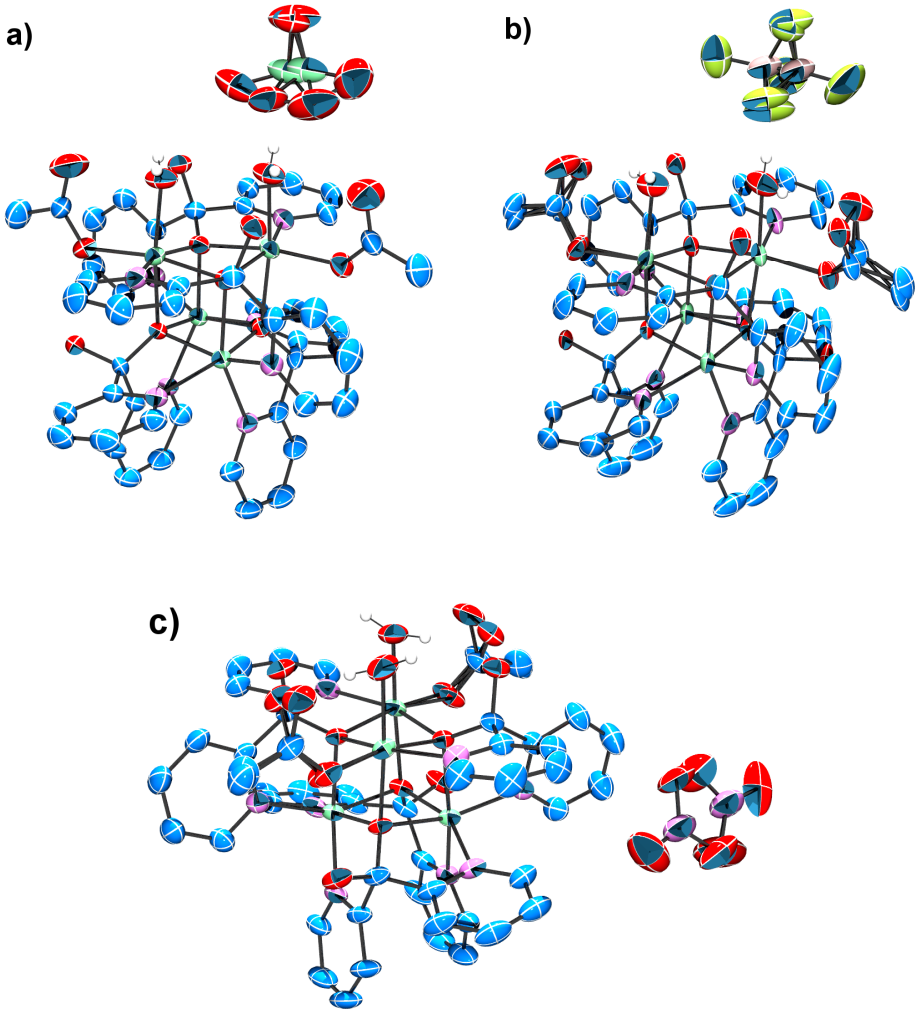

Figure S10. Thermal ellipsoid representations of **2-Co$_4$-ClO$_3$** (**a**), **-BF$_4$** (**b**), and **-NO$_3$** (**c**) at the 50 % probability level (solvent water molecules and ligand hydrogen atoms are omitted for clarity).

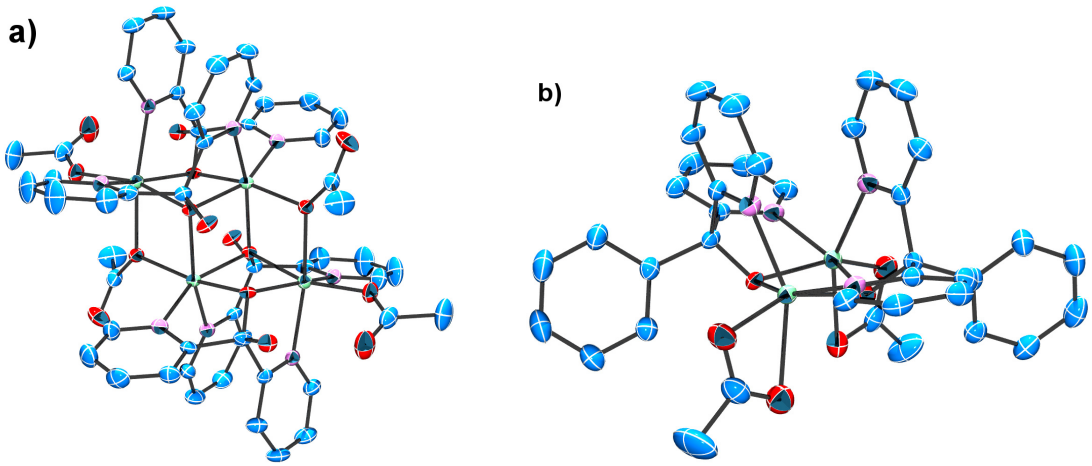

Figure S11. Thermal ellipsoid representations of defect [Co$_4$(dpy-C{OH}O)$_4$(OAc)$_4$] (**a**) and [Co$_2$(dpy-C{Ph}O)$_2$(μ-OAc)$_2$] (**b**) at the 50 % probability level (solvent molecules and ligand hydrogen atoms are omitted for clarity).

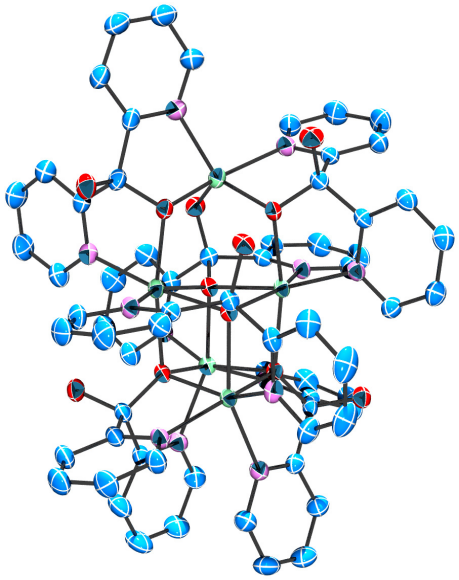

Figure S12. Thermal ellipsoid representations of cationic $[Co_5(dpy\text{-}C\{OH\}O)_5(dpy\text{-}C\{O\}_2)](NO_3)_3$ at the 50 % probability level (solvent water molecules, counteranions, and ligand hydrogen atoms are omitted for clarity).

Table S1. Crystallographic data of $[Co_4(dpy\text{-}C\{OH\}O)_4(OAc)_4]$, $[Co_4(dpy\text{-}C\{OH\}O)_4(Cl)_4]$, and $[Co_4(dpy\text{-}C\{OH\}O)_4(OAc)_2(H_2O)_2](BF_4)_2$.

Empirical formula	$C_{52}\ H_{94.6}\ Co_4\ N_8\ O_{37.3}$	$C_{44}\ H_{40}\ Cl_4\ Co_4\ N_8\ O_{10}$	$C_{48}\ H_{58}\ B_2\ Co_4\ F_8\ N_8\ O_{20}$
Formula weight	1664.47 $g\cdot mol^{-1}$	1218.36 $g\cdot mol^{-1}$	1476.36 $g\cdot mol^{-1}$
Temperature	183 K	183 K	183 K
Radiation wavelength	0.71073 Å	0.71073 Å	0.71073 Å
Crystal system	triclinic	cubic	monoclinic
Space group	*P*-1	*I*-43*d*	$P2_1/n$
a	14.6328(4) Å	23.9436(4) Å	15.4022(5) Å
b	14.6409(3) Å	23.9436(4) Å	24.0916(6) Å
c	18.1680(3) Å	23.9436(4) Å	16.0068(5) Å
α	94.984 (2)°	90°	90°
β	112.238(2)°	90°	96.849(3)°
γ	90.794(2)°	90°	90°
Volume	3584.52(14) $Å^3$	13726.8(6) $Å^3$	5897.2(3) $Å^3$
Z	2	12	4
Density calcd	1.542 $g\cdot cm^{-3}$	1.769 $g\cdot cm^{-3}$	1.663 $g\cdot cm^{-3}$
Absorption coefficient	1.008 mm^{-1} (Gaussian)	1.728 mm^{-1} (Gaussian)	1.211 mm^{-1} (Gaussian)
Crystal size	0.381 × 0.217 × 0.197 mm	0.198 × 0.173 × 0.146 mm	0.554 × 0.248 × 0.163 mm
Independent reflections	21812 [R_{int} = 0.0545]	2628 [R_{int} = 0.0397]	13494 [R_{int} = 0.0420]
Reflections collected	109212	23431	33367
θ range	2.268-30.508°	2.406-27.470°	2.563-27.481°
Completeness	0.9978 (θ = 30.44°)	0.9968 (θ = 27.42°)	0.9984 (θ = 27.42°)
F(000)	1738	7392	3008
Data/restraints/parameters	21812/1/986	2628/2/165	13494/0/855
$R_1[I>2\sigma(I)]^a$	0.0529	0.0281	0.0415
$wR_2[I>2\sigma(I)]^b$	0.1330	0.0687	0.0899
R_1^a (all data)	0.0716	0.0297	0.0671
wR_2^b (all data)	0.1447	0.0697	0.1032
Goodness-of-fit on F^2	1.046	1.058	1.034

$^a R_1 = \Sigma||F_o|-|F_c||/\Sigma|F_o|$; $^b wR_2 = \{\Sigma[w(F_o^2-F_c^2)^2]/\Sigma[w(F_o^2)^2]\}^{1/2}$

Table S2. Crystallographic data of $[Co_4(dpy\text{-}C\{OH\}O)_4(OAc)_3(H_2O)](ClO_3, \text{-}NO_3, \text{-}BF_4, \text{and -}PF_6)$.

Empirical formula	$C_{50}H_{52.6}ClCo_4N_8O_{20.4}$	$C_{50}H_{53}Co_4N_9O_{21}$	$C_{50}H_{51}BCo_4F_4N_8O_{17}$	$C_{50.50}H_{51}Co_4F_6N_8O_{16.50}P$
Formula weight	1362.81 g·mol^{-1}	1351.73 g·mol^{-1}	1358.51 g·mol^{-1}	1414.68 g·mol^{-1}
Temperature	160 K	180 K	183 K	160 K
Radiation wavelength	0.71073 Å	0.71073 Å	0.71073 Å	0.71073 Å
Crystal system	triclinic	triclinic	triclinic	triclinic
Space group	*P*-1	*P*-1	*P*-1	*P*-1
a	12.7097(2) Å	12.6957(4) Å	12.7299(4) Å	12.9163(4) Å
b	14.2447(3) Å	14.2283(5) Å	14.2087(5) Å	14.1420(3) Å
c	15.7479(3) Å	15.5843(4) Å	15.7489(8) Å	16.2926(4) Å
α	90.0964(15)°	90.190(2)°	89.780(3)°	89.681(2)°
β	105.6172(15)°	105.029(3)°	73.273(4)°	72.126(2)°
γ	92.2521(14)°	92.381(3)°	86.642(3)°	86.839(2)°
Volume	2743.48(8) Å^3	2716.20(15) Å^3	2723.13(19) Å^3	2827.90(13) Å^3
Z	2	2	2	2
Density calcd	1.650 g·cm^{-3}	1.653 g·cm^{-3}	1.657 g·cm^{-3}	1.661 g·cm^{-3}
Absorption coefficient	1.323 mm^{-1} (Gaussian)	1.289 mm^{-1} (Gaussian)	1.290 mm^{-1} (Gaussian)	1.278 mm^{-1} (Gaussian)
Crystal size	0.183 × 0.113 × 0.048 mm	0.323 × 0.228 × 0.121 mm	0.43 × 0.221 × 0.144 mm	0.195 × 0.146 × 0.124 mm
Independent reflections	13568 [Rint = 0.0431]	11102 [R_{int} = 0.0396]	11133 [R_{int} = 0.0528]	14037 [R_{int} = 0.0345]
Reflections collected	69749	30482	48988	64949
θ range	2.150-28.282	2.707-26.371°	2.701-26.372°	2.137-28.282°
Completeness	0.9987 (θ = 28.22°)	0.9988 (θ = 26.32°)	0.9987 (θ = 26.32°)	0.9988 (θ = 28.22°)
F(000)	1392	1384	1384	1438
Data/restraints/parameters	13568/268/851	11102/0/781	11133/0/767	14037/289/878
$R_1[I>2\sigma(I)]^a$	0.0401	0.0361	0.0441	0.0367
$wR_2[I>2\sigma(I)]^b$	0.1086	0.0843	0.1022	0.0921
R_1^a (all data)	0.0495	0.0491	0.0601	0.0459
wR_2^b (all data)	0.1135	0.0911	0.1111	0.0971
Goodness-of-fit on F^2	1.033	1.027	1.029	1.043

$^aR_1 = \Sigma||F_o|-|F_c||/\Sigma|F_o|$; $^bwR_2 = \{\Sigma[w(F_o^2-F_c^2)^2]/\Sigma[w(F_o^2)^2]\}^{1/2}$

Table S3. Crystallographic data of $[Co_xNi_{4-x}(dpy\text{-}C\{OH\}O)_4(OAc)_2(H_2O)_2](ClO_4, \text{-}BF_4, \text{-}PF_6, \text{and -}ClO_3)_2$ (0<x<4).

Empirical formula	$C_{48}H_{46}Cl_2Co_{1.92}Ni_{2.08}N_8O_{22}$	$C_{48}H_{46}B_2Co_{2.28}Ni_{1.72}F_8N_8O_{14}$	$C_{48}H_{46}Co_{1.64}Ni_{2.36}F_{12}N_8O_{14}P_2$	$C_{48}H_{48}Cl_2Co_{2.32}Ni_{1.68}N_8O_{21}$
Formula weight	1393.09 g·mol^{-1}	1367.89 g·mol^{-1}	1484.07 g·mol^{-1}	1379.19 g·mol^{-1}
Temperature	183 K	183 K	183 K	183 K
Radiation wavelength	0.71073 Å	0.71073 Å	0.71073 Å	0.71073 Å
Crystal system	monoclinic	monoclinic	triclinic	monoclinic
Space group	*C*2/*c*	*C*2/*c*	*P*-1	*C*2/*c*
a	22.7499(14) Å	22.7806(17) Å	12.2745(3) Å	22.4421(9) Å
b	12.1315(6) Å	12.0764(5) Å	13.3722(4) Å	12.0160(3) Å
c	21.1640(12) Å	21.2581(13) Å	19.5727(4) Å	21.2212(8) Å
α	90°	90°	88.324(2) °	90°
β	115.903(8)°	116.313(8)°	73.699(2) °	116.299(5)°
γ	90°	90°	64.454(3) °	90°
Volume	5254.2(6) Å^3	5242.3(6) Å^3	2766.35(14) Å^3	5130.3(4) Å^3
Z	4	4	2	4
Density calcd	1.761 g·cm^{-3}	1.733 g·cm^{-3}	1.782 g·cm^{-3}	1.786 g·cm^{-3}
Absorption coefficient	1.523 mm^{-1} (Gaussian)	1.420 mm^{-1} (Gaussian)	1.445 mm^{-1} (Gaussian)	1.541 mm^{-1} (Gaussian)
Crystal size	0.472 × 0.277 × 0.167 mm	0.387 × 0.267 × 0.109 mm	0.19 × 0.135 × 0.121 mm	0.491 × 0.357 × 0.346 mm
Independent reflections	6520 [R_{int} = 0.0242]	5353 [R_{int} = 0.0389]	20297 [R_{int} = 0.0658]	12436 [R_{int} = 0.0401]
Reflections collected	14532	14098	20297	64059
θ range	2.555-28.279°	2.553-26.368°	2.180-26.356°	2.450-36.316°
Completeness	0.9985 (θ = 28.22°)	0.9989 (θ = 26.32°)	0.9992 (θ = 26.32°)	0.9989 (θ = 36.23°)
F(000)	2840	2775	1501	2815
Data/restraints/parameters	6520/139/467	5353/158/464	20297/443/902	12436/249/467
$R_1[I>2\sigma(I)]^a$	0.0530	0.0519	0.0601	0.0410
$wR_2[I>2\sigma(I)]^b$	0.1344	0.1478	0.1896	0. 1009
R_1^a (all data)	0.0723	0.0647	0.0734	0. 0609
wR_2^b (all data)	0.1511	0.1615	0.1880	0.1171
Goodness-of-fit on F^2	1.040	1.046	0.1053	1.067

$^aR_1 = \Sigma||F_o|-|F_c||/\Sigma|F_o|$; $^bwR_2 = \{\Sigma[w(F_o^2-F_c^2)^2]/\Sigma[w(F_o^2)^2]\}^{1/2}$

Table S4. Crystallographic data of $[Co_xNi_{4-x}(dpy\text{-}C\{OH\}O)_4(OAc)_2(\mu\text{-}OAc)]ClO_4$, $-ClO_3$, $-BF_4$, $-PF_6$, $-NO_3$, and -Cl.

Empirical formula	$C_{50}H_{67}ClCo_{1.90}Ni_{2.10}N_8O_{29}$	$C_{50}H_{67}ClCo_{2.32}Ni_{1.68}N_8O_{28}$	$C_{50}H_{67}BCo_{1.54}Ni_{2.46}F_4N_8O_{25}$	$C_{50}H_{67}F_6N_8Co_{2.36}Ni_{1.64}O_{25}P$	$C_{50}H_{67}ClCo_{1.54}Ni_{2.46}N_9O_{28}$	$C_{50}H_{61}ClCo_{2.34}Ni_{1.66}N_8O_{22}$
Formula weight	1514.82 g·mol^{-1}	1498.91 g·mol^{-1}	1502.10 g·mol^{-1}	1560.44 g·mol^{-1}	1477.30 g·mol^{-1}	1396.87 g·mol^{-1}
Temperature	183 K	160 K	160 K	183 K	183 K	160 K
Radiation wavelength	0.71073 Å	0.71073 Å	0.71073 Å	0.71073 Å	0.71073 Å	0.71073 Å
Crystal system	monoclinic	monoclinic	monoclinic	monoclinic	monoclinic	Monoclinic
Space group	$P2_1/c$	$P2_1/c$	$P2_1/c$	$P2_1/c$	$P2_1/c$	$P2_1/c$
a	12.0492(2) Å	12.0091(3) Å	11.9719(3) Å	12.1050(3) Å	11.9277(3) Å	12.2353(7) Å
b	24.3545(4) Å	23.9541(7) Å	24.6331(6) Å	24.6661(8) Å	23.7667(6) Å	17.6400(10) Å
c	21.4569(4) Å	21.5009(5) Å	21.5467(5) Å	21.5614(6) Å	21.4551(5) Å	27.9435(14) Å
α	90°	90°	90°	90°	90°	90°
β	100.1181(17)°	100.068(2) °	101.719(3)°	100.632(2) °	99.791(2) °	99.120(5)°
γ	90°	90°	90°	90°	90°	90°
Volume	6198.63(19) Å^3	6089.9(3) Å^3	6221.8(3) Å^3	6327.3(3) Å^3	5993.6(3) Å^3	5954.8(6) Å^3
Z	4	4	4	4	4	4
Density calcd	1.623 g·cm^{-3}	1.635 g·cm^{-3}	1.604 g·cm^{-3}	1.638 g·cm^{-3}	1.637 g·cm^{-3}	1.558 g·cm^{-3}
Absorption coefficient	1.265 mm^{-1} (Gaussian)	1.270 mm^{-1} (Gaussian)	1.235 mm^{-1} (Gaussian)	1.218 mm^{-1} (Gaussian)	1.276 mm^{-1} (Gaussian)	1.285 mm^{-1} (Gaussian)
Crystal size	0.479 × 0.108 × 0.08 mm	0.217 × 0.051 × 0.03 mm	0.297 × 0.066 × 0.056 mm	0.53 × 0.287 × 0.085 mm	0.125 × 0.096 × 0.058 mm	0.4041 × 0.1949 × 0.097 mm
Independent reflections	17391 [R_{int} = 0.0324]	18488 [R_{int} = 0.0531]	18930 [R_{int} = 0.0311]	19306 [R_{int} = 0.0557]	14869 [R_{int} = 0.0486]	12144 [R_{int} = 0.0421]
Reflections collected	128647	96286	68983	123706	79048	33990
θ range	1.910-29.575°	2.103- 30.508	2.100-30.507°	2.268-30.508°	2.024- 29.298°	2.498-26.371°
Completeness	0.9996 (θ = 29.51°)	0.9947 (θ = 30.44°)	0.9974 (θ = 30.44°)	0.9992 (θ = 30.44°)	0.9985 (θ = 28.22°)	0.9979 (θ = 26.32°)
F(000)	3128	3095	3098	3207	3058	2879
Data/restraints/ parameters	17391/116/925	18488/69/926	18930/142/940	19306/326/956	14869/5/898	12144/0/841
$R_1[I>2\sigma(I)]^a$	0.0370	0.0366	0.0408	0.0504	0.0425	0.0567
$wR_2[I>2\sigma(I)]^b$	0.1052	0.0693	0.1168	0.1371	0.1032	0.1407
$R_1{}^a$ (all data)	0.0422	0.0576	0.0518	0.0724	0.0538	0.0747
$wR_2{}^b$ (all data)	0.1076	0.0746	0.1229	0.1538	0.1074	0.1498
Goodness-of-fit on F^2	1.091	1.013	1.054	1.033	1.041	1.100

$^aR_1 = \Sigma||F_o|-|F_c||/\Sigma|F_o|$; $^bwR_2 = \{\Sigma[w(F_o^2-F_c^2)^2]/\Sigma[w(F_o^2)^2]\}^{1/2}$

Table S5. Crystallographic data of $[Ni_4(dpy\text{-}C\{OH\}O)_4(OAc)_2(\mu\text{-}OAc)]ClO_4$, $-ClO_3$, $-NO_3$, $-BF_4$, $-PF_6$, and -Cl.

Empirical formula	$C_{50}H_{67}ClNi_4N_8O_{29}$	$C_{50}H_{67}ClN_8Ni_4O_{28}$	$C_{50}H_{67}Ni_4N_9O_{28}$	$C_{50}H_{67}BNi_4F_4N_8O_{25}$	$C_{50}H_{67}F_6N_8Ni_4O_{25}P$	$C_{50}H_{67}ClN_8Ni_4O_{25}$
Formula weight	1514.40 $g\cdot mol^{-1}$	1498.40 $g\cdot mol^{-1}$	1476.96 $g\cdot mol^{-1}$	1501.76 $g\cdot mol^{-1}$	1559.92 $g\cdot mol^{-1}$	1459.41 $g\cdot mol^{-1}$
Temperature	183 K	160 K	183 K	160 K	160 K	183 K
Radiation wavelength	0.71073 Å	0.71073 Å	0.71073 Å	0.71073 Å	0.71073 Å	0.71073 Å
Crystal system	monoclinic	monoclinic	monoclinic	monoclinic	monoclinic	monoclinic
Space group	$P2_1/c$	$P2_1/c$	$P2_1/c$	$P2_1/c$	$P2_1/c$	$P2_1/c$
a	12.0432(2) Å	11.9897(3) Å	11.9474(3) Å	11.9815(3) Å	12.0535(3) Å	11.9510(3) Å
b	24.3255(4) Å	23.9258(5) Å	23.7932(7) Å	24.6554(7) Å	24.6786(6) Å	24.1715(5) Å
c	21.4471(4) Å	21.4676(5) Å	21.4982(6) Å	21.5499(6) Å	21.4781(5) Å	21.5060(6) Å
α	90°	90°	90°	90°	90°	90°
β	100.2261(2)°	100.261(2) °	99.884(2)°	101.629(3)°	100.613(2)°	100.333(2) °
γ	90°	90°	90°	90°	90°	90°
Volume	6183.3(19) $Å^3$	6059.8(3) $Å^3$	6020.5(3) $Å^3$	6235.4(3) $Å^3$	6279.6(3) $Å^3$	6111.8(3) $Å^3$
Z	4	4	4	4	4	4
Density calcd	1.627 $g\cdot cm^{-3}$	1.642 $g\cdot cm^{-3}$	1.629 $g\cdot cm^{-3}$	1.582 $g\cdot cm^{-3}$	1.650 $g\cdot cm^{-3}$	1.586 $g\cdot cm^{-3}$
Absorption coefficient	1.337 mm^{-1} (Gaussian)	1.363 mm^{-1} (Gaussian)	1.328 mm^{-1} (Gaussian)	1.287 mm^{-1} (Multi-Scan)	1.311 mm^{-1} (Gaussian)	1.346 mm^{-1} (Gaussian)
Crystal size	0.405 × 0.235 × 0.199 mm^3	0.317 × 0.07 × 0.056 mm	0.265 × 0.043 × 0.029 mm	0.336 × 0.06 × 0.027 mm	0.378 × 0.073 × 0.065 mm	0.115 × 0.104 × 0.042 mm
Independent reflections	15336 [R_{int} = 0.0430]	13865 [R_{int} = 0.0410]	16171 [R_{int} = 0.0461]	14218 [R_{int} = 0.0394]	15562[R_{int} = 0.0570]	12486[R_{int} = 0.0441]
Reflections collected	76359	78189	73358	62059	81161	66759
θ range	2.275-28.282°	2.108-27.484°	2.020-29.130°	2.099-27.484°	1.989-28.282°	1.925-26.373°
Completeness	0.999 (θ = 28.22°)	0.9975 (θ = 27.42°)	0.9970 (θ = 29.07°)	0.9932 (θ = 27.42°)	0.9986 (θ = 28.22°)	0.9985 (θ = 26.32°)
F(000)	3136	3104	3038	3114	3216	3028
Data/restraints/ parameters	15336/179/932	13865/66/923	16171/0/892	14218/122/946	15562/309/943	12489/1/857
$R_1[I>2\sigma(I)]^a$	0.0424	0.0627	0.0382	0.0393	0.0596	0.0413
$wR_2[I>2\sigma(I)]^b$	0.1145	0.1572	0.0911	0.1003	0.1497	0.1141
$R_1{}^a$ (all data)	0.0499	0.0699	0.0567	0.0513	0.0679	0.0515
$wR_2{}^b$ (all data)	0.1201	0.1602	0.0979	0.1061	0.1532	0.1203
Goodness-of-fit on F^2	1.054	1.186	1.027	1.037	1.124	1.030

$^aR_1 = \Sigma||F_o|-|F_c||/\Sigma|F_o|$; $^bwR_2 = \{\Sigma[w(F_o^2-F_c^2)^2]/\Sigma[w(F_o^2)^2]\}^{1/2}$

Table S6. Crystallographic data of $[M_4(dpy\text{-}C\{OH\}O)_4(H_2O)_4](NO_3)_4$, $[Ni_4(dpy\text{-}C\{OH\}O)_4(OAc)(H_2O)_3](NO_3)_3$, and $[Ni_4(dpy\text{-}C\{OH\}O)_4(OAc)_2(H_2O)_2](NO_3)_2$.

Empirical formula	$C_{44}H_{56}Co_4N_{12}O_{30}$	$C_{44}H_{56}N_{12}Ni_4O_{30}$	$C_{46}H_{53}Ni_4N_{11}O_{26}$	$C_{48}H_{47.6}N_{10}Ni_4O_{21.4}$
Formula weight	1468.72 g·mol^{-1}	1467.84 g·mol^{-1}	1410.83 g·mol^{-1}	1342.12 g·mol^{-1}
Temperature	160 K	160 K	183 K	160 K
Radiation wavelength	0.71073 Å	1.54184 Å	1.54184 Å	1.54184 Å
Crystal system	triclinic	triclinic	triclinic	monoclinic
Space group	*P*-1	*P*-1	*P*-1	*C*2/*c*
a	11.7024(2) Å	11.60874(12) Å	11.7709(3) Å	22.5327(3)
b	12.9555(3) Å	12.86774(12) Å	13.3769(3) Å	11.87693(11)
c	19.8107(4) Å	19.73943(15) Å	17.3977(4) Å	21.4511(2)
α	91.1275(17)°	91.5430(7)°	91.475(2)°	90
β	100.3745(15)°	99.0305(8)°	100.300(2)°	116.4557(14)
γ	106.1227(17)°	106.2031(8)°	91.778(2)°	90
Volume	2830.49(10) Å^3	2788.63(5) Å^3	2692.59(12) Å^3	5139.54(11)
Z	2	2	2	4
Density calcd	1.723 g·cm^{-3}	1.748 g·cm^{-3}	1.740 g·cm^{-3}	1.735 g·cm^{-3}
Absorption coefficient	1.257 mm^{-1} (Gaussian)	2.455 mm^{-1} (Gaussian)	2.452 mm^{-1} (Multi-Scan)	2.462 mm^{-1} (Gaussian)
Crystal size	0.225 × 0.08 × 0.048 mm	0.239 × 0.067 × 0.033 mm	0.16 × 0.04 × 0.04 mm	0.167 × 0.126 × 0.068 mm
Independent reflections	14052 [R_{int} = 0.0325]	11652 [R_{int} = 0.0296]	10220 [R_{int} = 0.0526]	5419 [R_{int} = 0.0393]
Reflections collected	73069	47865	41551	30292
θ range	2.011-28.282°	3.587-77.381°	3.307-70.065°	4.320-77.382°
Completeness	0.9996 (θ = 28.22°)	0.9831 (θ = 77.17°)	0.9983 (θ = 69.95°)	0.9925 (θ = 77.17°)
F(000)	1504	1512	1452	2756
Data/restraints/parameters	14052/388/1020	11652/201/967	10220/3/820	5419/221/462
$R_1[I>2\sigma(I)]^a$	0.0517	0.0403	0.0351	0.0463
$wR_2[I>2\sigma(I)]^b$	0.1501	0.1129	0.0777	0.1256
R_1^a (all data)	0.0609	0.0442	0.0519	0.0508
wR_2^b (all data)	0.1575	0.1162	0.0840	0.1293
Goodness-of-fit on F^2	1.056	1.053	1.013	1.036

$^a R_1 = \Sigma||F_o|-|F_c||/\Sigma|F_o|$; $^b wR_2 = \{\Sigma[w(F_o^2-F_c^2)^2]/\Sigma[w(F_o^2)^2]\}^{1/2}$

Table S7. Crystallographic data of $[Co_4(dpy\text{-}C\{OH\}O)_4(OAc)_2(H_2O)_2](NO_3, \text{-}ClO_3, \text{and -}BF_4)_2$ and $[Co_5(dpy\text{-}C\{OH\}O)_5(dpy\text{-}C\{O\}_2)](NO_3)_3$

Empirical formula	$C_{48}H_{46}Co_4N_{10}O_{20}$	$C_{48}H_{46}Cl_2Co_4N_8O_{20}$	$C_{48}H_{46}B_2Co_4F_8N_8O_{14}$	$C_{66}H_{60.21}Co_5N_{15}O_{29.50}$
Formula weight	1318.67 g·mol^{-1}	1361.55 g·mol^{-1}	1368.27 g·mol^{-1}	1830.15 g·mol^{-1}
Temperature	160 K	160 K	160 K	160 K
Radiation wavelength	1.54184 Å	1.54184 Å	0.71073 Å	1.54184 Å
Crystal system	monoclinic	monoclinic	monoclinic	triclinic
Space group	*C*2/*c*	*C*2/*c*	*C*2/*c*	*P*-1
a	22.5898(6) Å	22.3692(6) Å	22.6584(5) Å	11.93210(10) Å
b	11.9550(2) Å	12.07776(19) Å	12.1359(3) Å	13.38640(10) Å
c	21.4009(6) Å	21.0774(5) Å	21.1615(5) Å	23.8027(2) Å
α	90°	90°	90°	91.2810(10)°
β	116.258(3) °	115.686(3) °	115.784(3)°	92.0850(10)°
γ	90°	90°	90°	107.5810(10)°
Volume	5183.2(2) Å^3	5131.7(2) Å^3	5239.7(2) Å^3	3619.75(5) Å^3
Z	4	4	4	2
Density calcd	1.690 g·cm^{-3}	1.762 g·cm^{-3}	1.735 g·cm^{-3}	1.679 g·cm^{-3}
Absorption coefficient	10.631 mm^{-1} (Gaussian)	11.683 mm^{-1} (Multi-Scan)	1.348 mm^{-1} (Gaussian)	9.644 mm^{-1} (Gaussian)
Crystal size	0.086 × 0.047 × 0.021 mm	0.156 × 0.086 × 0.041 mm	0.252 × 0.148 × 0.099 mm	0.139 × 0.081 × 0.028 mm
Independent reflections	5291 [R_{int} = 0.0494]	5405 [R_{int} = 0.0528]	6020 [R_{int} = 0.0304]	15055 [R_{int} = 0.0456]
Reflections collected	27903	21680	39800	60044
θ range	4.294-74.484°	4.267-77.306°	1.952-27.484°	3.466-77.379°
Completeness	0.9993 (θ = 74.33°)	0.9860 (θ = 77.17°)	0.9995 (θ = 27.42°)	0.995 (θ = 67.684°)
F(000)	2688	2768	2768	1864
Data/restraints/ parameters	5291/270/456	5405/154/418	6020/357/478	15055/97/1204
$R_1[I>2\sigma(I)]^a$	0.0507	0.0564	0.0484	0.0419
$wR_2[I>2\sigma(I)]^b$	0.1510	0.1574	0.1375	0.1068
R_1^a (all data)	0.0571	0.0679	0.0529	0.0515
wR_2^b (all data)	0.1572	0.1669	0.1422	0.1144
Goodness-of-fit on F^2	1.057	1.048	1.026	1.053

$^a R_1 = \Sigma||F_o|-|F_c||/\Sigma|F_o|$; $^b wR_2 = \{\Sigma[w(F_o^2-F_c^2)^2]/\Sigma[w(F_o^2)^2]\}^{1/2}$

Table S8. Crystallographic data of $[Co_4(dpy\text{-}C\{OH\}O)_4(OAc)_4]$ (defect cubane), $[Co_4(dpy\text{-}C\{OH\}O)_4(OAc)_4]$, and $[Co_2(dpy\text{-}C\{Ph\}O)_2(OAc)_2]$.

Empirical formula	$C_{60}H_{72}Co_4N_8O_{20}$	$C_{52}H_{90}Co_4N_8O_{37}$	$C_{40}H_{37}Co_2N_5O_7$
Formula weight	1460.97 g·mol^{-1}	1655.03 g·mol^{-1}	817.60 g·mol^{-1}
Temperature	183 K	160 K	183 K
Radiation wavelength	0.71073 Å	0.71073 Å	0.71073 Å
Crystal system	monoclinic	triclinic	monoclinic
Space group	$P2_1/c$	P-1	$P2_1/n$
a	12.6067(10) Å	14.7712 (2) Å	9.2864(2) Å
b	14.0325(6) Å	17.5108 (3) Å	21.6644(5) Å
c	18.7571(12) Å	17.9137 (2) Å	18.8463(5) Å
α	90°	60.079 (2)°	90°
β	106.059(7)°	70.4300 (10)°	95.987(2)°
γ	90°	65.817 (2)°	90°
Volume	3188.7(4) Å^3	3704.60 (12) Å^3	3770.90(16) Å^3
Z	2	2	4
Density calcd	1.522 g·cm^{-3}	1.484 g·cm^{-3}	1.440 g·cm^{-3}
Absorption coefficient	1.103 mm^{-1} (Analytical)	0.975 mm^{-1} (Multi-scan)	0.936 mm^{-1} (Gaussian)
Crystal size	0.305 × 0.125 × 0.064 mm	0.13 × 0.08 × 0.08 mm	0.379 × 0.207 × 0.107 mm
Independent reflections	6049 [R_{int} = 0.0641]	22603 [R_{int} = 0.0437]	7715 [R_{int} = 0.0580]
Reflections collected	28602	139318	76910
θ range	2.415-25.680°	2.186-30.508°	2.355-26.370°
Completeness	0.9991 (θ = 25.63°)	0.9994 (θ = 26.32°)	0.9992 (θ = 26.32°)
F(000)	1512	1724	1688
Data/restraints/ parameters	6049/86/457	22603/0/956	7715/524/91
$R_1[I>2\sigma(I)]^a$	0.0489	0.0594	0.0353
$wR_2[I>2\sigma(I)]^b$	0.1129	0.1707	0.0784
R_1^a (all data)	0.0788	0.0793	0.0442
wR_2^b (all data)	0.1272	0.1876	0.0828
Goodness-of-fit on F^2	1.020	1.014	1.031

$^a R_1 = \Sigma||F_o|-|F_c||/\Sigma|F_o|$; $^b wR_2 = \{\Sigma[w(F_o^2-F_c^2)^2]/\Sigma[w(F_o^2)^2]\}^{1/2}$

Table S9. Selected bond lengths of **type 1**{Co_4O_4} cubanes.

	1-4OAc	1-3OAc-ClO_3	1-3OAc-BF_4	1-3OAc-PF_6	1-3OAc-NO_3	1-2OAc-BF_4	1-4Cl
Co1–O1	2.0420(17)	2.0405(15)	2.038(2)	2.0489(14)	2.0410(16)	2.0486(18)	2.026(2)
Co1–O2	2.2577(18)	2.1617(15)	2.162(2)	2.1616(14)	2.1578(17)	2.1727(17)	
Co1–O3	2.1000(18)	2.1583(15)	2.123(2)	2.1314(14)	2.1597(18)	2.1060(16)	
Co2–O1	2.2452(17)	2.2383(14)	2.222(2)	2.2345(14)	2.2399(17)	2.1786(18)	
Co2–O2	2.0404(18)	2.0491(15)	2.040(2)	2.0485(14)	2.0466(17)	2.0568(18)	
Co2–O4	2.0989(18)	2.1060(14)	2.109(2)	2.1218(14)	2.1087(17)	2.1071(16)	
Co3–O1	2.1099(18)	2.0938(15)	2.100(2)	2.1029(14)	2.0940(17)	2.1441(16)	
Co3–O3	2.2649(18)	2.2346(14)	2.216(2)	2.2327(14)	2.2306(16)	2.1743(18)	
Co3–O4	2.0266(18)	2.0300(14)	2.029(2)	2.0230(14)	2.0225(16)	2.0540(17)	
Co4–O2	2.1121(18)	2.1219(14)	2.108(2)	2.1099(14)	2.1118(17)	2.1508(16)	
Co4–O3	2.0333(18)	2.0541(14)	2.049(2)	2.0481(14)	2.0582(17)	2.0535(17)	
Co4–O4	2.2783(18)	2.2358(14)	2.244(2)	2.2582(14)	2.2394(16)	2.1799(17)	
Co1–N1	2.154(2)	2.1263(19)	2.113(3)	2.1196(18)	2.124(2)	2.132(2)	2.144(3)
Co1–N3	2.108(2)	2.1414(18)	2.135(3)	2.1441(17)	2.139(2)	2.094(2)	
Co2–N2	2.102(2)	2.0923(19)	2.098(3)	2.1063(19)	2.091(2)	2.106(2)	2.096(3)
Co2–N4	2.153(2)	2.1545(19)	2.151(3)	2.1672(19)	2.155(2)	2.130(2)	
Co3–N5	2.098(2)	2.1088(18)	2.108(3)	2.1061(17)	2.108(2)	2.109(2)	
Co3–N7	2.168(2)	2.1358(18)	2.135(3)	2.1449(18)	2.137(2)	2.131(2)	
Co4–N6	2.164(2)	2.1819(19)	2.178(3)	2.1810(18)	2.178(2)	2.129(2)	
Co4–N8	2.098(2)	2.0988(17)	2.099(3)	2.0970(18)	2.099(2)	2.119(2)	

Table S10. Selected bond lengths of **2-Co_4-ClO_4**, **2-Co_xNi_{4-x}**, and **2-Ni_4-ClO_4** cubanes.

	2-Co_4-ClO_4[5]	2-Co_xNi_{4-x}-ClO_4	2-Co_xNi_{4-x}-ClO_3	2-Co_xNi_{4-x}-BF_4	2-Ni_4-ClO_4		2-Co_xNi_{4-x}-PF_6
M1–O1 M1′–O1′	2.067(3)	2.049(2)	2.0506(11)	2.052(2)	2.028(2)	M1–O1	2.039(3)
						M2–O2	2.050(3)
M1–O1′ M1′–O1	2.138(3)	2.133(2)	2.1278(12)	2.140(3)	2.123(2)	M1–O2	2.133(3)
						M2–O1	2.159(3)
M1–O2′ M1′–O2	2.175(3)	2.145(2)	2.1567(11)	2.152(2)	2.116(2)	M1–O4	2.145(3)
						M2–O3	2.134(3)
M2–O1 M2′–O1′	2.151(3)	2.134(3)	2.1298(12)	2.130(3)	2.122(3)	M3–O1	2.137(3)
						M4–O2	2.139(3)
M2–O2 M2′–O2′	2.050(3)	2.040(3)	2.0384(12)	2.044(3)	2.031(3)	M3–O3	2.054(3)
						M4–O4	2.051(3)
M2–O2′ M2′–O2	2.116(3)	2.102(2)	2.0982(11)	2.109(2)	2.100(2)	M3–O4	2.124(3)
						M4–O3	2.125(3)
M1–N1 M1’–N1’	2.128(4)	2.112(3)	2.1145(16)	2.112(4)	2.078(3)	M1–N1	2.105(4)
						M2–N3	2.112(4)
M2–N2 M2’–N2’	2.071(4)	2.044(3)	2.0525(15)	2.055(3)	2.031(3)	M3–N2	2.070(4)
						M4–N4	2.062(4)
M2–N3 M2’–N3’	2.131(4)	2.103(3)	2.0994(15)	2.104(3)	2.088(3)	M3–N5	2.106(4)
						M4–N8	2.107(4)
M2–N4’ M2’–N4	2.134(4)	2.100(3)	2.1022(15)	2.097(3)	2.079(3)	M3–N7	2.100(4)
						M4–N6	2.109(4)

Table S11. Selected bond lengths of **2-μ-OAc-Co_xNi_{4-x}** cubanes.

	2-μ-OAc-Co_xNi_{4-x}-ClO_4	**2-μ-OAc-Co_xNi_{4-x}-ClO_3**	**2-μ-OAc-Co_xNi_{4-x}-BF_4**	**2-μ-OAc-Co_xNi_{4-x}-PF_6**	**2-μ-OAc-Co_xNi_{4-x}-NO_3**	**2-μ-OAc-Co_xNi_{4-x}-Cl**
M1–O1	2.0623(15)	2.0626(12)	2.0513(14)	2.0550(19)	2.0543(17)	2.055(3)
M1–O2	2.1370(15)	2.1393(11)	2.1214(13)	2.1277(18)	2.1233(17)	2.170(3)
M1–O4	2.2118(15)	2.2263(11)	2.1932(14)	2.2196(19)	2.2138(17)	2.198(3)
M2–O1	2.1356(15)	2.1386(11)	2.1136(14)	2.1376(18)	2.1261(17)	2.111(3)
M2–O2	2.0606(15)	2.0617(11)	2.0598(14)	2.0695(19)	2.0483(17)	2.064(3)
M2–O3	2.2234(14)	2.2201(11)	2.1833(13)	2.2046(18)	2.2010(17)	2.211(3)
M3–O1	2.0886(14)	2.0971(11)	2.0826(14)	2.0875(19)	2.0828(17)	2.076(3)
M3–O3	2.0496(15)	2.0369(11)	2.0436(13)	2.0397(18)	2.0303(17)	2.028(3)
M3–O4	2.1185(14)	2.1063(11)	2.1134(14)	2.1110(19)	2.1063(17)	2.116(3)
M4–O2	2.0955(15)	2.0844(11)	2.0871(14)	2.0912(18)	2.0780(17)	2.073(3)
M4–O3	2.1105(15)	2.1212(11)	2.1191(14)	2.1161(18)	2.1196(17)	2.110(3)
M4–O4	2.0377(15)	2.0544(11)	2.0381(14)	2.0484(18)	2.0484(17)	2.051(3)
M1–N1	2.1234(19)	2.0952(19)	2.0847(18)	2.097(2)	2.080(2)	2.137(4)
M2–N3	2.0989(19)	2.1199(15)	2.1090(17)	2.122(2)	2.103(2)	2.085(4)
M3–N2	2.0600(19)	2.0601(14)	2.0504(18)	2.056(2)	2.047(2)	2.087(3)
M3–N5	2.0919(18)	2.0979(14)	2.0822(17)	2.093(2)	2.093(2)	2.117(3)
M3–N7	2.1114(18)	2.1049(14)	2.0971(18)	2.109(2)	2.093(2)	2.097(4)
M4–N4	2.0538(19)	2.0663(15)	2.0503(18)	2.057(2)	2.059(2)	2.069(3)
M4–N6	2.1040(19)	2.1170(14)	2.0908(17)	2.109(2)	2.104(2)	2.117(3)
M4–N8	2.1003(18)	2.0927(14)	2.0832(18)	2.096(2)	2.080(2)	2.103(4)

Table S12. Selected bond lengths of **2-μ-OAc-Ni_4** cubanes.

	2-μ-OAc-Ni_4-ClO_4	**2-μ-OAc-Ni_4-ClO_3**	**2-μ-OAc-Ni_4-BF_4**	**2-μ-OAc-Ni_4-PF_6**	**2-μ-OAc-Ni_4-NO_3**	**2-μ-OAc-Ni_4-Cl**
Ni1–O1	2.0460(17)	2.042(3)	2.0473(17)	2.048(2)	2.0339(14)	2.0436(19)
Ni1–O2	2.1087(17)	2.099(3)	2.0964(17)	2.099(3)	2.1060(14)	2.090(2)
Ni1–O4	2.1934(17)	2.183(3)	2.1589(17)	2.171(2)	2.1733(14)	2.1580(19)
Ni2–O1	2.1186(17)	2.106(3)	2.0945(17)	2.088(3)	2.0938(14)	2.102(2)
Ni2–O2	2.0451(17)	2.040(3)	2.0397(17)	2.039(3)	2.0421(15)	2.036(2)
Ni2–O3	2.1832(17)	2.173(3)	2.1761(17)	2.182(3)	2.1867(15)	2.179(2)
Ni3–O1	2.0843(18)	2.082(3)	2.0853(17)	2.083(2)	2.0759(14)	2.075(2)
Ni3–O3	2.0315(17)	2.028(3)	2.0371(17)	2.036(3)	2.0404(14)	2.046(2)
Ni3–O4	2.1051(17)	2.097(3)	2.1218(17)	2.109(2)	2.1157(14)	2.1197(19)
Ni4–O2	2.0819(17)	2.076(3)	2.0850(17)	2.078(3)	2.0793(15)	2.080(2)
Ni4–O3	2.1099(17)	2.111(3)	2.1170(17)	2.110(3)	2.1050(15)	2.101(2)
Ni4–O4	2.0388(17)	2.042(3)	2.0405(17)	2.029(3)	2.0271(14)	2.0257(19)
Ni1–N1	2.078(2)	2.056(4)	2.084(2)	2.082(3)	2.0792(18)	2.075(3)
Ni2–N3	2.099(2)	2.083(4)	2.062(2)	2.069(3)	2.059(2)	2.058(3)
Ni3–N2	2.037(2)	2.038(4)	2.041(2)	2.035(3)	2.0448(19)	2.043(3)
Ni3–N5	2.085(2)	2.077(4)	2.075(2)	2.078(3)	2.0675(18)	2.066(3)
Ni3–N7	2.090(2)	2.082(4)	2.083(2)	2.092(3)	2.0894(17)	2.085(3)
Ni4–N4	2.045(2)	2.044(4)	2.043(2)	2.036(3)	2.0437(19)	2.040(3)
Ni4–N6	2.094(2)	2.092(4)	2.087(2)	2.087(3)	2.0812(18)	2.082(3)
Ni4–N8	2.076(2)	2.066(4)	2.081(2)	2.077(3)	2.0794(19)	2.080(3)

Table S13. Selected bond lengths of **2-Co_4** and **2-(*gem*-aqua)-Co_4-NO_3** cubanes.

	2-Co_4-ClO_4[5]	**2-Co_4-ClO_3**	**2-Co_4-NO_3**	**2-Co_4-BF_4**		**2-(*gem*-aqua)-Co_4-NO_3**
Co1–O1	2.067(3)	2.070(3)	2.071(2)	2.0700(19)	Co1–O1	2.0815(19)
Co1′–O1′					Co2–O2	2.084(2)
Co1–O1′	2.138(3)	2.138(3)	2.141(2)	2.1298(19)	Co1–O2	2.119(2)
Co1′–O1					Co2–O1	2.1185(19)
Co1–O2′	2.175(3)	2.186(3)	2.185(2)	2.175(2)	Co1–O4	2.208(2)
Co1′–O2					Co2–O3	2.189(2)
Co2–O1	2.151(3)	2.148(3)	2.136(2)	2.153(2)	Co3–O1	2.119(2)
Co2′–O1′					Co4–O2	2.164(2)
Co2–O2	2.050(3)	2.059(3)	2.051(2)	2.051(2)	Co3–O3	2.063(2)
Co2′–O2′					Co4–O4	2.064(2)
Co2–O2′	2.116(3)	2.114(3)	2.116(2)	2.1146(19)	Co3–O4	2.126(2)
Co2′–O2					Co4–O3	2.119(2)
Co1–N1	2.128(4)	2.132(4)	2.128(3)	2.121(3)	Co1–N1	2.124(3)
Co1’–N1’					Co2–N3	2.106(3)
Co2–N2	2.071(4)	2.079(3)	2.073(3)	2.070(3)	Co3–N2	2.089(2)
Co2’–N2’					Co4–N4	2.073(3)
Co2–N3	2.131(4)	2.122(3)	2.127(3)	2.128(3)	Co3–N5	2.125(3)
Co2’–N3’					Co4–N8	2.144(3)
Co2–N4’	2.134(4)	2.135(3)	2.124(3)	2.128(3)	Co3–N7	2.140(3)
Co2’–N4					Co4–N6	2.120(3)

Table S14. Selected bond lengths of **2-Ni_4** and **2-(*gem*-aqua** and –**half *gem*-aqua)-Ni_4-NO_3** cubanes.

	2-Ni_4-ClO_4	**2-Ni_4-NO_3**		**2-(*gem*-aqua)-Ni_4-NO_3**	**2-(half *gem*-aqua)-Ni_4-NO_3**
Ni1–O1	2.028(2)	2.0478(17)	Ni1–O1	2.0363(15)	2.0229(16)
Ni1′–O1′			Ni2–O2	2.0410(15)	2.0377(16)
Ni1–O1′	2.123(2)	2.1325(17)	Ni1–O2	2.1092(15)	2.1005(16)
Ni1′–O1			Ni2–O1	2.0988(15)	2.1075(16)
Ni1–O2′	2.116(2)	2.1464(18)	Ni1–O4	2.1389(15)	2.0986(16)
Ni1′–O2			Ni2–O3	2.1133(15)	2.1506(16)
Ni2–O1	2.122(3)	2.1210(18)	Ni3–O1	2.0942(15)	2.1188(16)
Ni2′–O1′			Ni4–O2	2.1265(16)	2.1172(17)
Ni2–O2	2.031(3)	2.0359(18)	Ni3–O3	2.0356(15)	2.0285(16)
Ni2′–O2′			Ni4–O4	2.0279(15)	2.0345(16)
Ni2–O2′	2.100(2)	2.0968(17)	Ni3–O4	2.1105(15)	2.1010(16)
Ni2′–O2			Ni4–O3	2.1135(15)	2.1179(16)
Ni1–N1	2.078(3)	2.097(2)	Ni1–N1	2.070(2)	2.059(2)
Ni1’–N1’			Ni2–N3	2.0563(19)	2.059(2)
Ni2–N2	2.031(3)	2.042(2)	Ni3–N2	2.0463(18)	2.028(2)
Ni2’–N2’			Ni4–N4	2.0391(19)	2.045(2)
Ni2–N3	2.088(3)	2.097(2)	Ni3–N5	2.0837(19)	2.086(2)
Ni2’–N3’			Ni4–N8	2.0913(19)	2.084(2)
Ni2–N4’	2.079(3)	2.095(2)	Ni3–N7	2.0870(18)	2.081(2)
Ni2’–N4			Ni4–N6	2.0932(19)	2.061(2)

Anionic disorder and hydrogen bonds in type 1 cubanes: Generally, the **type 1** cubane cations do not exhibit significant disorder, except for one acetate ligand of **1-3OAc-ClO$_3$** (C(46)H$_3$C(45)O(11)O(10)$^-$), which was positionally refined with partial occupancies of 0.592:0.408. This compound also displays anionic disorder, as well as its structural analogue **1-3OAc-PF$_6$**. ClO_3^- was refined into two moieties with relative occupancies of 0.778:0.222, while PF_6^- was described with a disorder model with two different F positions (F1-6A and F1-6B, 0.447:0.553) surrounding a P center.

The acetate ligands of all **type 1** cubanes are approximately parallel to their respective {Co-O-Co-O} faces, and the proximity of their carbonyl oxygen atoms to oxygen atoms of the neighboring dpy-C{OH}O- ligands lead to intramolecular hydrogen bonds (1.745-1.864 Å), which were crystallographically refined. In all representatives of the **1-3OAc** cubanes, such hydrogen bonds are not present between O9 of the aqua ligand and O5 of the dpy-C{OH}O- ligand located on the same polar face at a distance of approx. 3.9 Å. Instead, O5 and O9 bond through their hydrogen atoms to two ligands on the opposite polar face, namely O12 of acetate and O7 of dpy-C{OH}O$^-$. A relay of hydrogen bonds can be refined through O15, O7, O9, solvent water (O16 and 17), and counteranions (cf. CIF files 1891283-1891285), and this relay is even further extended for **1-2OAc-2BF$_4$**.

Anionic disorder and hydrogen bonds in type 2 edge-site cubanes: **2-Co$_x$Ni$_{4-x}$** edge-site cubanes were obtained with different counteranions (cf. Scheme 1) and display positional disorder of acetate ligands, such as respective occupancies of 0.184:0.816, 0.282:0.718, and 0.279:0.721 refined for **2-Co$_{1.92}$Ni$_{2.08}$-ClO$_4$**, **2-Co$_{2.32}$Ni$_{1.68}$-ClO$_3$**, and **2-Co$_{2.28}$Ni$_{1.72}$-BF$_4$**. The anions in **type 2** cubanes frequently exhibit positional disorder, which was refined for ClO_4^-, ClO_3^-, and BF_4^- of the above cubanes into two intact anion fractions with relative occupancies of 0.277:0.723, 0.466:0.534, and 0.373:0.627; respectively (see the CIF files 1891347-1891349). In **2-Co$_{1.64}$Ni$_{2.36}$-PF$_6$**, disorder in the PF_6^- counteranion is limited to the fluorine centers surrounding the same P, with refined occupancies for P1F$_6^-$ and P2F$_6^-$ of 0.420:0.580 for F3-6A and F3-6B and 0.443:0.557 for F7-12A and F7-12B, respectively. Other than in the **type 1** cubanes, the acetate ligands of all **type 2** cubanes are almost perpendicular to their respective {M-O-M-O} faces, giving rise to intramolecular hydrogen bonds (1.838-2.078 Å) between carbonyl oxygen atoms and aqua ligands coordinated to the same metal atom. A second type of intramolecular hydrogen bonds is formed between acetate oxygen atoms and dpy-C{OH}O$^-$ hydroxyl groups located on the opposite polar face (1.841-1.892 Å).

In addition to these intramolecular hydrogen bonds, **2-Co$_{2.32}$Ni$_{1.68}$-ClO$_3$** displays two different types of intermolecular hydrogen bonds between hydroxyl groups of dpy-C{OH}O$^-$ (located on the edge-site) and aqua ligands or disordered anions, respectively. Obviously, the edge-site dpy-C{OH}O$^-$ cannot participate in such hydrogen bonds with anions in the cases of **2-Co$_{1.92}$Ni$_{2.08}$-ClO$_4$** and **2-Co$_{2.28}$Ni$_{1.72}$-BF$_4$**. However, refinement after releasing the corresponding H U_{iso} points to a stable hydrogen -O3H position directed towards O9 of ClO_4^- and F3 of BF_4^-, respectively, indicating a less pronounced intermolecular interaction. While the distances between aqua ligands and PF_6^- in **2-Co$_{1.64}$Ni$_{2.36}$-PF$_6$** are rather long, hydrogen bonds were instead observed as O14-H14A (aqua ligand)···O5 (hydroxyl O of dpy-C{OH}O$^-$) as well as for a larger relay involving O12 (acetate carbonyl), O14, O5, and F4.

Anionic disorder and hydrogen bonds in 2-μ-OAc type 2 cubanes: Except for **2-μ-OAc-Co$_{1.54}$Ni$_{2.46}$-NO$_3$**, all other **2-μ-OAc-Co$_x$Ni$_{4-x}$** cubanes display positional anion disorder. In the case of **2-μ-OAc-Co$_{1.90}$Ni$_{2.10}$-ClO$_4$**, **2-μ-OAc-Co$_{1.52}$Ni$_{2.48}$-BF$_4$**, and **2-μ-OAc-Co$_{2.36}$Ni$_{1.64}$-PF$_6$**, the disordered O and F atoms are still centered around a single respective central atom. Occupancies of 0.235:0.765, 0.336:0.664, and 0.429:0.571 were refined for the disordered O and F sites on ClO_4^-, BF_4^-, and PF_6^-, respectively. As for **2-μ-OAc-Co$_{2.32}$Ni$_{1.68}$-ClO$_3$** and **2-μ-OAc-Co$_{2.34}$Ni$_{1.62}$-Cl**, both ClO_3^- and Cl^- can be refined into two disordered parts with occupancies of 0.122:0.878 and 0.308:0.692.

All **2-μ-OAc-Co$_x$Ni$_{4-x}$** cubane cations exhibit two types of intramolecular H bonds: the first (1.850-1.962 Å) occurs between carbonyl O10 and O12 of the acetate ligand and hydroxyl groups of O6 and O5 of dpy-C{OH}O$^-$. The second type (1.867- 1.926 Å) is located between O9 and 11 of acetate ligands and hydroxyl groups O8 and O7 of dpy-C{OH}O$^-$, respectively. A much more extended and stable hydrogen bonding network of acetate moieties, hydroxyl groups of dpy-C{OH}O$^-$, crystal water molecules, and anions exists around most of the **2-μ-OAc-Co$_x$Ni$_{4-x}$** cubanes in their solid state (see the CIF files).

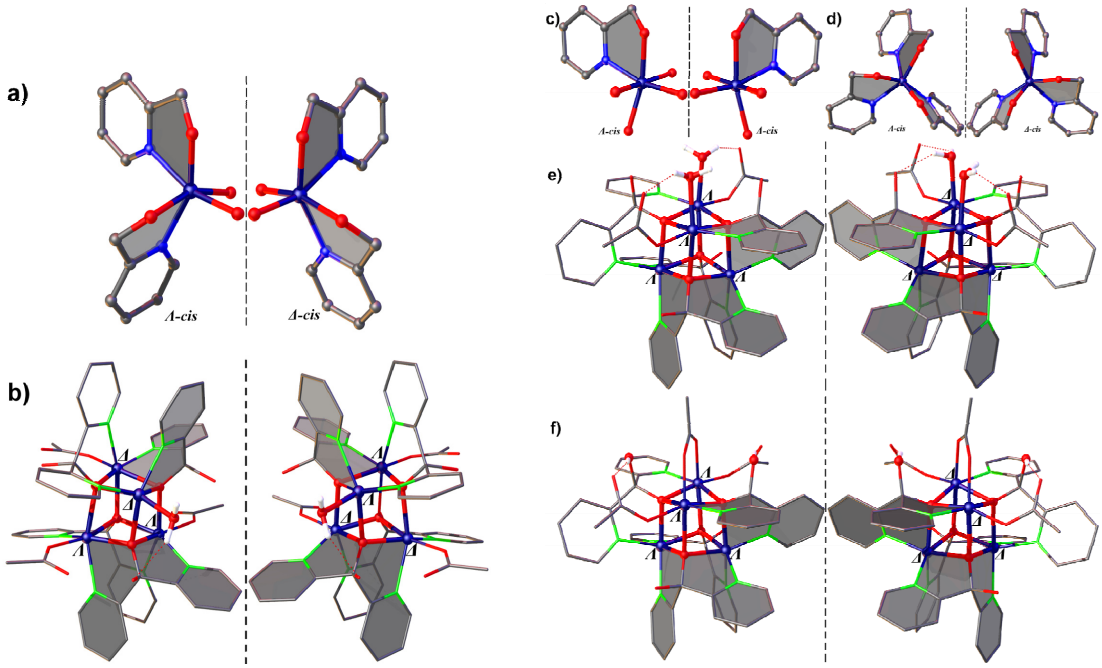

Figure S13. (**a**) Enantiomeric pair of the [Co(py-C{OH}O)$_2$O$_2$] building block (H atoms, acetyl, and hydroxyls are omitted) and (**b**) enantiomers of [Co$_4$(dpy{OH}O)$_4$(OAc)$_3$(H$_2$O)]$^+$. Enantiomeric pairs of the [M(py-C{OH}O)O$_4$] (**c**) and [M(py-C{OH}O)$_3$] (**d**) building blocks and enantiomers of [Co$_x$Ni$_{4-x}$(dpy-C{OH}O}$_4$(OAc)$_2$(H$_2$O)$_2$]$^{2+}$ (**e**) and [Co$_x$Ni$_{4-x}$(dpy-C{OH}O)$_4$(OAc)$_2$(μ-OAc)]$^+$ (**f**).

Stereochemistry of type 1 and type 2 cubanes: On the cations of **1-2OAc** and **1-3OAc**, a pair of enantiomeric moieties with defect propeller shapes bearing two five-membered rings {CoOCCN} as paddle faces displays clockwise and counterclockwise rotation that gives rise to the respective *Λ*- and *Δ*- configurations (Fig. S13). However, all **1-2OAc** and **1-3OAc** bulk compounds crystallize as racemates in the centrosymmetric space groups $P2_1/n$ and P-1, respectively. Also of note is that the $\bar{4}$ rotational axes within their cubane moieties render **1-4OAc** and **1-4Cl** meso-forms. Two pairs of enantiomeric moieties ([M(py-C{OH}O)O$_4$] and [M(py-C{OH}O)$_3$] (Fig. S13**c-d**) are present in **type 2** cubanes having the same configuration (Fig. S13 **e-f**), and molecular chirality arises from the exclusive presence of 2-fold rotational axes.

HR-ESI-MS analyses were performed on representative cubanes in order to investigate three main aspects: (1) integrity of the cubane core under ionization conditions, (2) observation of their fragmentation patterns and (3) the presence of heterometallic Co/Ni cubane cores.

Given that fragments of the $[M_4\{dpy\text{-}C(OH)O\}_4]$ building block representing intact cubane cores are present as the dominant ionized species in all of the **HR-ESI-MS** measurements, the cubanes indeed show high stability under ionizing conditions.

However, for bulk purity analyses, we refer to the according analytical strategies described on p. S34 below.

***HR-ESI-MS analyses of type 1 cubanes*:** The mass spectra of **1-4OAc**, **1-2OAc-2BF$_4$** and of all **1-3OAc** cubanes all have the most abundant mass signal *m/z* 579^{2+} in common (Figs. S14 and S15). It can be assigned to the $[Co_4(dpy\text{-}C\{OH\}O)_4(OAc)_2]^{2+}$ fragment (Fig. S17**a**), arising from dissociation of two acetate and two aqua ligands, or one aqua and one acetate ligand from **1-4OAc**, or the cations of **1-2OAc-2BF$_4$** and **1-3OAc**, respectively. A rather weak mass signal around *m/z* 1217^{+} often appears in the spectra of the above compounds, which can be assigned to the $[Co_4(dpy\text{-}C\{OH\}O)_4(OAc)_3]^{+}$ fragment (Fig. S19**a**). Furthermore, all according spectra display the $[Co_4(dpy\text{-}C\{OH\}O)_3(dpy\text{-}C\{O\}O)(OAc)]^{2+}$ (*m/z* 549^{2+}) fragment due to dissociation of a further acetate ligand from $[Co_4(dpy\text{-}C\{OH\}O)_4(OAc)_2]^{2+}$, together with loss of a –OH proton of one dpy-C{OH}O^{-} ligand, accounting for the 2+ charge (Fig. S18**a**). **1-Co$_x$Ni$_{4-x}$-3OAc** cubanes display analogous results, taking into account a slight shift of the above *m/z* values due to the presence of lighter Ni^{2+} centers in the mixed cores (Fig. S43-S45).

HR-ESI-MS analyses of 1-4Cl cubanes: The fragments $[Co_4(dpy\text{-}C\{OH\}O)_4(Cl)_2]^{2+}$ (*m/z* 555^{2+}) and $[Co_4(dpy\text{-}C\{OH\}O)_4(Cl)_3]^{+}$ (*m/z* 1145^{+}) were observed in the mass spectrum of **1-4Cl** as the most abundant species (Fig. S16), and its Co/Ni mixed analogues give rise to related results (Fig. S60).

HR-ESI-MS analyses of type 2 cubanes: The most pronounced fragment in the mass spectra of both **2-μ-OAc** and the edge-site cubanes is $[M_4(dpy\text{-}C\{OH\}O)_4(OAc)_2]^{2+}$ (*m/z* $578\text{-}579^{2+}$, Figs. S17**b** and S20-S23), arising from the loss of the bridging acetate ligand or two aqua ligands, respectively. The signal *m/z* $548\text{-}549^{2+}$ can be observed as well in the spectra of the **type 2** series, and a possible fragmentation is given in Fig. S18**b** for their Co analogue. Furthermore, fragments of weaker intensity with *m/z* $1215\text{-}1217^{+}$ were observed throughout all spectra of **type 2** cubanes, and they may arise from a $[M_4(dpy\text{-}C\{OH\}O)_4(OAc)_3]^{+}$ moiety with a bridging acetate coordinated to the M atoms in the edge-site position (Fig. S19**b**).

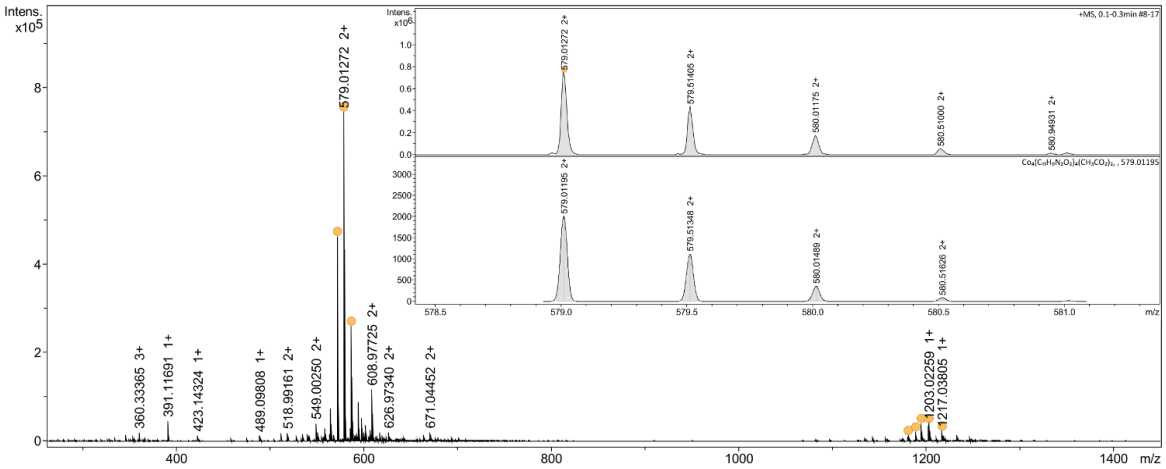

Figure S14. HR-ESI-MS spectrum of **1-4OAc** and the isotope patterns related to the fragmentation of $[Co_4(dpy\text{-}C\{OH\}O)_4(OAc)_2]^{2+}$.

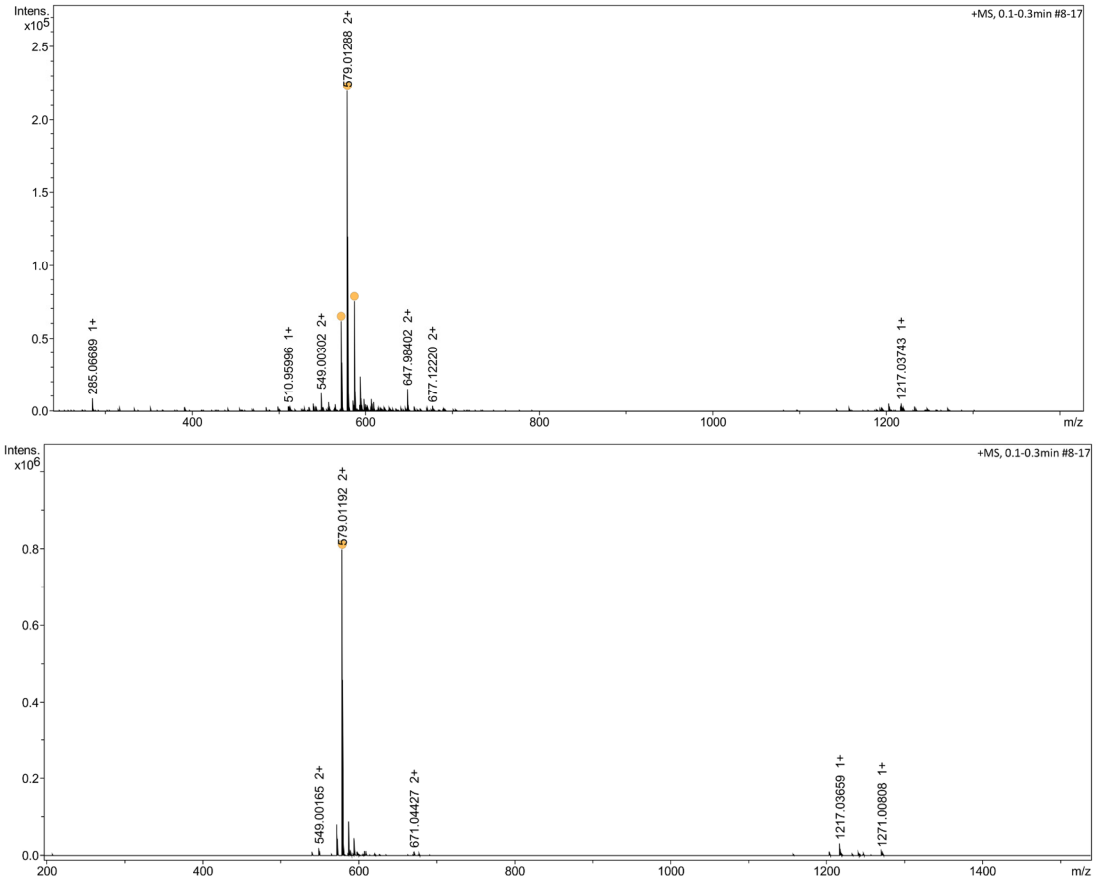

Figure S15. HR-ESI-MS spectrum of **1-2OAc-2BF$_4$** (top) and of **1-3OAc-ClO$_3$** (bottom).

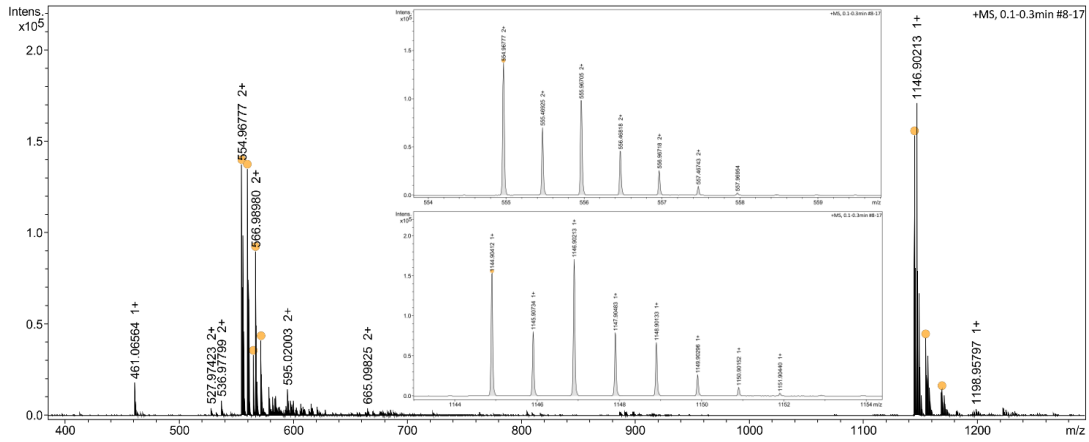

Figure S16. HR-ESI-MS spectrum of **1-4Cl** and the isotope patterns related to the fragmentations of $[Co_4(dpy\text{-}C\{OH\}O)_4(Cl)_2]^{2+}$ (*m/z* 555^{2+}) and $[Co_4(dpy\text{-}C\{OH\}O)_4(Cl)_3]^{+}$ (*m/z* 1145^{+}).

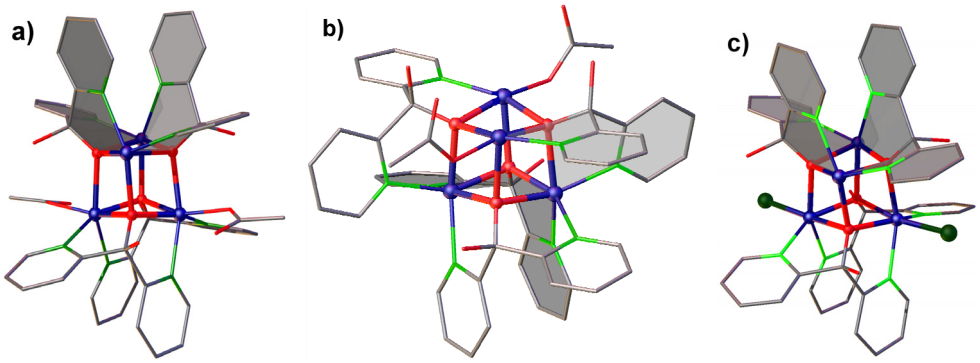

Figure S17. Possible structures of fragments $[M_4(dpy\text{-}C\{OH\}O)_4(OAc)_2]^{2+}$ (**type 1**, (**a**)), $[M_4(dpy\text{-}C\{OH\}O)_4(OAc)_2]^{2+}$ (**type 2**, (**b**)), and $[M_4(dpy\text{-}C\{OH\}O)_4(Cl)_2]^{2+}$ (**c**).

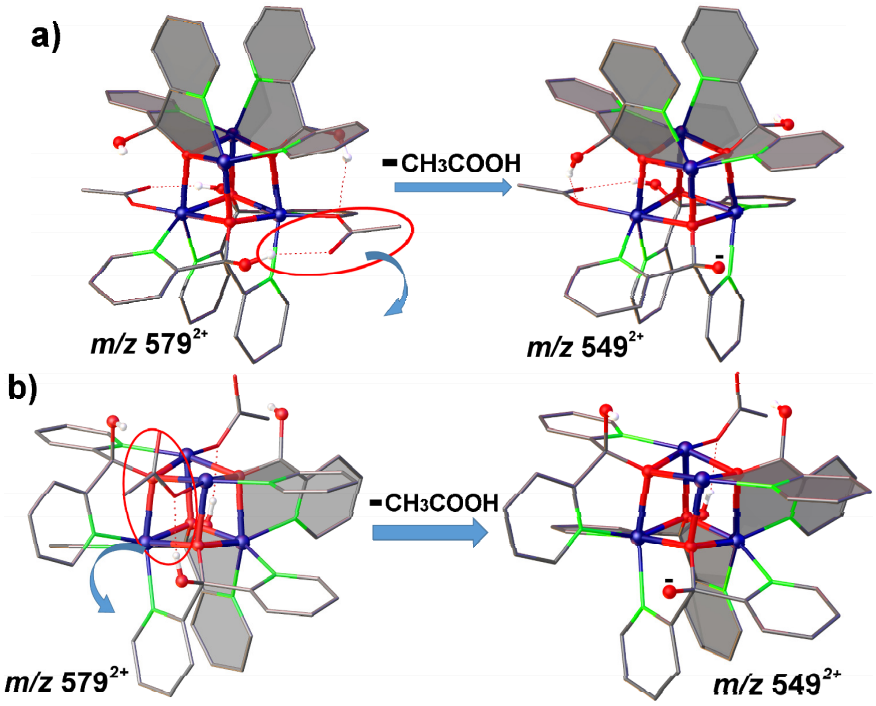

Figure S18. Possible formation routes of fragments with *m/z* 549^{2+} ($[Co_4(dpy\text{-}C\{OH\}O)_3(dpy\text{-}C\{OH\}O)(OAc)]^{2+}$) starting from the respective fragment *m/z* 579^{2+} ($[Co_4(dpy\text{-}C\{OH\}O)_4(OAc)_2]^{2+}$) during HR-ESI-MS.

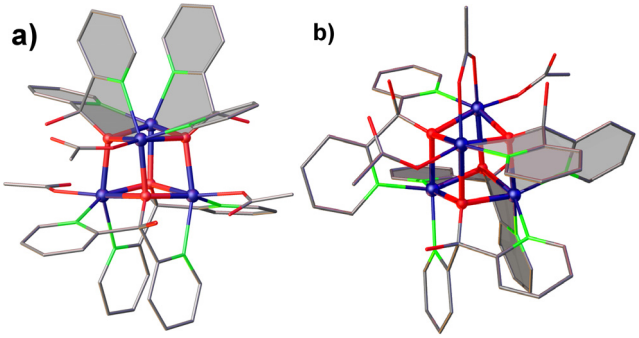

Figure S19. Possible structures of the fragments $[M_4(dpy\text{-}C\{OH\}O)_4(OAc)_3]^{+}$ of **type 1** (**a**) and **2** (**b**).

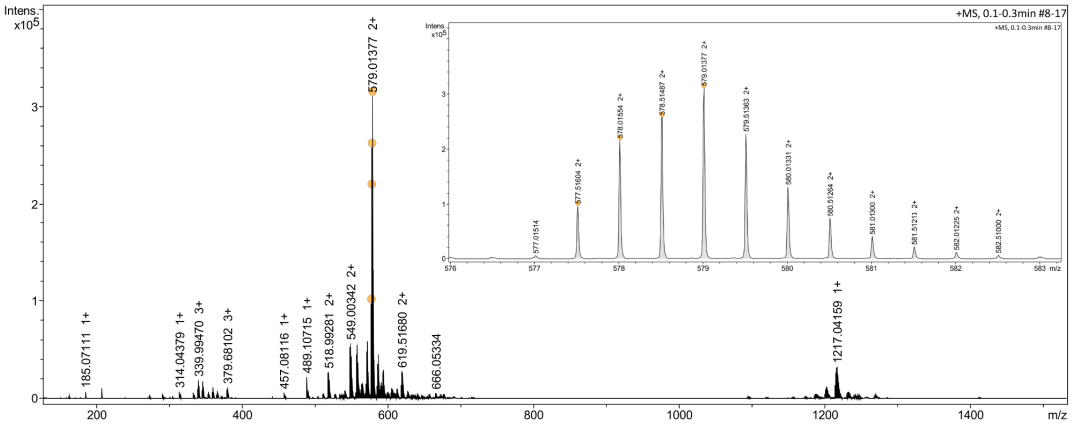

Figure S20. HR-ESI-MS spectrum of **2-Co$_{2.32}$Ni$_{1.68}$-ClO$_3$** and the isotope patterns related to the fragmentation of $[M_4(dpy\text{-}C\{OH\}O)_4(OAc)_2]^{2+}$.

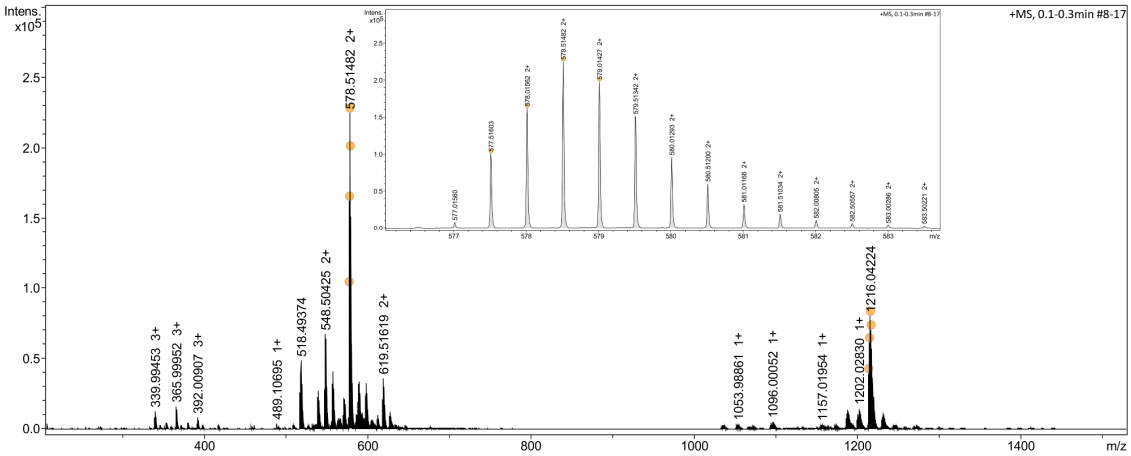

Figure S21. HR-ESI-MS spectrum of **2-μ-Co$_x$Ni$_{4-x}$-Cl** and the isotope patterns related to the fragmentation of $[M_4(dpy\text{-}C\{OH\}O)_4(OAc)_2]^{2+}$.

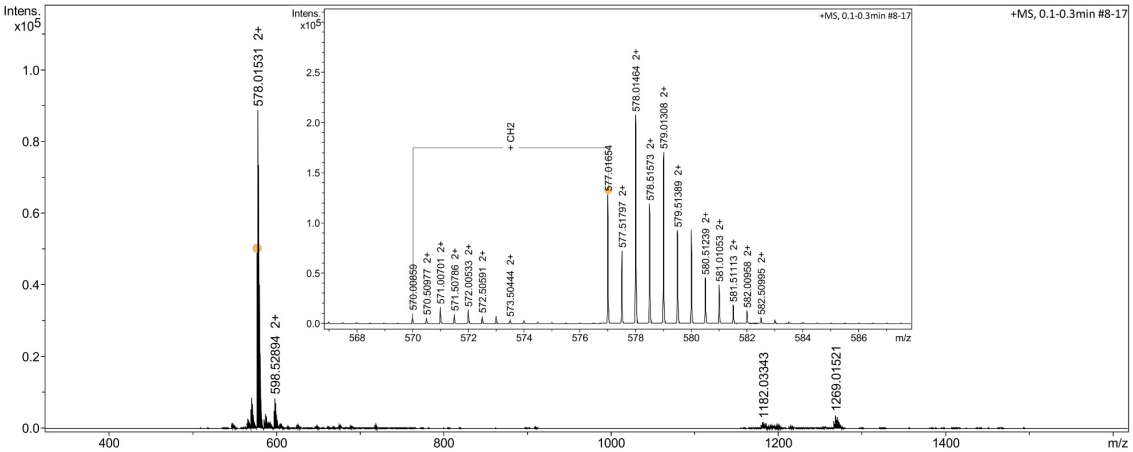

Figure S22. HR-ESI-MS spectrum of **2-Ni$_4$-ClO$_4$** and the isotope patterns related to the fragmentation of $[Ni_4(dpy\text{-}C\{OH\}O)_4(OAc)_2]^{2+}$.

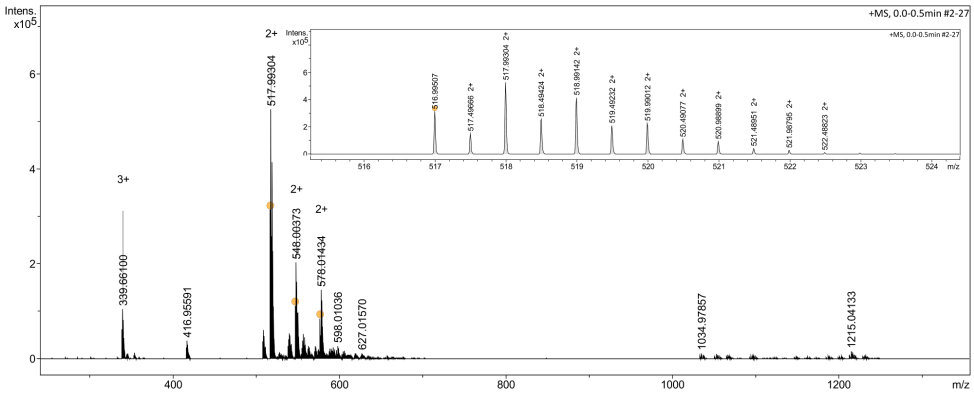

Figure S23. HR-ESI-MS spectrum of **2-μ-OAc-Ni$_4$-BF$_4$** and the isotope patterns related to the fragmentation of $[Ni_4(dpy\text{-}C\{OH\}O)_4(OAc)_2]^{2+}$.

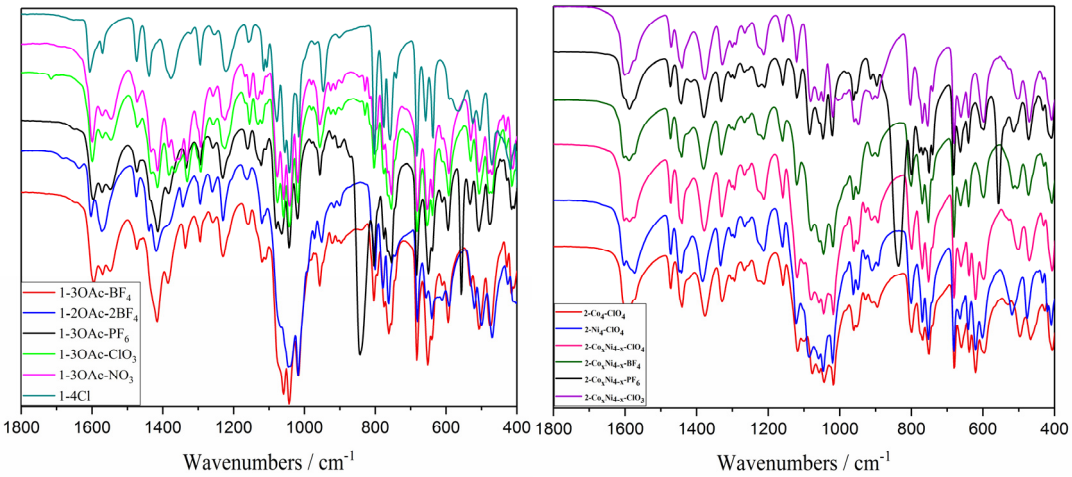

Figure S24. FT-IR spectra of **type 1** (left) and **type 2** (right) cubanes.

Bulk analytical strategies for type 1 and type 2 cubanes

First, representative examples for detailed **type 1** and **2** cubane characterizations with ^{1}H NMR spectroscopy are given. Next, three complementary and tailored analytical protocols are discussed to address special challenges associated with different cubane sample types.

***^{1}H NMR spectroscopic characterizations of cobalt cubanes*:** ^{1}H NMR spectra and T_1 relaxation times of each ^{1}H signal were recorded for the **1-4OAc**, **1-2OAc-2BF$_4$**, and **1-3OAc** series, and the ^{1}H signals were then assigned through the proportional relation between the respective ^{1}H−Co distance and T_1. As observed in previous studies on **2-Co$_4$-ClO$_4$**,[5] the ortho-H signals of all **type 1** cubanes appear in the highest investigated chemical shift range (100-320 ppm, Figs. 4, S25, and S26). The H atoms in meta- and para-positions are located within lower chemical shift ranges of 13-75 ppm and -12-24 ppm, respectively. The ^{1}H NMR spectra of **1-4OAc**, **1-2OAc-2BF$_4$**, and **1-3OAc** reflect the respective expected cubane symmetry in solution in contrast to the observed space group, such as a $\bar{4}$ axis in **1-4OAc** (cf. triclinic solid state symmetry in Table S1). Indeed, a set of 2 ortho-H, 4 meta-H, 2 para-H, 1 ^{1}HO-, and 1 $^1H_3COO^-$ signals was observed (Fig. S25), indicating that all Co centers of **1-4OAc** display the same coordination environment. **1-2OAc-2BF$_4$** can be structurally derived from **1-4OAc** through replacing 2 acetates by 2 aqua ligands at the same polar side, giving rise to two different types of cobalt coordination. This was verified through the presence of a set of 4 ortho-H, 8 meta-H, 4 para-H, 2 ^{1}HO- and 2 $^1H_3COO^-$ signals (Fig. 4). In the case of **1-3OAc**, a four- and twofold number of signals compared

to **1-4OAc** and **1-2OAc-2BF$_4$**, respectively, appear in the respective chemical shift range. Together with a stronger paramagnetic character, signal overlaps for **1-3OAc** are thus far more likely. In this context, the 8 ortho-H, 14 meta-H, 6 para-H, 4 ^{1}HO-, and 3 ^{1}H$_3$COO-signals observed for **1-3OAc** still reasonably reflect its structure in solution (Fig. S26), despite the absence of 2 meta-H and 2 para-H signals.

***^{1}H NMR spectroscopic characterizations of nickel-containing cubanes*:** Protons could neither be assigned in the recorded ^{1}H NMR spectra of **2-Ni$_4$-ClO$_4$** (Fig. S41), nor for the entire Co/Ni mixed cubane series (Fig. S42). Given that the **2-Co$_4$**, **2-Co$_x$Ni$_{4-x}$**, and **2-Ni$_4$** cubane types display only minor structural differences (Table S10), the stark contrast in the quality of the respective spectroscopic data is most likely due to the different magnetic properties of the Ni centers.

Analytical protocol 1 (**1-2OAc-2BF$_4$** as an example): First, bulk purity of the crystalline fraction of **1-2OAc-2BF$_4$** is evident from the very good correspondence of PXRD data with the calculated powder pattern (Fig. S44**b**). Next, the purity of potential non-crystalline product fractions was checked with ^{1}H NMR measurements. The exclusive presence of signals clearly assigned to **1-2OAc-2BF$_4$** showed that no side products were present in solution either (Fig. 4). Third, the agreement of elemental analysis results with calculated data (cf. SI) ruled out the formation of significant amounts of cobalt oxides. This three-step approach was applied to confirm the purity of **2-Co$_4$-ClO$_4$**, **1-4OAc**, **1-4Cl**, and of all **1-Co$_4$-3OAc** cubanes.

Analytical protocol 2 (**2-Co$_{2.32}$Ni$_{1.68}$-ClO$_3$** as an example): While comparison of experimental and calculated PXRD patterns demonstrated phase purity of the crystalline main fraction (Fig. S45**b**), the strongly paramagnetic Ni centers hampered the ^{1}H NMR analysis of possible amorphous fractions in the case of **2-Co$_{2.32}$Ni$_{1.68}$-ClO$_3$**. Therefore, the obtained large single crystals of **2-Co$_{2.32}$Ni$_{1.68}$-ClO$_3$** (Fig. S46) were used as a reference for Raman spectroscopy, and their good correspondence with bulk spectra clearly indicated bulk purity (Fig. S47). The Raman detection limit was estimated from reference spectra of pure **2-Co$_{2.32}$Ni$_{1.68}$-ClO$_3$** spiked with increasing amounts of **1-3OAc-ClO$_3$** representing possible **type 1** impurities. Even though the Raman spectra of pure **1-3OAc-ClO$_3$** and **2-Co$_{2.32}$Ni$_{1.68}$-ClO$_3$** are very closely related, they can still be clearly distinguished through a Raman signal shift 298 cm^{-1} that is observed for **1-3OAc-ClO$_3$**, but is absent in **2-Co$_{2.32}$Ni$_{1.68}$-ClO$_3$** (Fig. S48). As the lowest detection limit for this characteristic peak is 2% **1-3OAc-ClO$_3$** within a **2-Co$_{2.32}$Ni$_{1.68}$-ClO$_3$** sample (Fig. S48), we conclude that as-synthesized bulk **2-Co$_{2.32}$Ni$_{1.68}$-ClO$_3$** is > 98 % pure. Purity of all **1-Co$_x$Ni$_{4-x}$** and **2-Co$_x$Ni$_{4-x}$** compounds was assessed with this second protocol.

Analytical protocol 3 (explained for **2-μ-OAc-Co$_x$Ni$_{4-x}$-ClO$_4$**): Given that **2-μ-OAc-Co$_x$Ni$_{4-x}$** and **2-μ-OAc-Ni$_4$** cubanes display pronounced crystal weathering upon exposure to air, PXRD purity checks were not applicable. Nevertheless, large crystals were available as standards for Raman spectroscopy checks with min. 98 % accuracy (protocol 2, cf. also Fig. S48), where spectra of bulk **2-μ-OAc-Co$_x$Ni$_{4-x}$-ClO$_4$** were found to be identical with the single-crystal standard (Fig. S49). Furthermore, the absence of the characteristic Raman shifts at 136 cm^{-1} and 345 cm^{-1} in bulk **2-μ-OAc-Co$_x$Ni$_{4-x}$-ClO$_4$** compared to its edge-site analogue **2-Co$_x$Ni$_{4-x}$-ClO$_4$** and at 297 cm^{-1} compared to its **type 1** analogue **1-Co$_4$-3OAc-ClO$_4$** (Fig. S50) confirms high purity. Protocol 3 was applied to control the phase purity of all **2-μ-OAc-Co$_x$Ni$_{4-x}$** and **2-μ-OAc-Ni$_4$** cubanes.

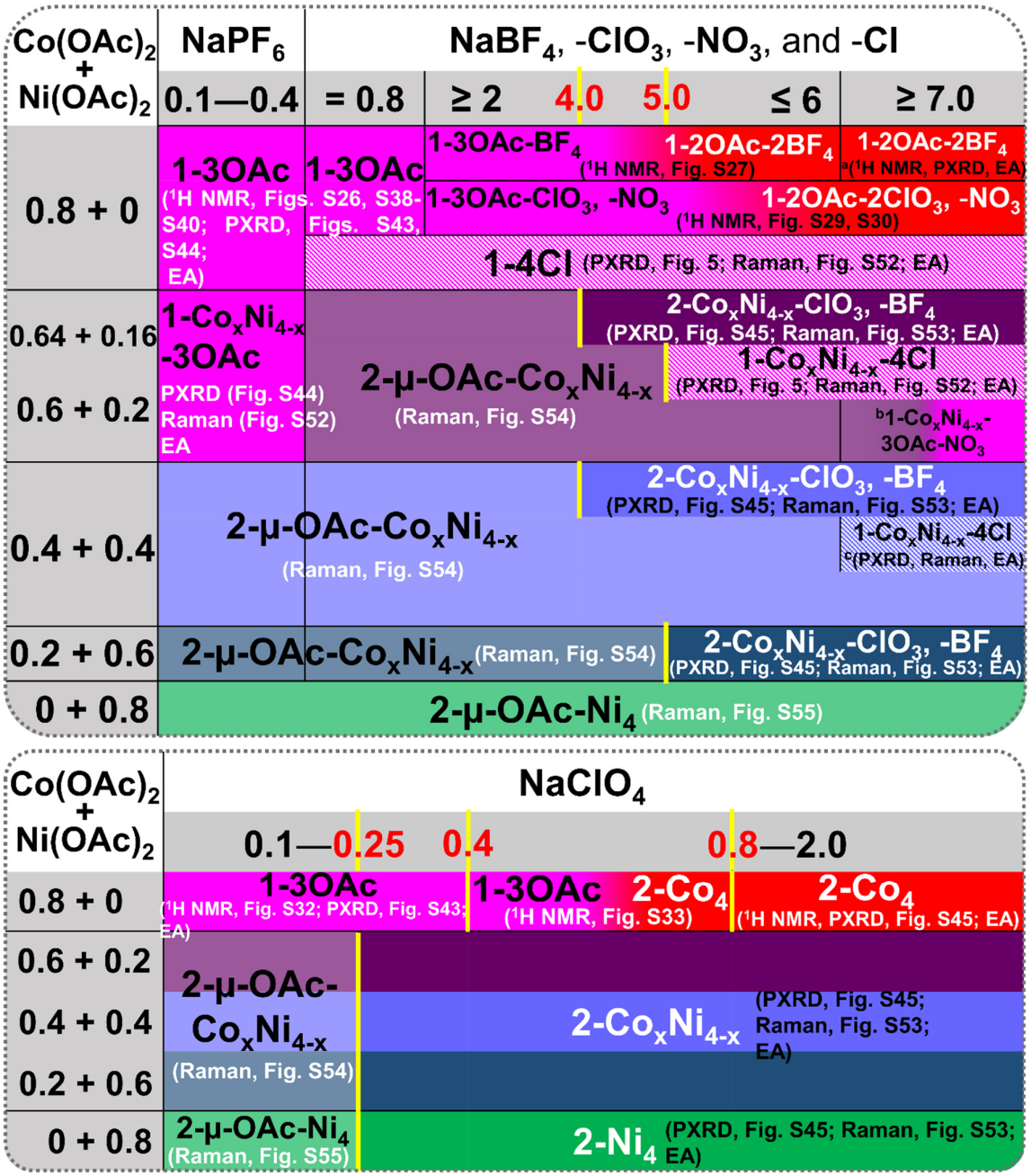

Scheme S1. Counteranion-directed access to $\{Co_4O_4\}$, $\{Co_xNi_{4-x}O_4\}$, and $\{Co_4O_4\}$ cubanes as outlined in Scheme 1 in the main text and the corresponding bulk analyses. [a]cf. Figs. 4 and S44**a**. [b]Coexistence of crystals of **type 1** and **2** cubanes has been observed microscopically under polarized light and was further structurally confirmed by single-crystal X-ray diffraction. [c]cf. Figs. 5 and S52.

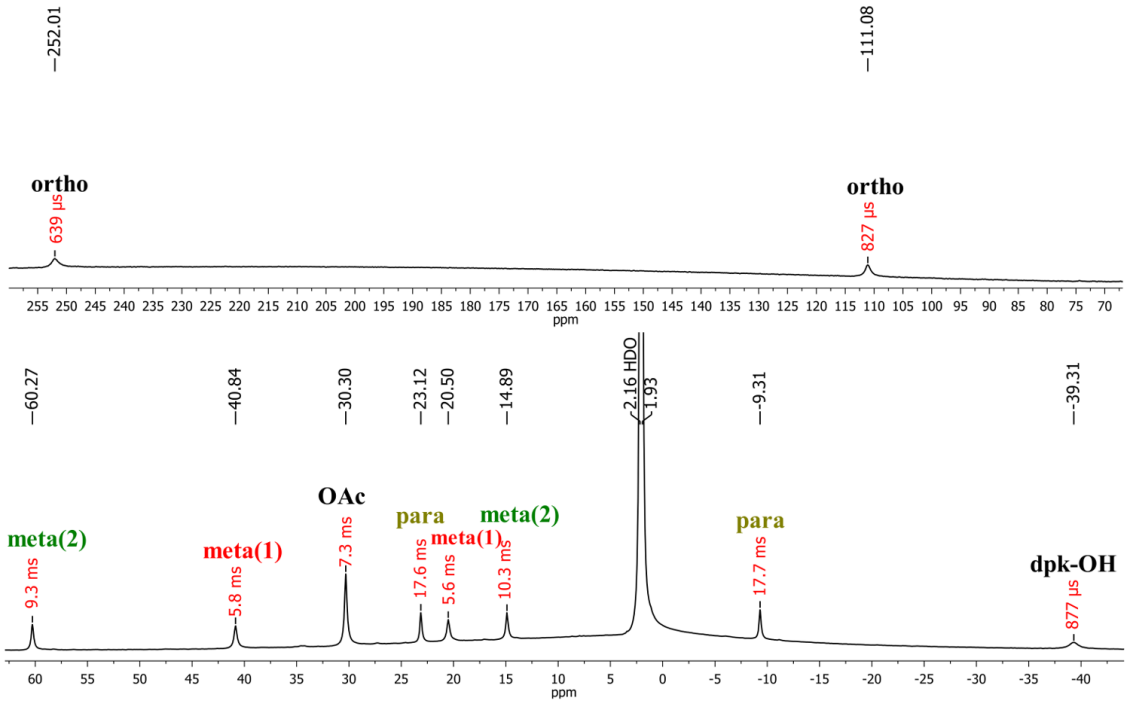

Figure S25. ^{1}H NMR spectrum of **1-4OAc**.

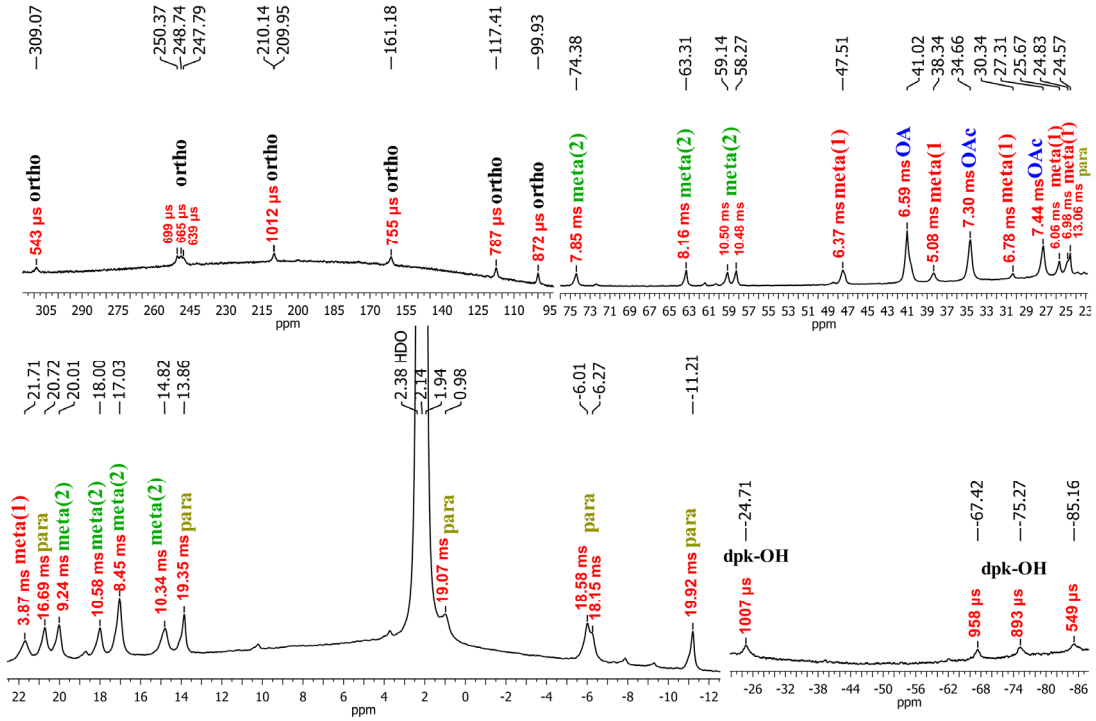

Figure S26. ^{1}H NMR spectrum of **1-3OAc-BF$_4$**.

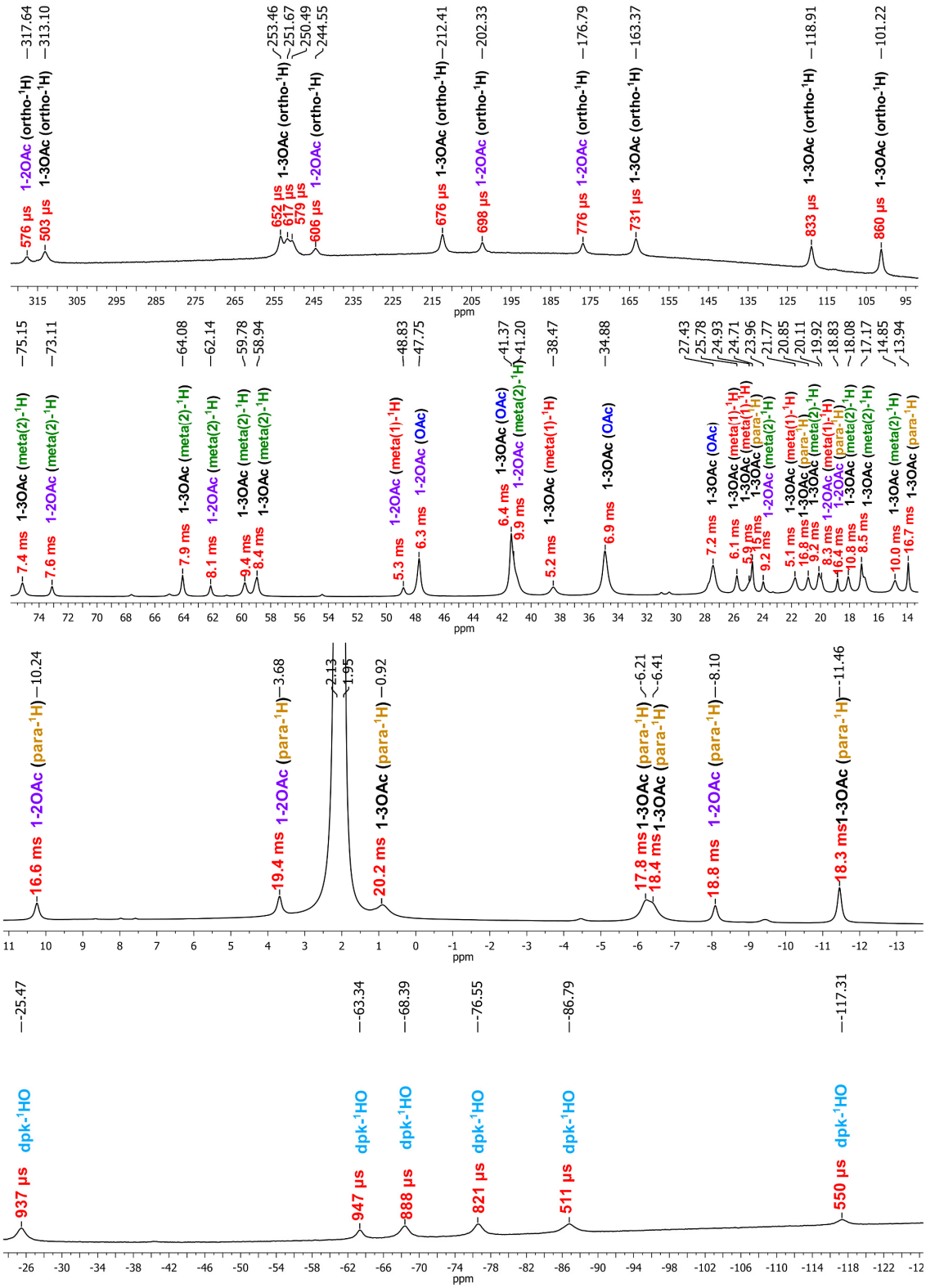

Figure S27. ^{1}H NMR spectrum of the as-synthesized mixture of **1-3OAc-BF$_4$** and **1-2OAc-2BF$_4$**.

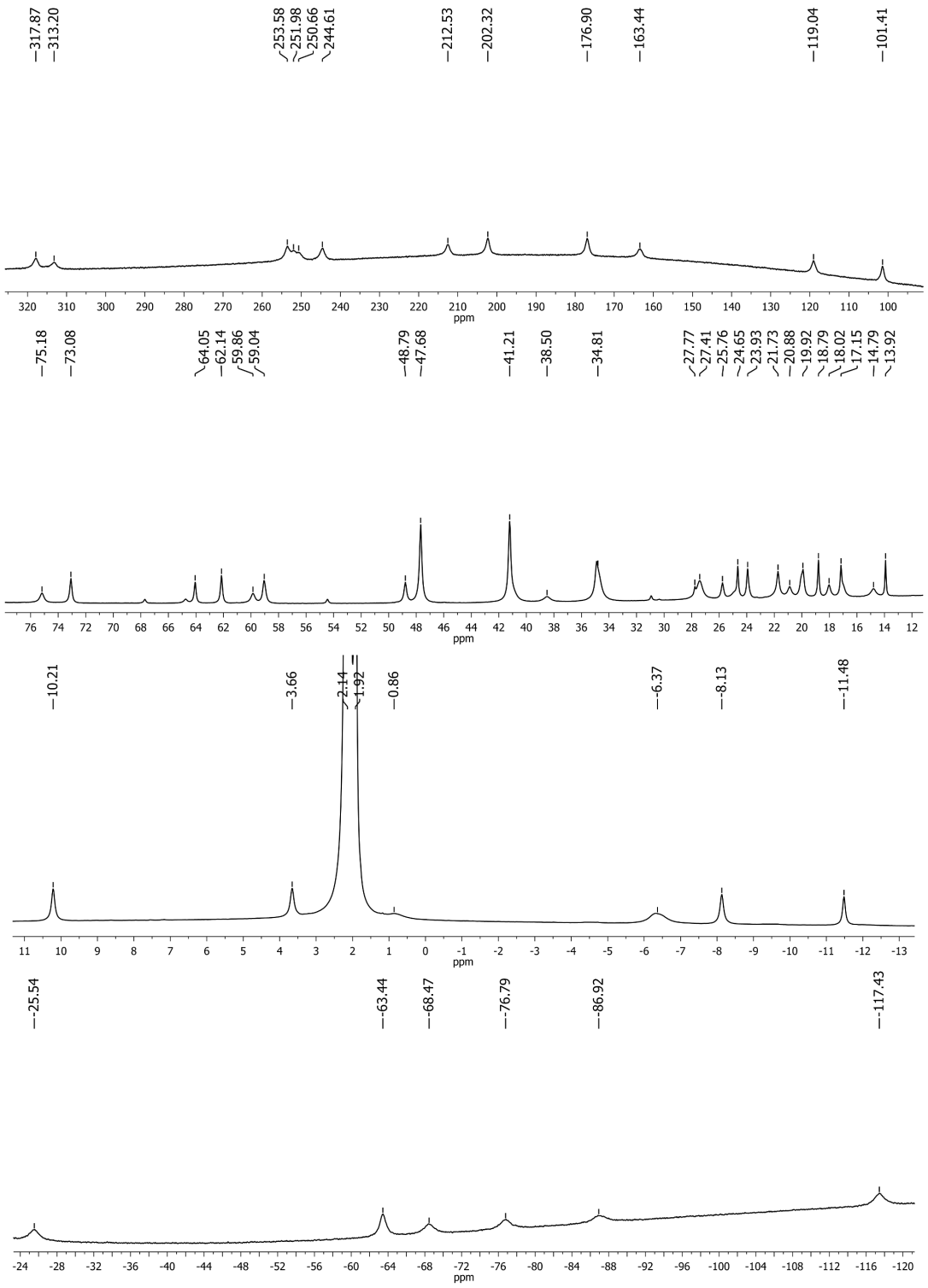

Figure S28. ^{1}H NMR spectrum of a mixture of pure **1-3OAc-BF$_4$** and **1-2OAc-2BF$_4$** (3:2). The chemical shift assignments are listed in Table S15.

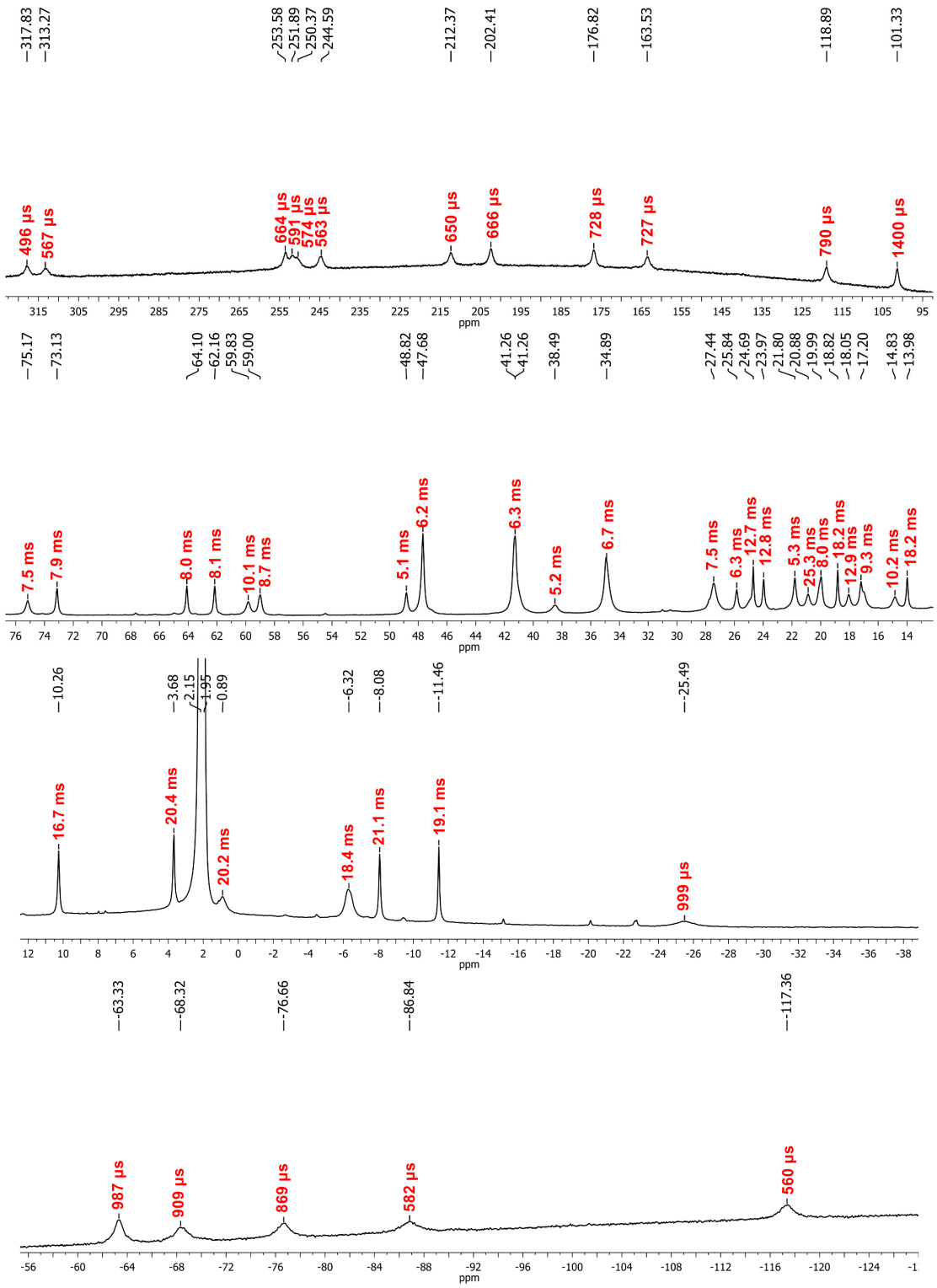

Figure S29. ^{1}H NMR spectrum of the as-synthesized mixture of **1-3OAc-NO$_3$** and **1-2OAc-2NO$_3$**. The chemical shift assignments are listed in Table S15.

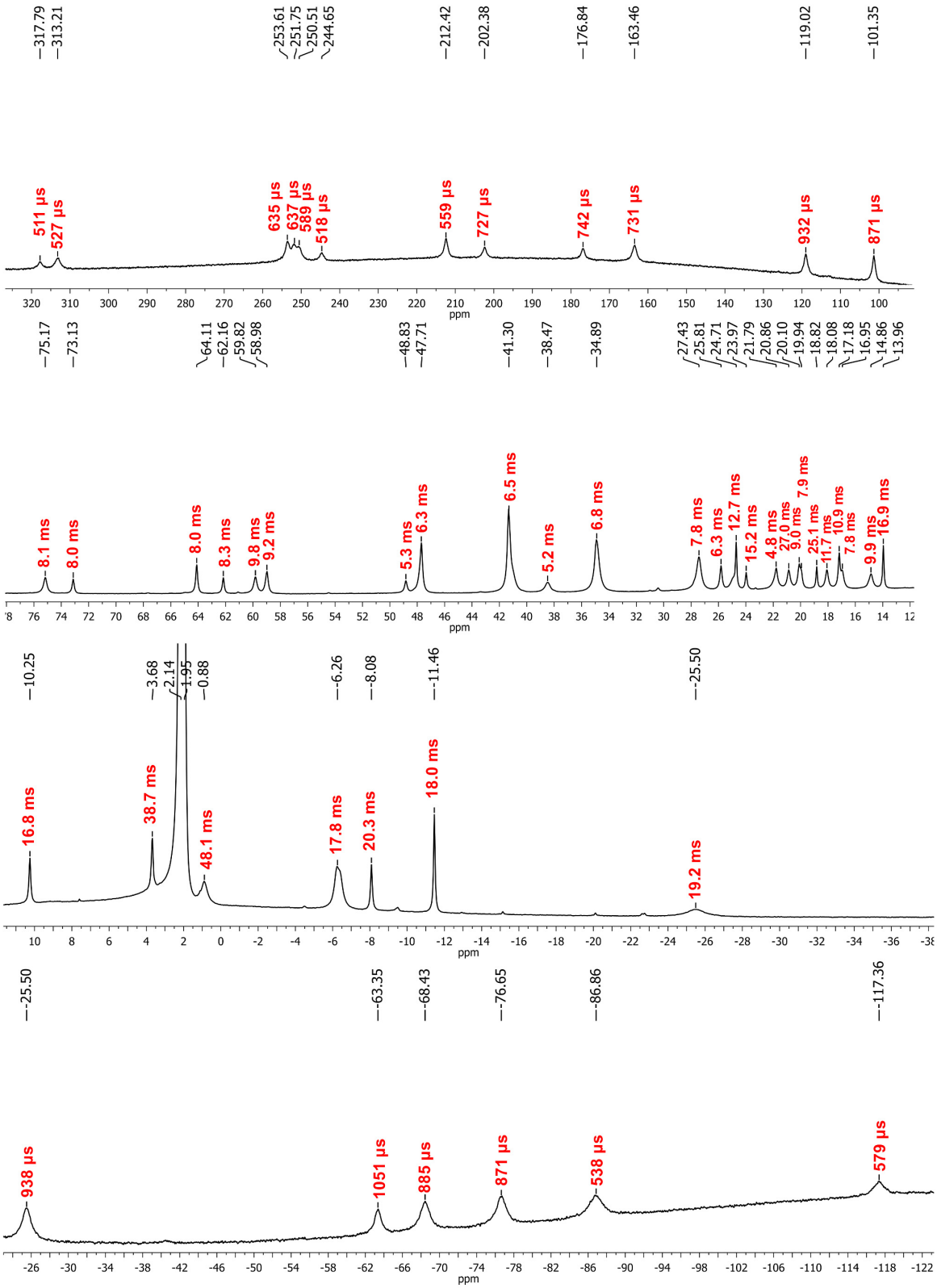

Figure S30. ^{1}H NMR spectrum of the as-synthesized mixture of **1-3OAc-ClO$_3$** and **1-2OAc-2ClO$_3$**. The chemical shift assignments are listed in Table S15.

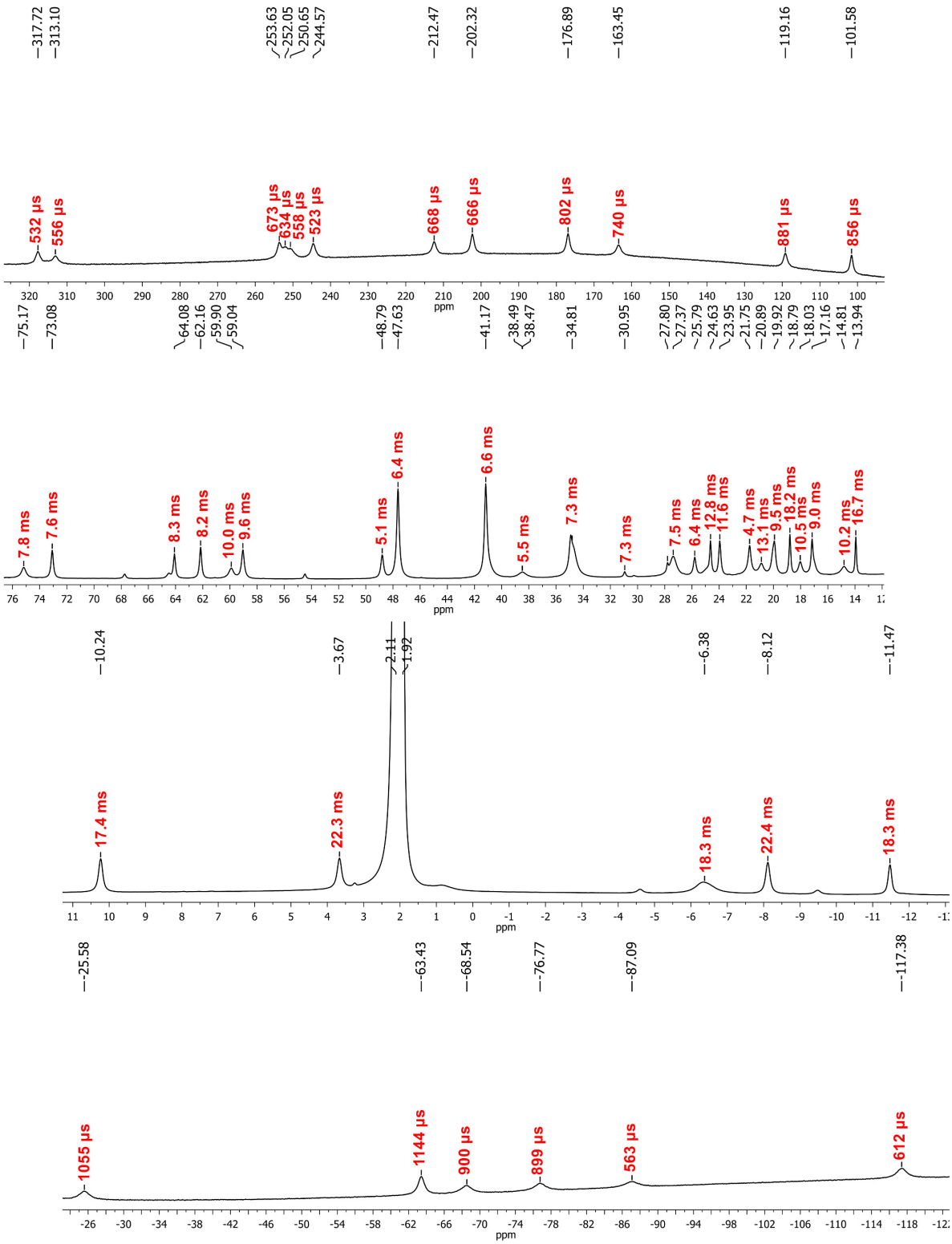

Figure S31. ^{1}H NMR spectrum of the as-synthesized mixture of **1-3OAc-PF$_6$** and **1-2OAc-2PF$_6$** upon addition of > 0.4 mmol $NaPF_6$. (cf. analogous assignments in Table S15).

Table S15. ^{1}H NMR chemical shift assignments for Figures S26-S30.

^{1}H	Pure **1-3OAc-BF$_4$** (Fig. S26)	Pure **1-2OAc-2BF$_4$** (Fig. 4)	BF$_4^-$ counteranion (Fig. S27)	NO$_3^-$ counteranion (Fig. S29)	ClO$_3^-$ counteranion (Fig. S30)	**1-3OAc-BF$_4$: 1-2OAc-2BF$_4$ 3:2** (Fig. S28)
Ortho-		**317.78** (542 µs)	**317.64** (576 µs)	**317.83** (496 µs)	**317.79** (511 µs)	**317.85**
	309.07 (534 µs)		[a]**313.10** (503 µs)	**313.27** (567 µs)	**313.21** (527 µs)	**313.18**
	250.37 (699 µs)		**253.46** (652 µs)	**253.58** (664 µs)	**253.61** (635 µs)	**253.56**
	248.74 (665 µs)		**251.67** (617 µs)	**251.89** (591 µs)	**251.75** (637 µs)	**252.05**
	247.79 (639 µs)		**250.49** (579 µs)	**250.37** (574 µs)	**250.51** (589 µs)	**250.59**
		244.54 (538 µs)	**244.55** (606 µs)	**244.59** (563 µs)	**244.65** (518 µs)	**244.55**
	210.14 (1012 µs)		**212.41** (676 µs)	**212.37** (650 µs)	**212.42** (559 µs)	**212.48**
		202.29 (710 µs)	**202.33** (698 µs)	**202.41** (666 µs)	**202.38** (727 µs)	**202.32**
		176.79 (715 µs)	**176.79** (776 µs)	**176.82** (728 µs)	**176.84** (742 µs)	**176.91**
	161.18 (755 µs)		**163.37** (731 µs)	**163.53** (727 µs)	**163.46** (731 µs)	**163.37**
	117.41 (787 µs)		**118.91** (833 µs)	**118.89** (790 µs)	**119.02** (932 µs)	**119.09**
	99.93 (872 µs)		**101.22** (860 µs)	**101.33** (1400 µs)	**101.35** (871 µs)	**101.40**
Meta-	**74.38** (7.8 ms)		**75.15** (7.4 ms)	**75.17** (7.8 ms)	**75.17** (8.1 ms)	**75.17**
		73.08 (7.6 ms)	**73.11** (7.6 ms)	**73.13** (7.9 ms)	**73.13** (8.0 ms)	**73.07**
	63.31 (8.2 ms)		**64.08** (7.9 ms)	**64.10** (8.0 ms)	**64.11** (8.0 ms)	**64.05**
		62.13 (8.1 ms)	**62.14** (8.1 ms)	**62.16** (8.1 ms)	**62.16** (8.3 ms)	**62.14**
	59.14 (10.5 ms)		**59.78** (9.4 ms)	**59.83** (10.1 ms)	**59.82** (9.8 ms)	**59.85**
	58.27 (10.5 ms)		**58.94** (8.4 ms)	**59.00** (8.7 ms)	**58.98** (9.2 ms)	**59.04**
Meta-		**48.80** (5.3 ms)	**48.83** (5.3 ms)	**48.82** (5.1 ms)	**48.83** (5.3 ms)	**48.78**
OAc-		**47.71** (6.4 ms)	**47.75** (6.4 ms)	**47.68** (6.2 ms)	**47.71** (6.3 ms)	**47.67**
Meta-	**47.51** (6.4 ms)		[b]**OL with** [c]**47.75**	**OL with 47.68**	**OL with 47.71**	**OL with 47.67**
Meta-		**41.19** (10.0 ms)	**41.20** (9.9 ms)	**OL with 41.26**	**OL with 41.30**	**OL with 41.21**

Continued on the next page

^{1}H	Pure **1-3OAc-BF$_4$** (Fig. S26)	Pure **1-2OAc-2BF$_4$** (Fig. 4)	BF$_4^-$ counteranion (Fig. S27)	NO$_3^-$ counteranion (Fig. S29)	ClO$_3^-$ counteranion (Fig. S30)	**1-3OAc-BF$_4$: 1-2OAc-2BF$_4$ 3:2** (Fig. S28)
OAc-	**41.02** (6.6 ms)		**41.37** (9.9 ms)	**41.26** (6.3 ms)	**41.30** (6.5 ms)	**41.21**
Meta-	**38.34** (5.1 ms)		**38.47** (5.5 ms)	**38.49** (5.2 ms)	**38.47** (5.2 ms)	**38.48**
		34.92 (6.3 ms)	**OL with 38.47**	**OL with 38.49**	**OL with 38.47**	**OL with 38.48**
OAc-	**34.66** (7.3 ms)		**34.88** (6.9 ms)	**34.89** (6.7 ms)	**34.89** (6.8 ms)	**34.89**
Meta-	**30.34** (6.8 ms)		**Missing**	**Missing**	**Missing**	**Missing**
OAc-	**27.31** (7.4 ms)		**27.43** (7.4 ms)	**27.44** (7.5 ms)	**27.43** (7.8 ms)	**27.41**
Meta-	**25.67** (6.1 ms)		**25.78** (5.5 ms)	**25.84** (6.3 ms)	**25.81** (6.3 ms)	**25.76**
	24.83 (7.0 ms)		**24.93** (5.9 ms)	**OL with 24.69**	**OL with 24.71**	**OL with 24.56**
Para-	**24.57** (13.1 ms)		**24.71** (13.9 ms)	**24.69** (12.7 ms)	**24.71** (12.7 ms)	**24.65**
Meta-		**23.94** (10.7 ms)	**23.96** (9.4 ms)	**23.97** (12.8 ms)	**23.97** (15.2 ms)	**23.93**
Meta-		**21.73** (6.6 ms)	**21.77** (5.1 ms)	**21.89** (5.3 ms)	**21.79** (4.8 ms)	**21.72**
	21.71 (3.9 ms)		**OL with 21.77**	**OL with 21.89**	**OL with 21.79**	**OL with 21.72**
Para-	**20.72** (16.7 ms)		**20.85** (16.8 ms)	**20.88** (25.3 ms)	**20.86** (27.0 ms)	**20.88**
Meta-	**20.01** (9.2 ms)		**20.11** (9.2 ms)	**OL with 19.99**	**20.10** (9.0 ms)	**OL with 19.91**
Meta-		**19.91** (6.7 ms)	**19.92** (8.3 ms)	**19.99** (8.0 ms)	**19.94** (7.9 ms)	**19.91**
Para-		**18.81** (15.3 ms)	**18.83** (16.4 ms)	**18.82** (18.2 ms)	**18.82** (25.1 ms)	**18.79**
Meta-	**18.00** (10.6 ms)		**18.08** (10.8 ms)	**18.05** (12.9 ms)	**18.08** (11.7 ms)	**18.02**
	17.03 (8.4 ms)		**17.17** (8.5 ms)	**17.20** (9.3 ms)	**17.18** (10.9 ms)	**17.15**
	14.82 (10.3 ms)		**14.85** (10.0 ms)	**14.83** (10.2 ms)	**14.86** (9.9 ms)	**14.79**
Para-	**13.86** (19.4 ms)		**13.94** (16.7 ms)	**13.98** (18.2 ms)	**13.96** (16.9 ms)	**13.91**
		10.22 (16.7 ms)	**10.24** (16.6 ms)	**10.25** (16.7 ms)	**10.25** (16.8 ms)	**10.21**
		3.67 (18.3 ms)	**3.68** (19.4 ms)	**3.68** (20.4 ms)	**3.68** (38.7 ms)	**3.65**
	0.98 (19.1 ms)		**0.92** (20.2 ms)	**0.89** (20.2 ms)	**0.88** (48.1 ms)	**0.86**

Continued on the next page

^{1}H	Pure **1-3OAc-BF$_4$** (Fig. S26)	Pure **1-2OAc-2BF$_4$** (Fig. 4)	BF$_4^-$ counteranion (Fig. S27)	NO$_3^-$ counteranion (Fig. S29)	ClO$_3^-$ counteranion (Fig. S30)	**1-3OAc-BF$_4$: 1-2OAc-2BF$_4$ 3:2** (Fig. S28)
Para-	**-6.01** (18.6 ms)		**-6.21** (17.8 ms)	**-6.32** (18.4 ms)	**-6.26** (17.8 ms)	**-6.32**
	-6.27 (18.2 ms)		**-6.41** (18.4 ms)	**OL with -6.32**	**OL with -6.26**	**OL with -6.32**
		-8.11 (18.6 ms)	**-8.10** (18.8 ms)	**-8.08** (21.1 ms)	**-8.08** (20.3 ms)	**-8.13**
	-11.21 (19.9 ms)		**-11.46** (18.3 ms)	**-11.46** (19.1 ms)	**-11.46** (18.0 ms)	**-11.49**
HO-	**-24.71** (1107 µs)		**-25.47** (937 µs)	**-25.49** (999 µs)	**-25.50** (938 µs)	**-25.56**
		-63.37 (970 µs)	**-63.34** (947 µs)	**-63.33** (987 µs)	**-63.35** (1051 µs)	**-63.64**
	-67.42 (985 µs)		**-68.39** (905 µs)	**-68.32** (909 µs)	**-68.43** (885 µs)	**-68.41**
	-75.27 (893 µs)		**-76.55** (888 µs)	**-76.66** (869 µs)	**-76.65** (871 µs)	**-76.84**
	-85.16 (549 µs)		**-86.79** (511 µs)	**-86.84** (582 µs)	**-86.86** (538 µs)	**-86.85**
		-117.38 (582 µs)	**-117.31** (550 µs)	**-117.36** (560 µs)	**-117.36** (579 µs)	**-117.47**

[a]Larger chemical shift differences between the pure **1-3OAc** and those of **1-3OAc** containing **1-2OAc** are attributed to the strong paramagnetic influence of **1-2OAc**. [b]OL = overlapped. [c]Assignments of overlapped shifts were made on the basis of the more dominant component and the T_1 times related to the corresponding pure component.

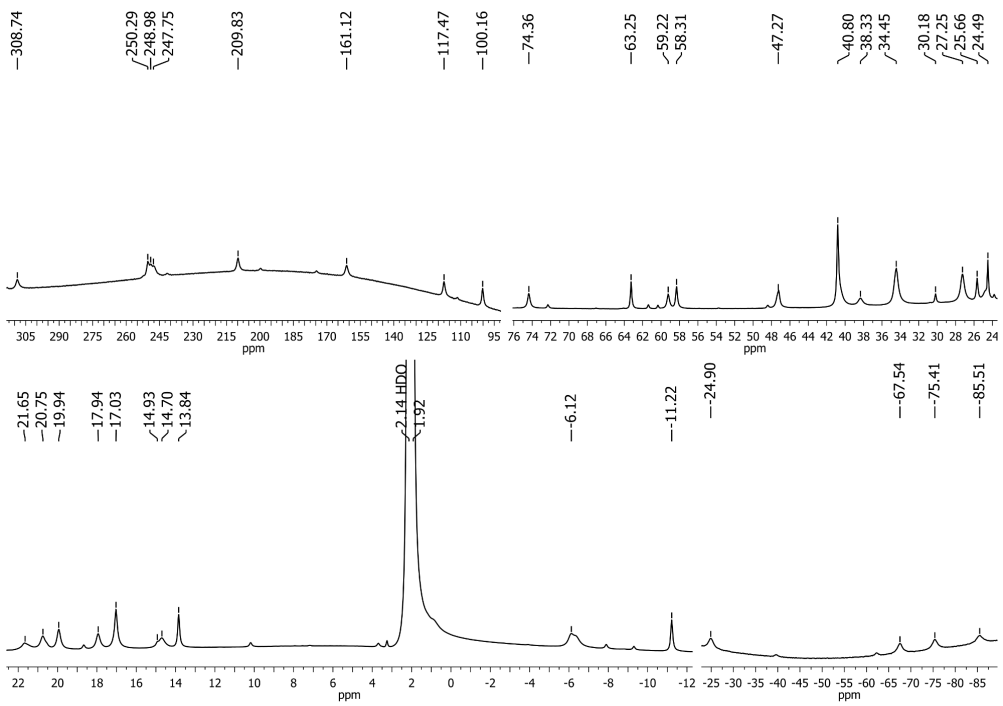

Figure S32. ^{1}H NMR spectrum of **1-3OAc-ClO$_4$**; cf. signal assignments of **1-3OAc-BF$_4$** (Fig. S26).

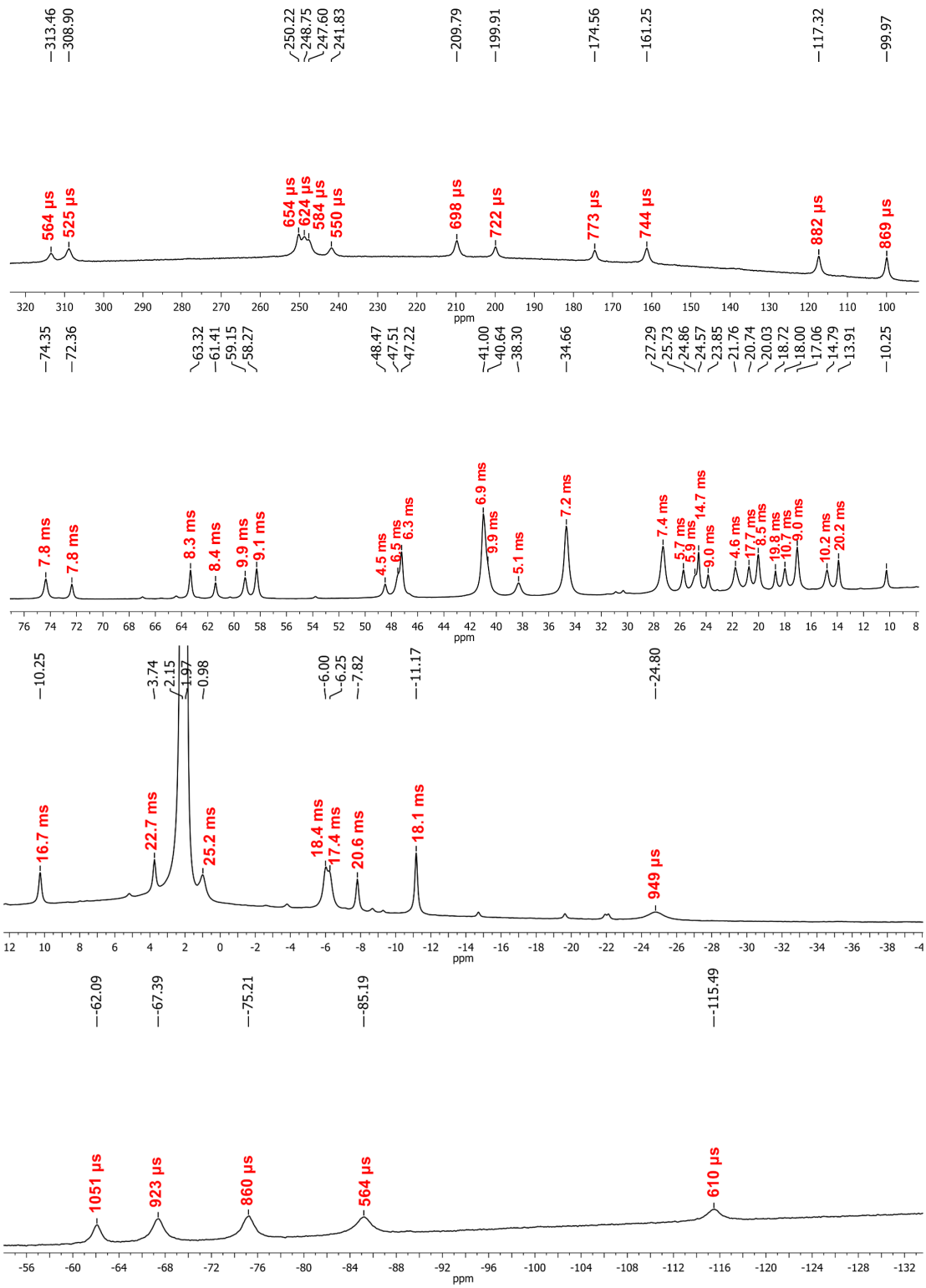

Figure S33. ^{1}H NMR spectrum of the as-synthesized mixture of **1-3OAc-ClO$_4$** and **2-Co$_4$-ClO$_4$** (cf. Table S16 for the chemical shift assignments).

Table S16. ^{1}H NMR chemical shift assignment list of Figure S33.

^{1}H	Pure **1-3OAc-BF_4**	Pure **2-Co_4-ClO_4**[5]	ClO_4^- counteranion (Fig. S33)
Ortho-		**313.55** (542 μs)	**313.46** (554 μs)
	309.07 (534 μs)		**308.90** (525 μs)
	250.37 (699 μs)		**250.22** (654 μs)
	248.74 (665 μs)		**248.75** (624 μs)
	247.79 (639 μs)		**247.60** (584 μs)
		241.82 (538 μs)	**241.83** (550 μs)
	210.14 (1012 μs)		**209.79** (698 μs)
		199.96 (710 μs)	**199.91** (722 μs)
		174.62 (715 μs)	**174.56** (773 μs)
	161.18 (755 μs)		**161.25** (744 μs)
	117.41 (787 μs)		**117.32** (882 μs)
	99.93 (872 μs)		**99.97** (869 μs)
Meta-	**74.38** (7.8 ms)		**74.35** (7.8 ms)
		72.35 (7.6 ms)	**72.36** (7.8 ms)
	63.31 (8.2 ms)		**63.32** (8.3 ms)
		61.41 (8.1 ms)	**61.41** (8.4 ms)
	59.14 (10.5 ms)		**59.15** (9.9 ms)
	58.27 (10.5 ms)		**58.27** (9.1 ms)
Meta-		**48.46** (5.3 ms)	**48.47** (4.5 ms)
	47.51 (6.4 ms)		**47.51** (6.5 ms)
OAc-		**47.21** (6.4 ms)	**47.22** (6.3 ms)
	41.02 (6.6 ms)		**41.00** (6.9 ms)

^{1}H	Pure **1-3OAc-BF_4**	Pure **2-Co_4-ClO_4**[5]	ClO_4^- counteranion (Fig. S33)
Meta-		**40.84** (10.0 ms)	**40.64** (9.9 ms)
Meta-	**38.34** (5.1 ms)		**38.30** (5.1 ms)
		34.71 (6.3 ms)	**Overlapped**
OAc-	**34.66** (7.3 ms)		**34.66** (7.2 ms)
Meta-	**30.34** (6.8 ms)		**Missing**
OAc-	**27.31** (7.4 ms)		**27.29** (7.4 ms)
Meta-	**25.67** (6.1 ms)		**25.73** (5.7 ms)
	24.83 (7.0 ms)		**24.86** (5.9 ms)
Para-	**24.57** (13.1 ms)		**24.57** (14.7 ms)
Meta-		**23.82** (10.7 ms)	**23.85** (9.0 ms)
Meta-		**21.74** (6.6 ms)	**OL**
	21.71 (3.9 ms)		**21.76** (4.6 ms)
Para-	**20.72** (16.7 ms)		**20.74** (17.7 ms)
Meta-	**20.01** (9.2 ms)		**20.03** (8.5 ms)
Meta-		**19.99** (6.7 ms)	**Overlapped**
Para-		**18.69** (15.3 ms)	**18.72** (19.8 ms)
Meta-	**18.00** (10.6 ms)		**18.00** (10.7 ms)
	17.03 (8.4 ms)		**17.06** (9.0 ms)
	14.82 (10.3 ms)		**14.79** (10.2 ms)
Para-	**13.86** (19.4 ms)		**13.91** (20.2 ms)
		10.22 (16.7 ms)	**10.25** (16.7 ms)
		3.72 (18.3 ms)	**3.74** (22.7 ms)

Continued on the next page.

^{1}H	Pure **1-3OAc-BF_4**	Pure **2-Co_4-ClO_4**[5]	ClO_4^- counteranion (Fig. S33)
Para-	**0.98** (19.1 ms)		**0.98** (25.2 ms)
	-6.01 (18.6 ms)		**-6.00** (18.4 ms)
	-6.27 (18.2 ms)		**-6.25** (17.4 ms)
		-7.86 (18.6 ms)	**-7.82** (20.6 ms)
	-11.21 (19.9 ms)		**-11.17** (18.1 ms)

^{1}H	Pure **1-3OAc-BF_4**	Pure **2-Co_4-ClO_4**[5]	ClO_4^- counteranion (Fig. S33)
HO-	**-24.71** (1107 µs)		**-24.80** (949 µs)
		-62.22 (970 µs)	**-62.09** (1051 µs)
	-67.42 (985 µs)		**-67.39** (923 µs)
	-75.27 (893 µs)		**-75.21** (860 µs)
	-85.16 (549 µs)		**-85.19** (564 µs)
		-115.57 (582 µs)	**-115.49** (610 µs)
	-24.71 (1107 µs)		**-24.80** (949 µs)

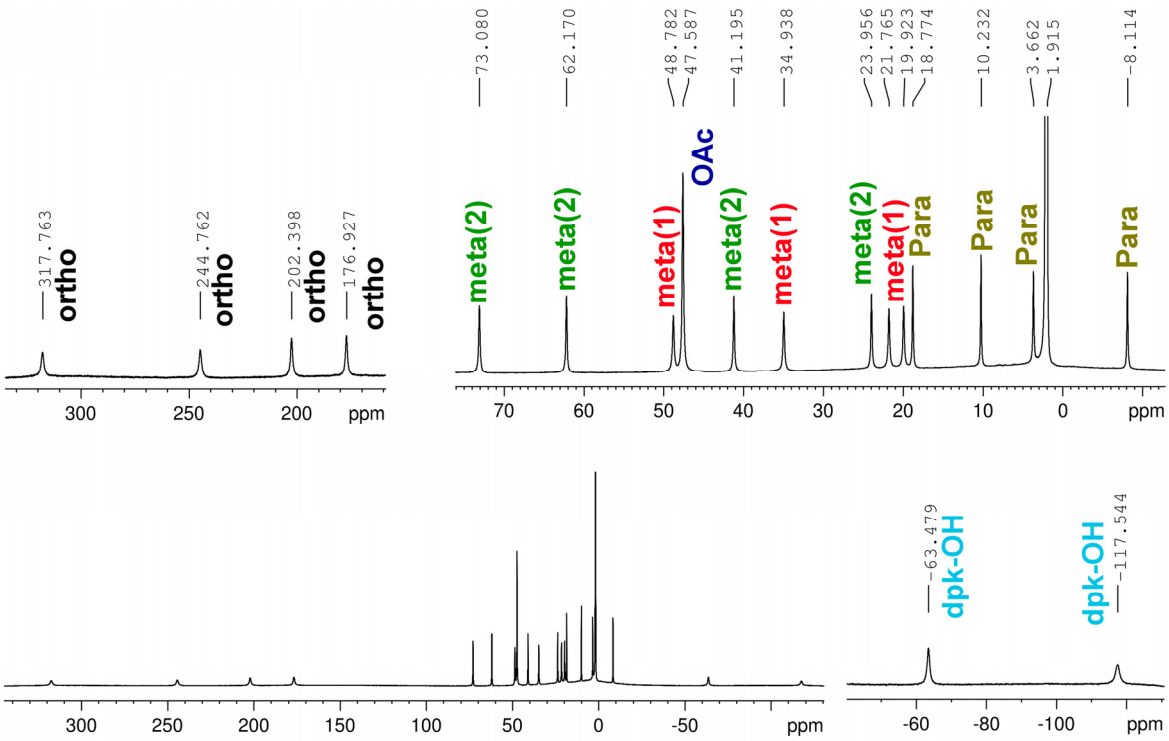

Figure S34. ^{1}H NMR spectrum of **1-2OAc-2ClO_4**. Chemical shift assignments were made on the basis of **1-2OAc-2BF_4** (cf. Fig. 4).

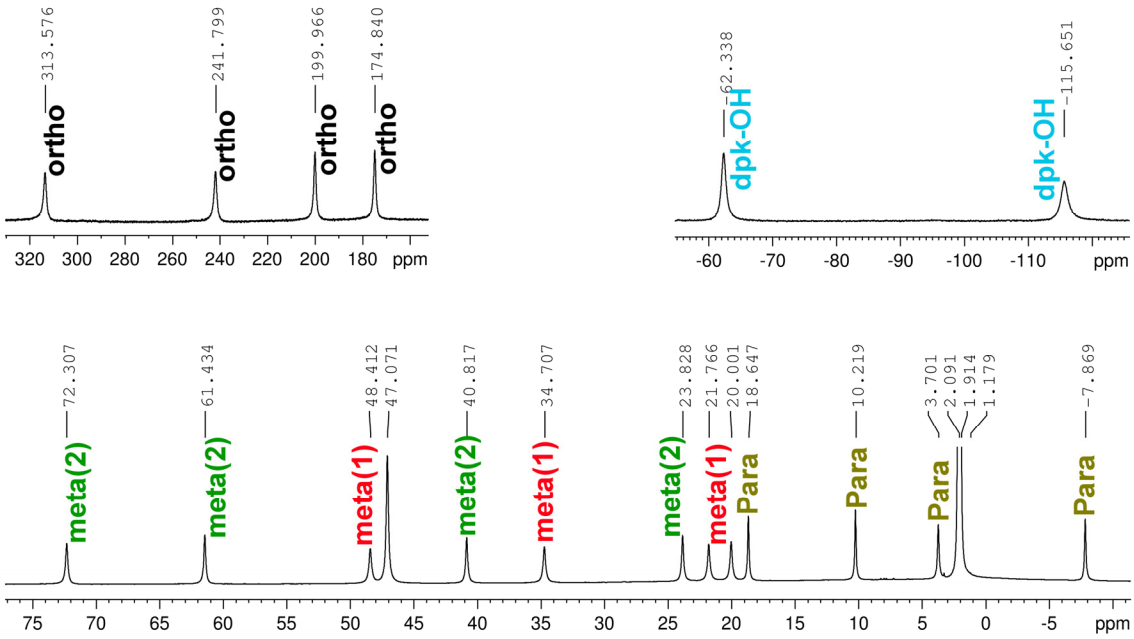

Figure S35. ^{1}H NMR spectrum of **2-Co$_4$-NO$_3$**. Chemical shift assignments were made on the basis of **2-Co$_4$-ClO$_4$**.

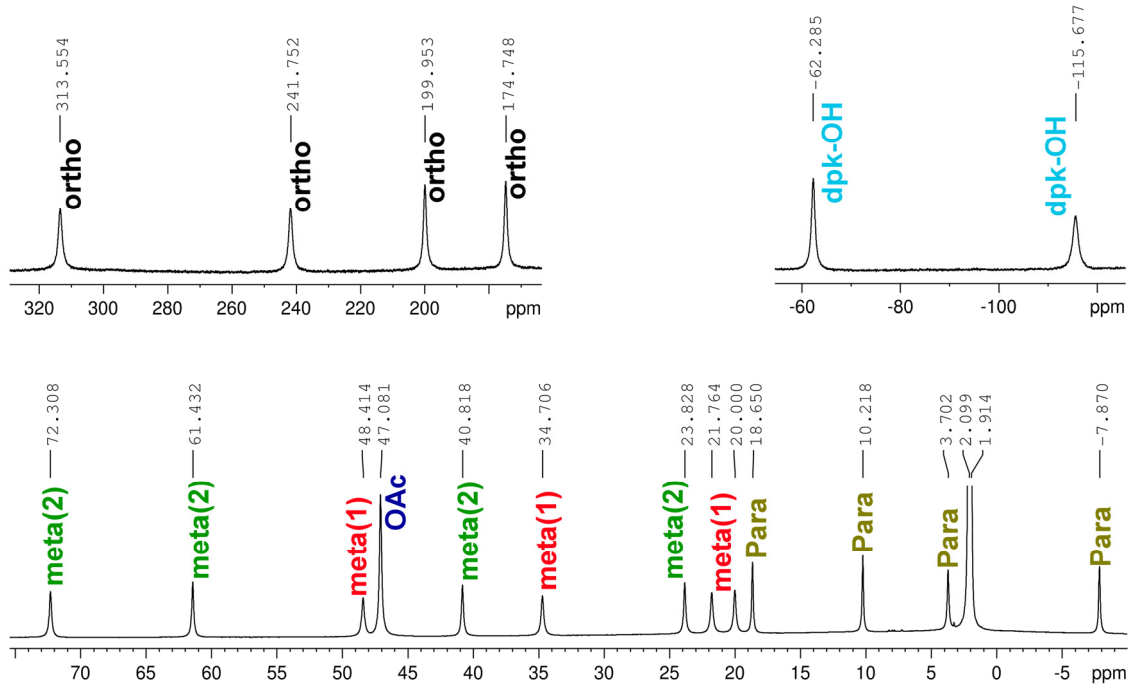

Figure S36. ^{1}H NMR spectrum of **2-Co$_4$-BF$_4$**. Chemical shift assignments were made on the basis of **2-Co$_4$-ClO$_4$**.

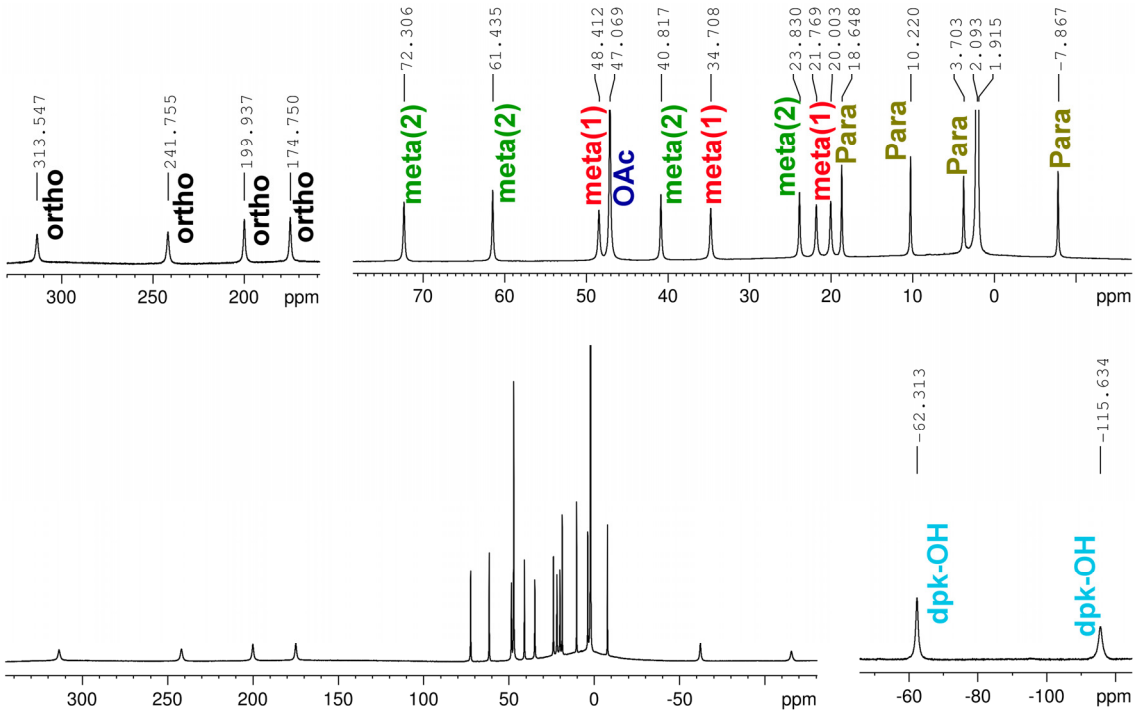

Figure S37. ^{1}H NMR spectrum of **2-Co$_4$-ClO$_3$**. Chemical shift assignments were made on the basis of **2-Co$_4$-ClO$_4$**.

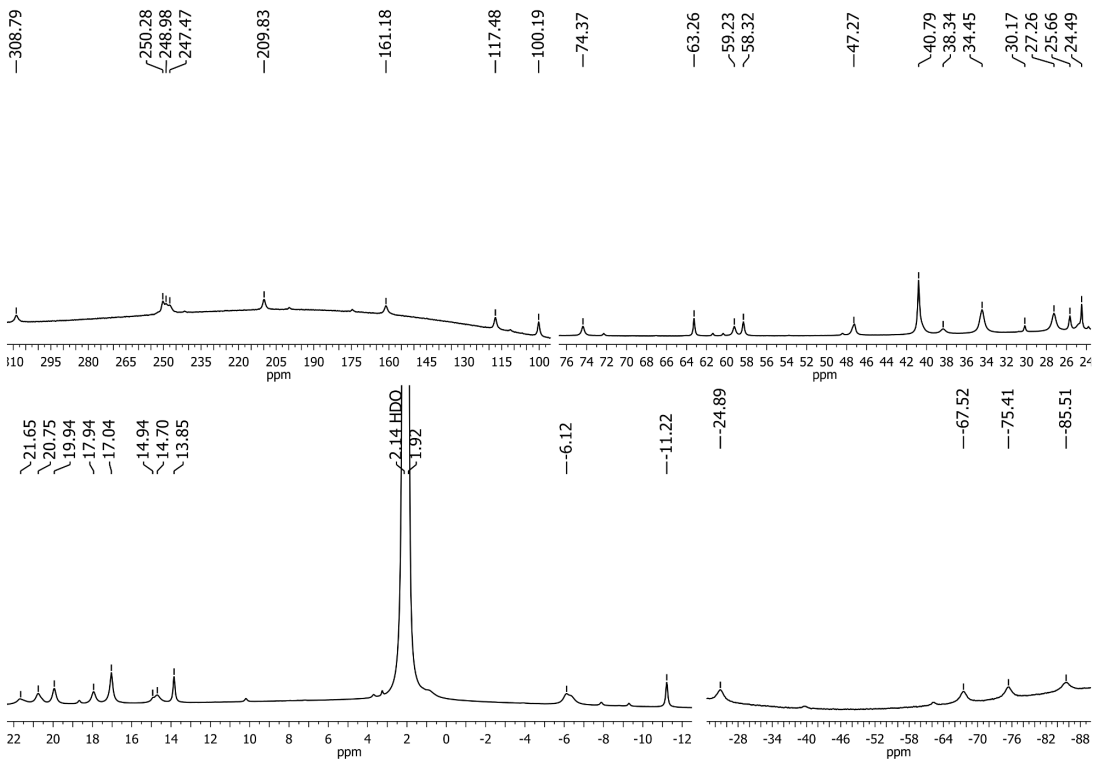

Figure S38. ^{1}H NMR spectrum of **1-3OAc-NO$_3$**; cf. signal assignments of **1-3OAc-BF$_4$** (Fig. S26).

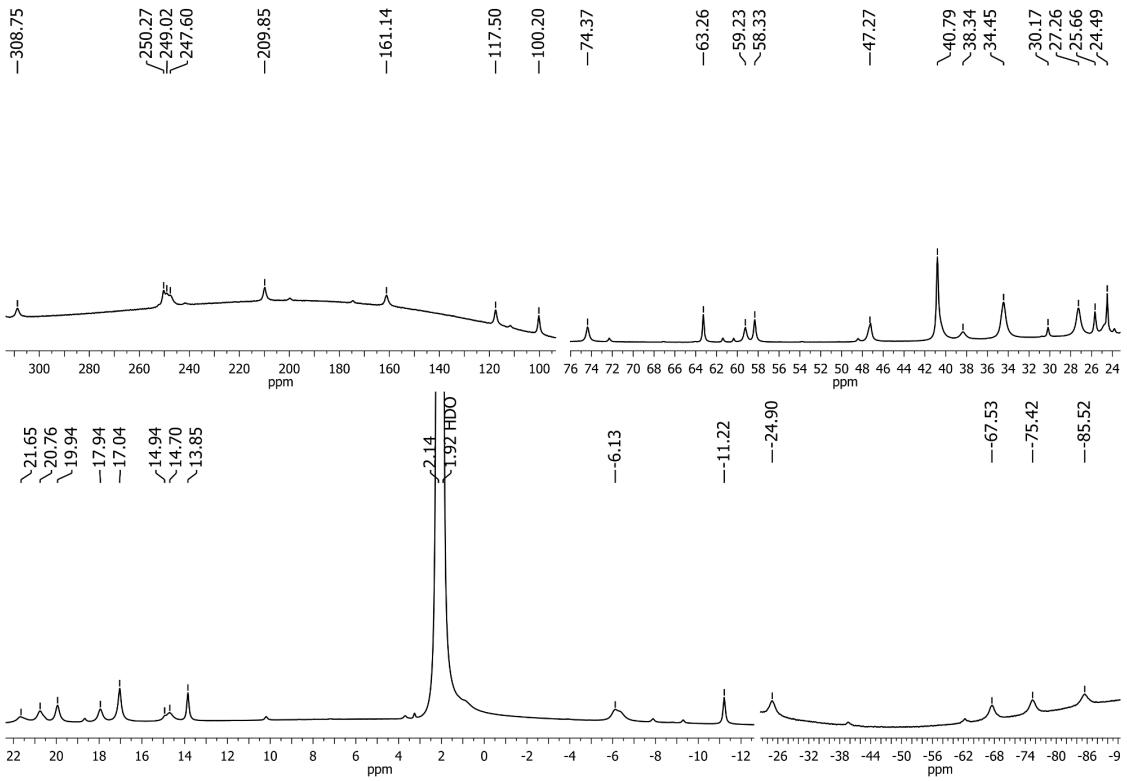

Figure S39. ^{1}H NMR spectrum of **1-3OAc-ClO$_3$**; cf. signal assignments of **1-3OAc-BF$_4$** (Fig. S26).

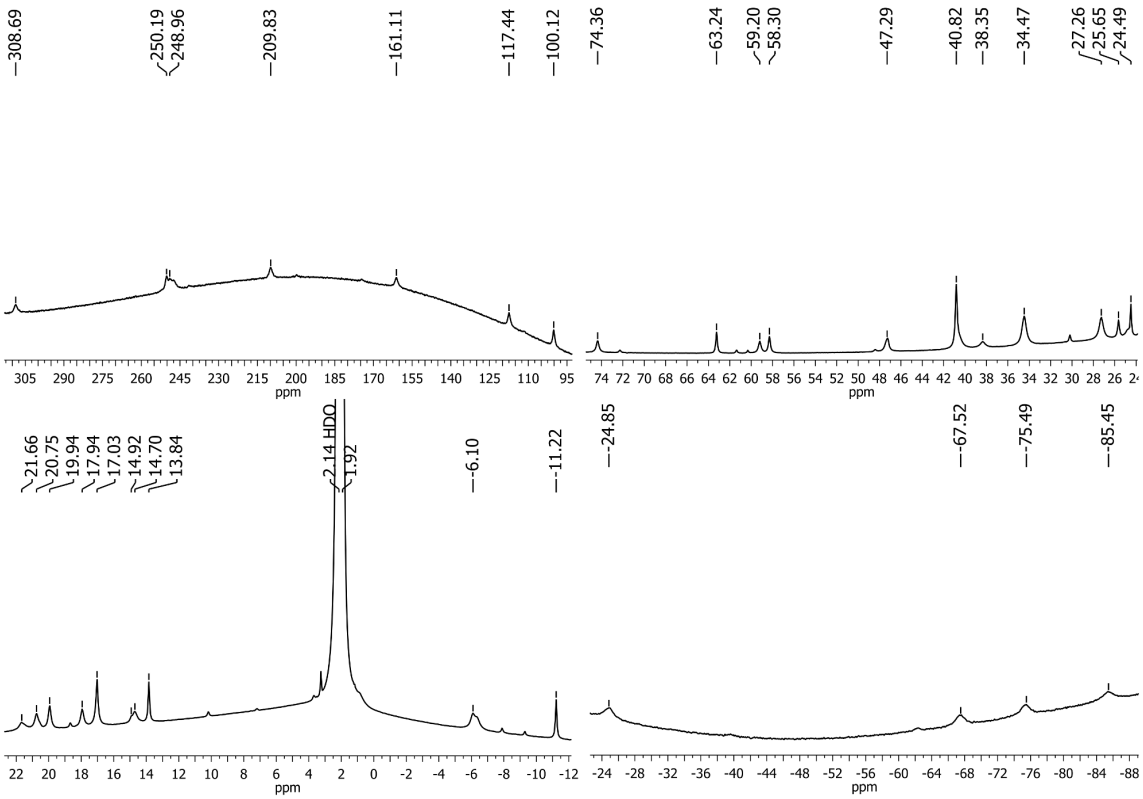

Figure S40. ^{1}H NMR spectrum of **1-3OAc-PF$_6$**; cf. signal assignments of **1-3OAc-BF$_4$** (Fig. S26).

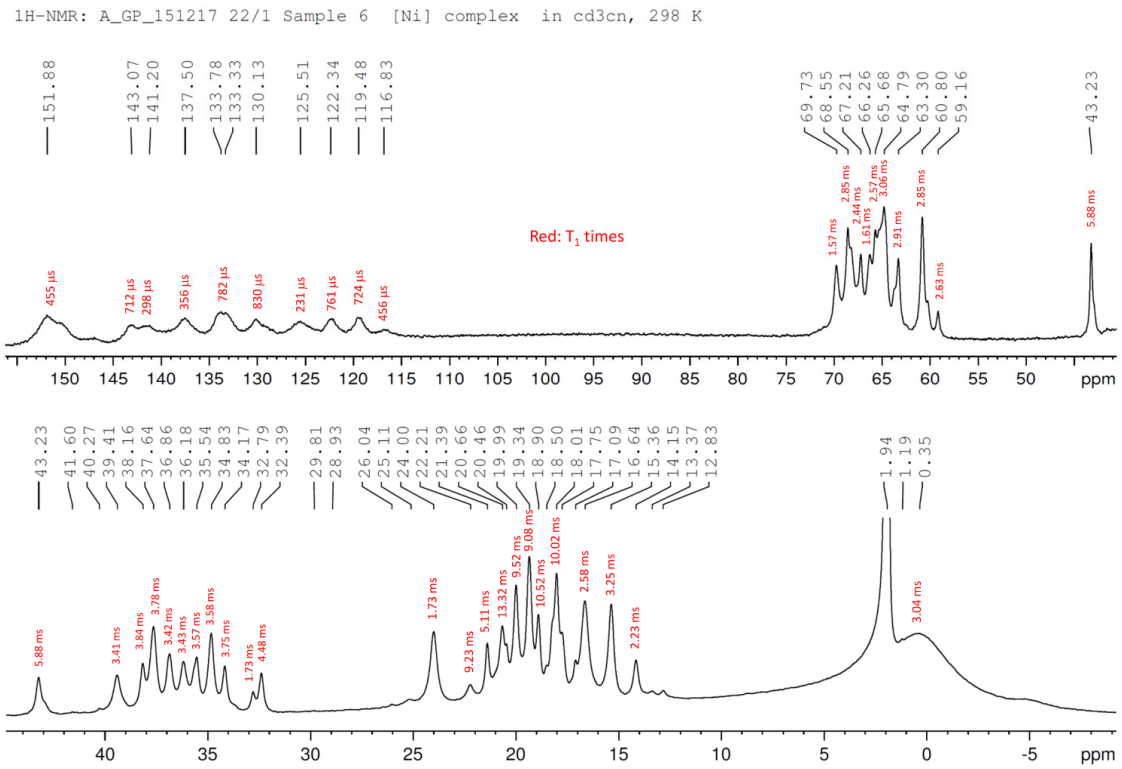

Figure S41. ^{1}H NMR spectrum of **2-Ni$_4$-ClO$_4$**.

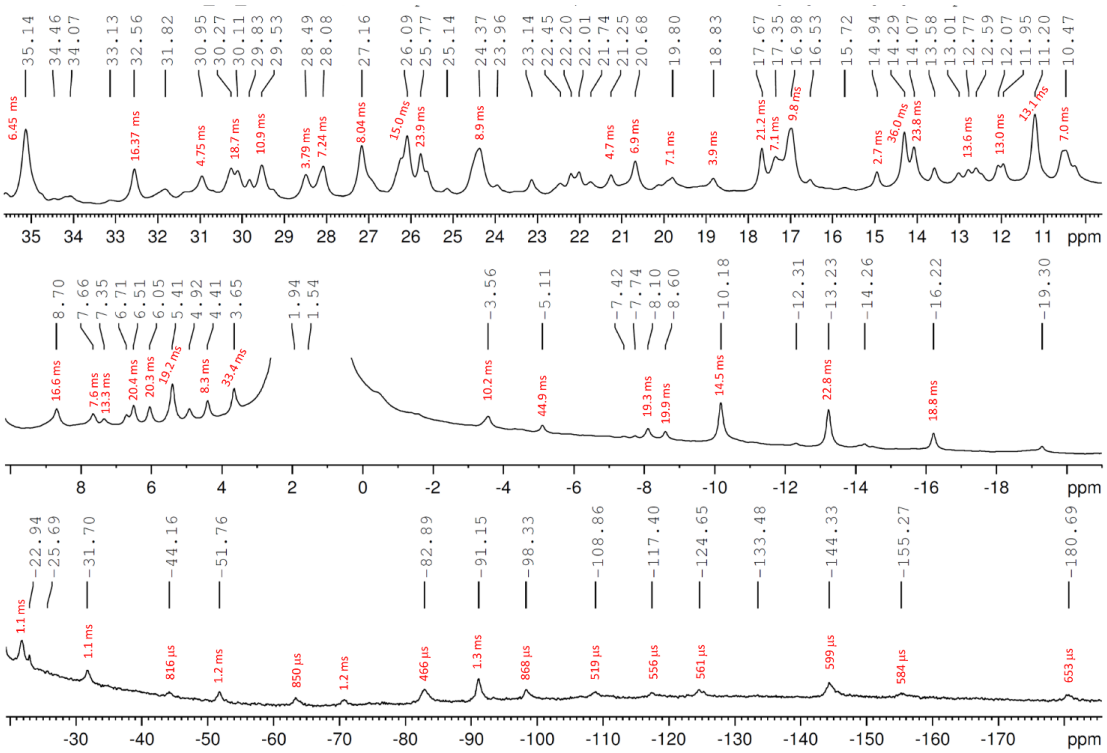

Figure S42. ^{1}H NMR spectrum of **2-Co$_{2.28}$Ni$_{1.72}$-BF$_4$**.

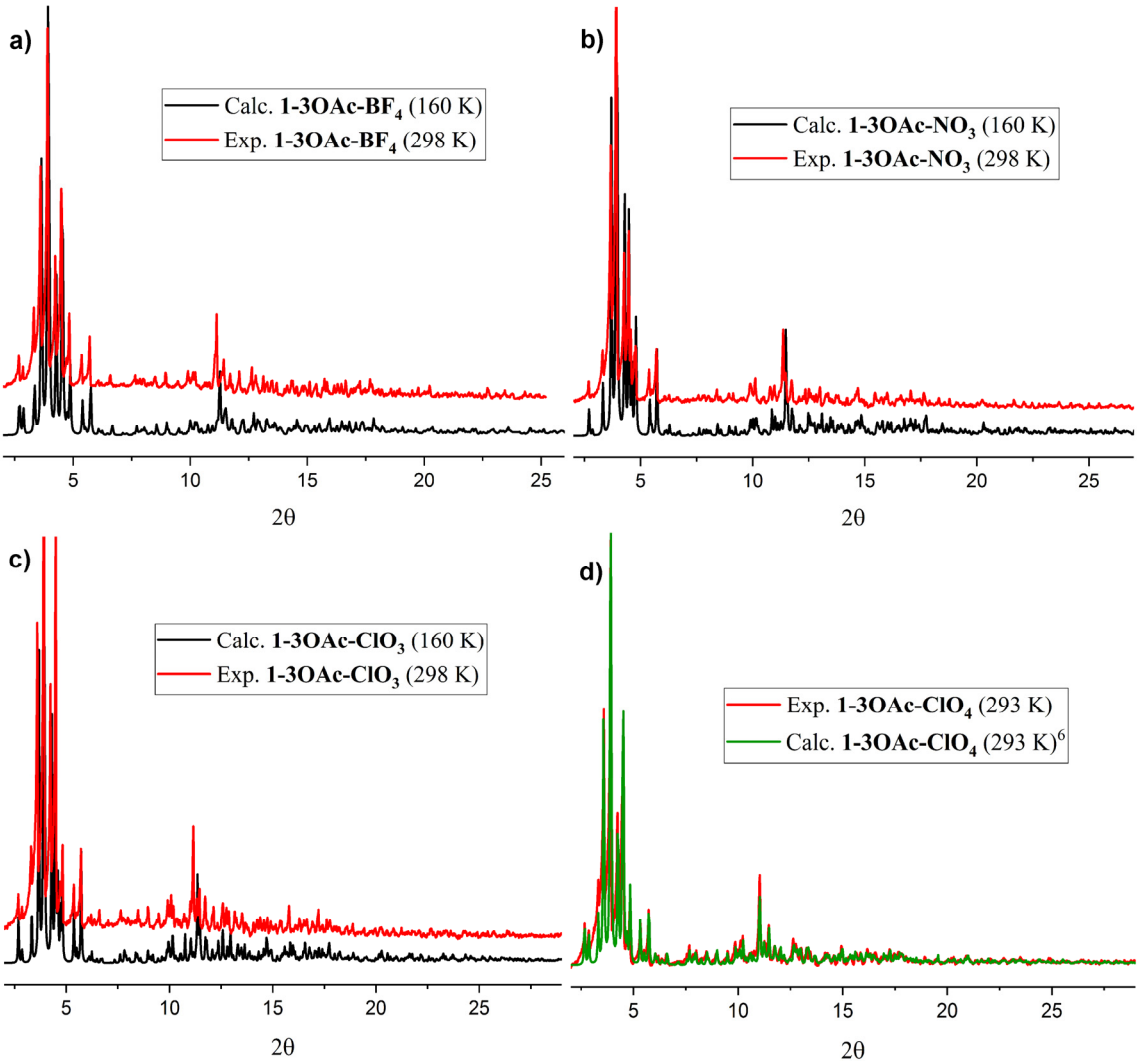

Figure S43. Calculated (**1-3OAc-ClO$_4$**)[6] and experimental PXRD patterns of **1-3OAc** cubanes.

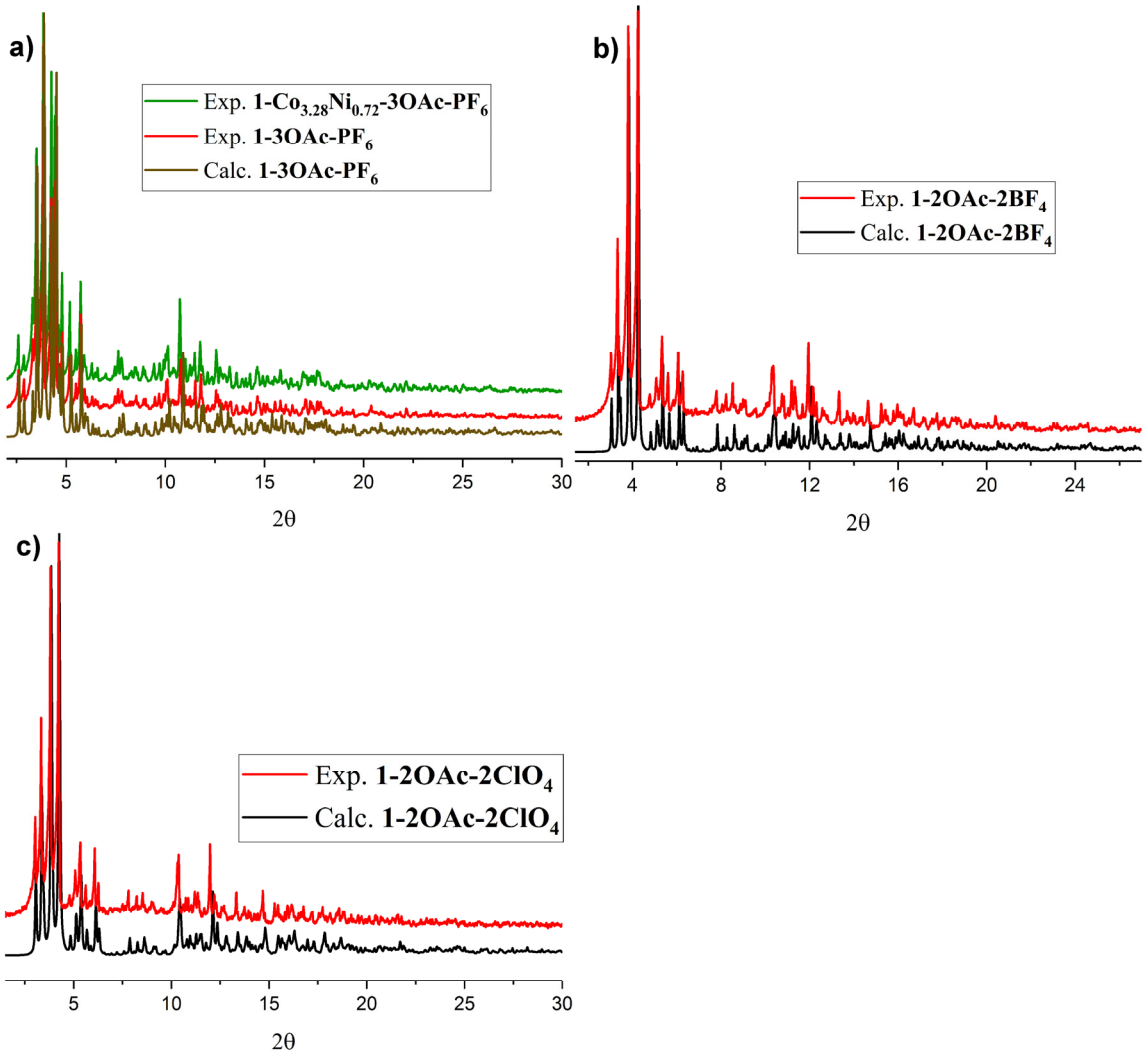

Figure S44. (**a**) Experimental PXRD patterns of **1-3OAc-PF$_6$** and **1-Co$_{3.28}$Ni$_{0.72}$-3OAc-PF$_6$** vs. the calculated pattern of **1-3OAc-PF$_6$**. (**b**, **c**) Calculated and experimental PXRD patterns of **1-2OAc-2BF$_4$** and **-ClO$_4$**.

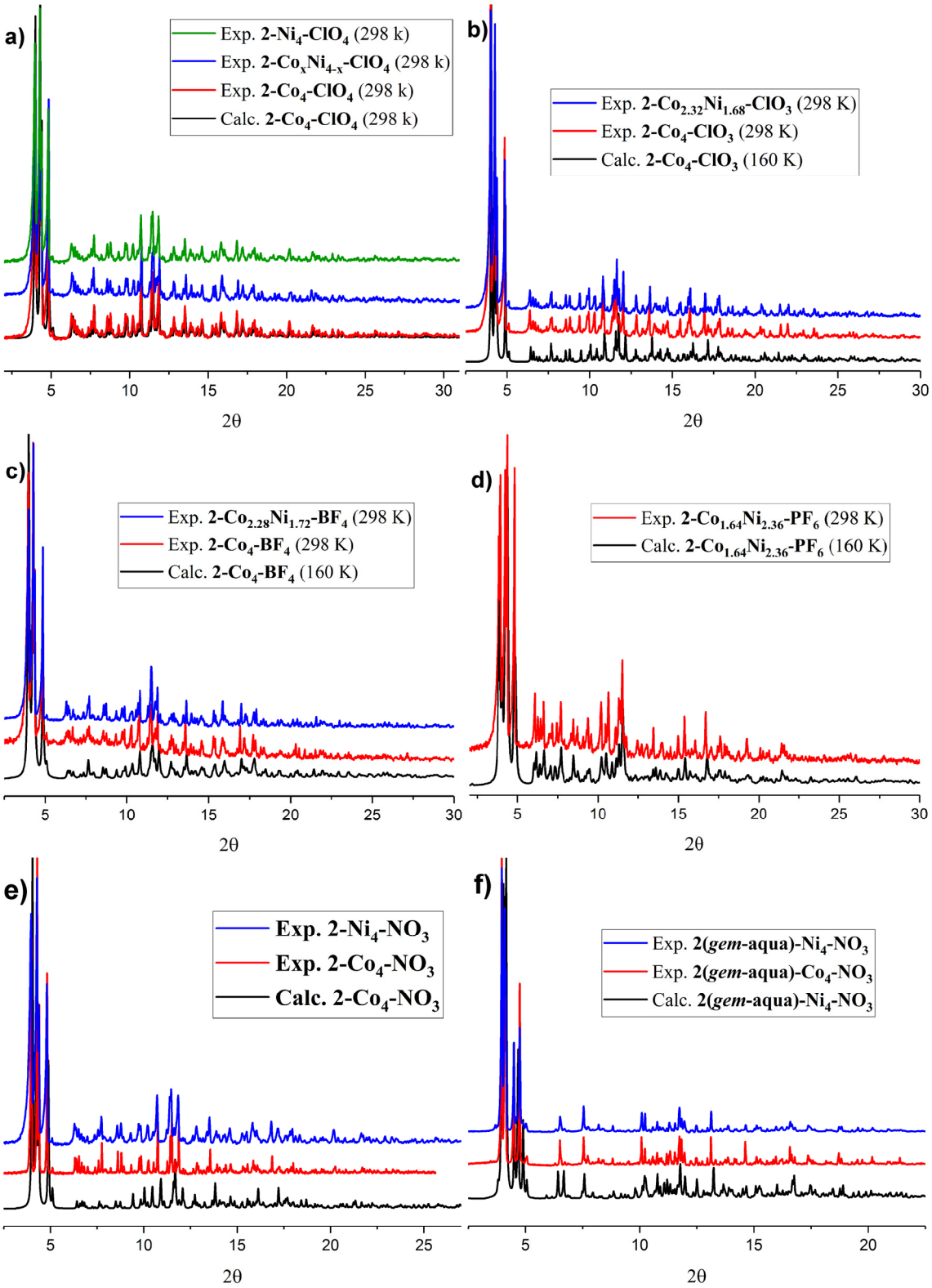

Figure S45. Calculated and experimental PXRD patterns of **2-edge-site** cubanes.

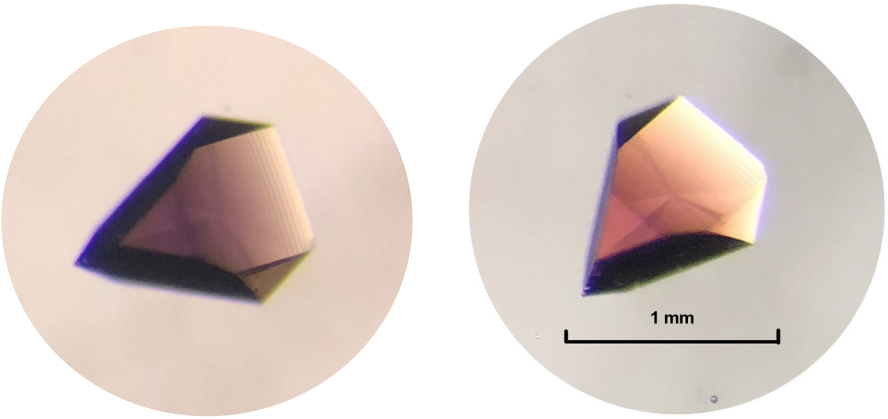

Figure S46. Photographs of large single crystals of **2-$Co_{2.32}Ni_{1.68}$-ClO_3** (both photos were taken with the same magnification).

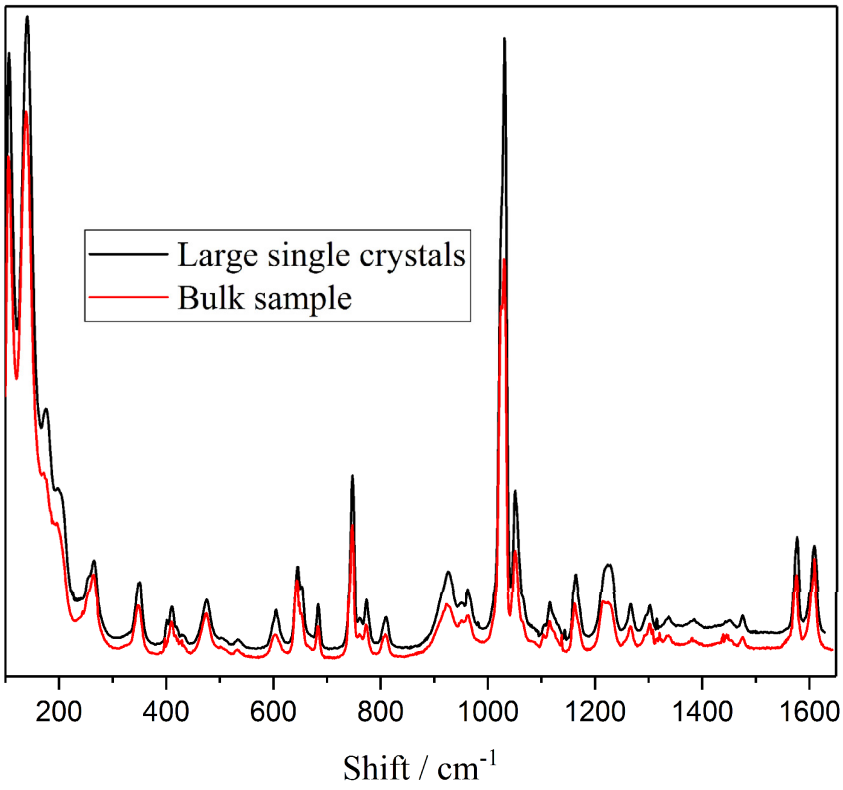

Figure S47. Raman spectra of **2-$Co_{2.32}Ni_{1.68}$-ClO_3**: large single crystals and bulk product.

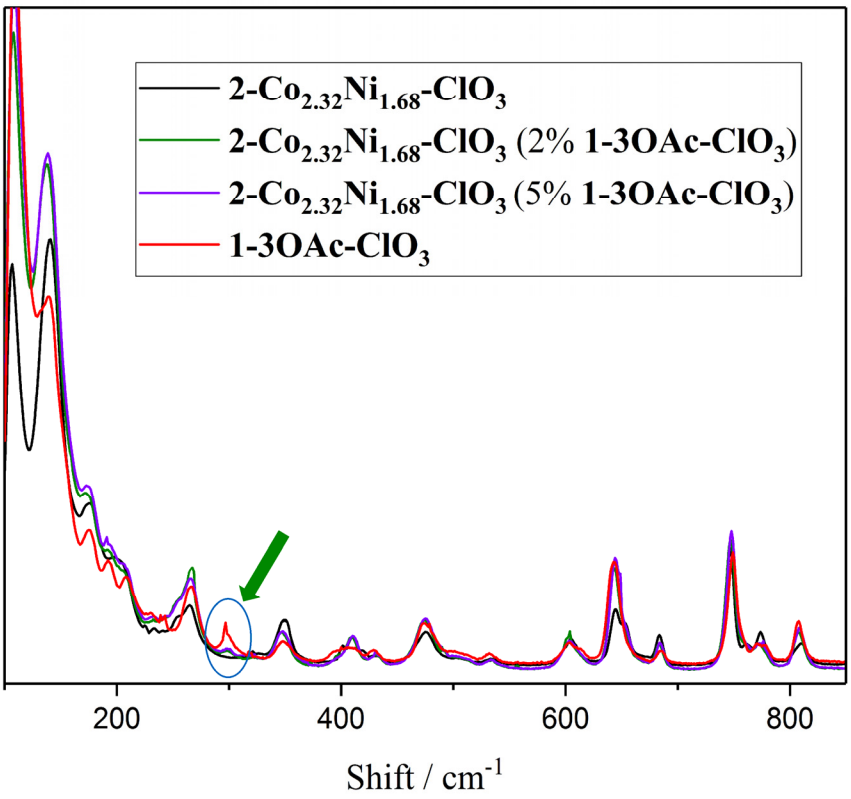

Figure S48. Raman spectra of standard **1-3OAc-ClO_3** and of **2-$Co_{2.32}Ni_{1.68}$-ClO_3** spiked with 0, 2, and 5% **1-3OAc-ClO_3**, respectively.

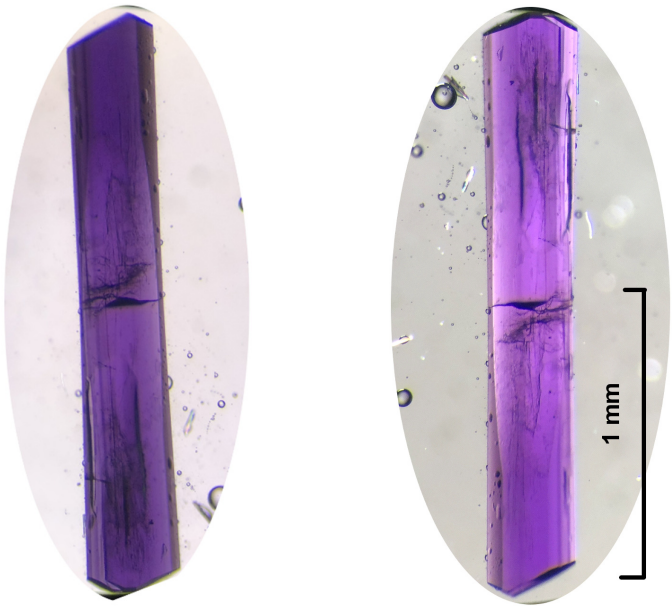

Figure S49. Photographs of large single crystals of **2-μ-OAc-Co_xNi_{4-x}-ClO_4** (both photos were recorded with the same magnification).

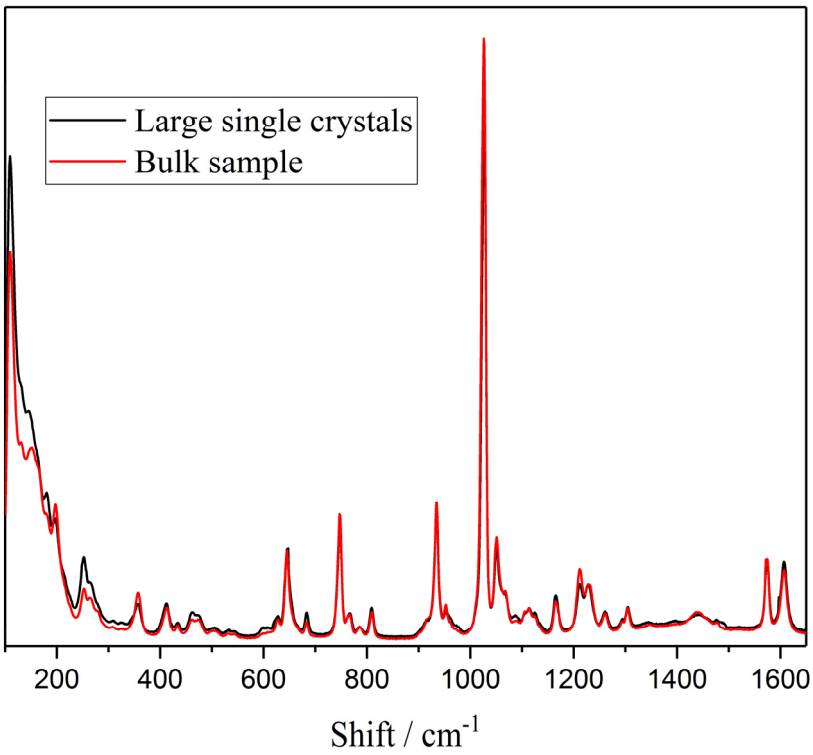

Figure S50. Raman spectra of **2-μ-OAc-Co_xNi_{4-x}-ClO_4**: large single crystals and bulk product.

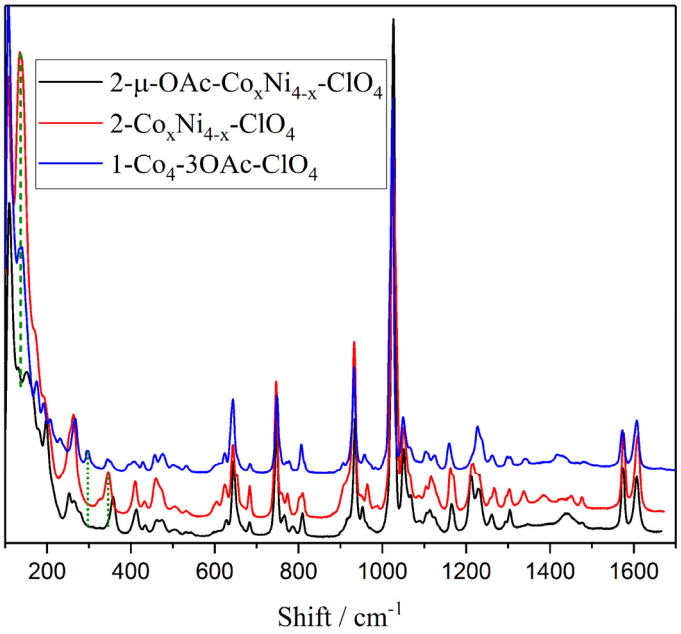

Figure S51. Raman spectra of bulk **2-μ-OAc–Co_xNi_{4-x}-ClO_4** (black) and of single crystals of **2-Co_xNi_{4-x}-ClO_4** and **1-3OAc-ClO_4**.

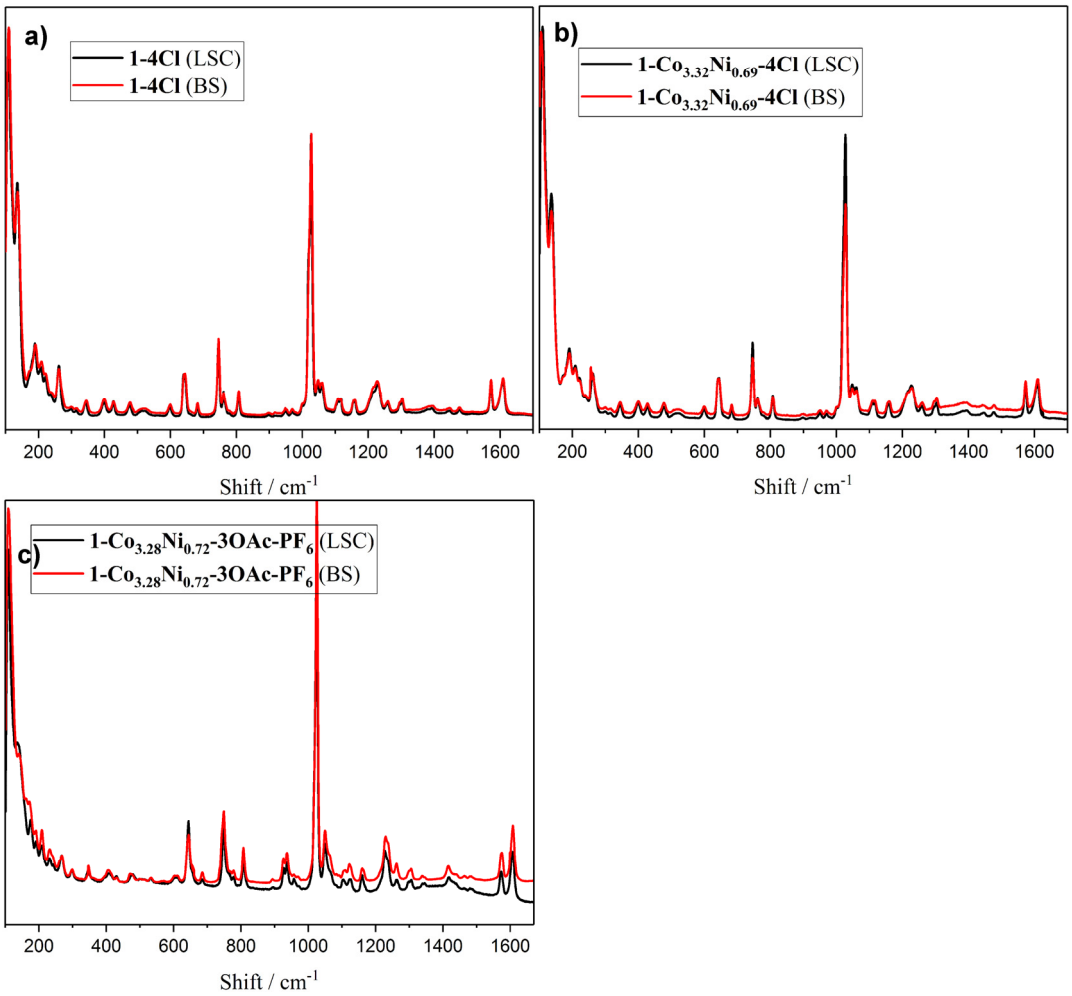

Figure S52. Raman spectra of large single crystals (LSC) and bulk sample (BS) of **1-4Cl** (**a**), **1-$Co_{3.32}Ni_{0.69}$-4Cl** (**b**), and **1-$Co_{3.28}Ni_{0.72}$-3OAc-PF_6** (**c**), respectively. **1-$Co_{3.32}Ni_{0.69}$-4Cl** results are representative for the **1-Co_xNi_{4-x}-4Cl** series.

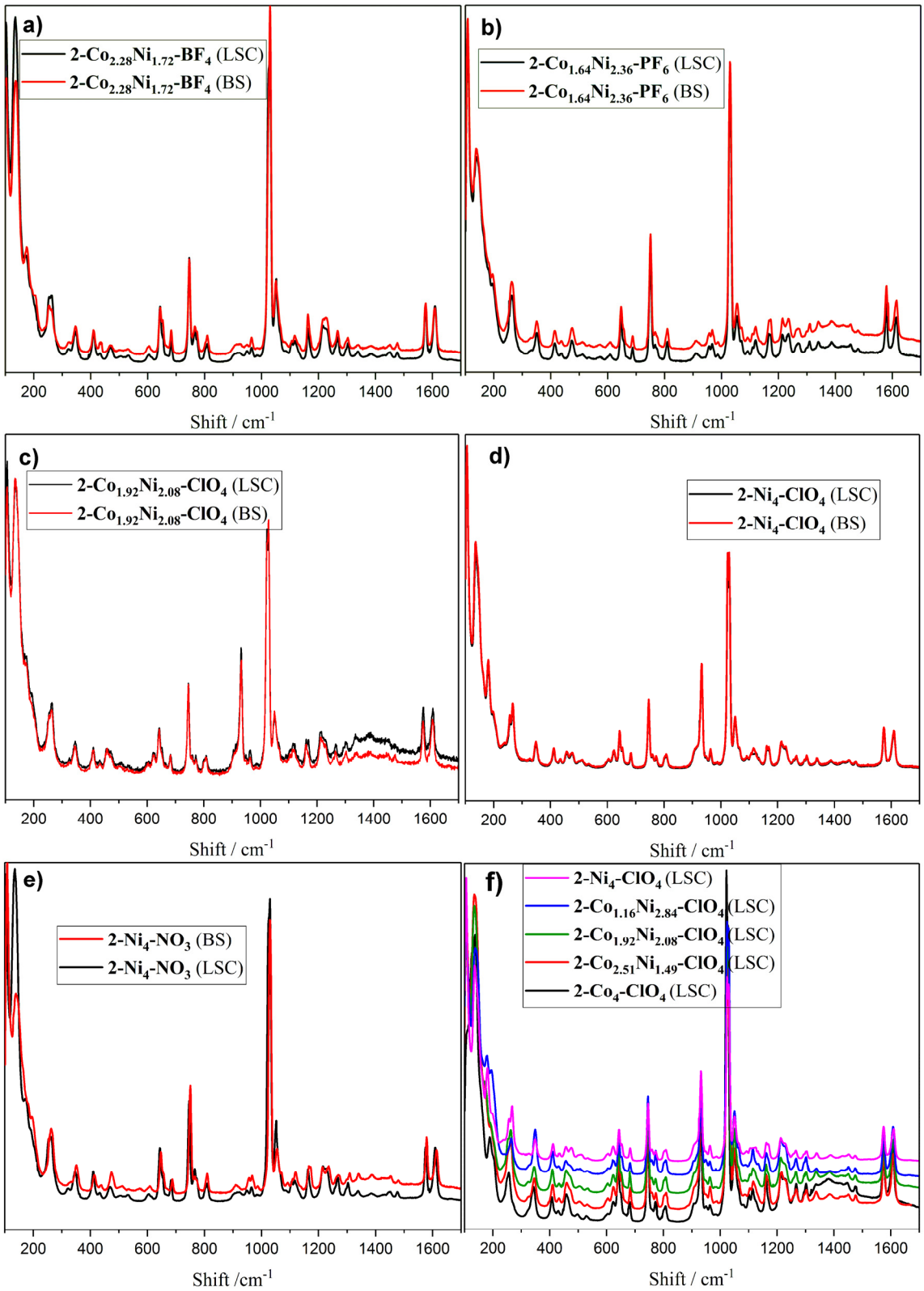

Figure S53. Raman spectra of large single crystals (LSC) and bulk sample (BS) of **2-$Co_{2.28}Ni_{1.72}$-BF_4** (**a**), **2-$Co_{1.64}Ni_{2.36}$-PF_6** (**b**), **2-$Co_{1.92}Ni_{2.08}$-ClO_4** (**c**), and **2-Ni_4-ClO_4** (**d**) respectively. (**e**) Raman spectra of large single crystals of the **2-Co_xNi_{4-x}-ClO_4** series vs. their {Co_4O_4} and {Ni_4O_4} analogues. **2-$Co_{2.28}Ni_{1.72}$-BF_4** results are representative for the **2-Co_xNi_{4-x}-BF_4** series.

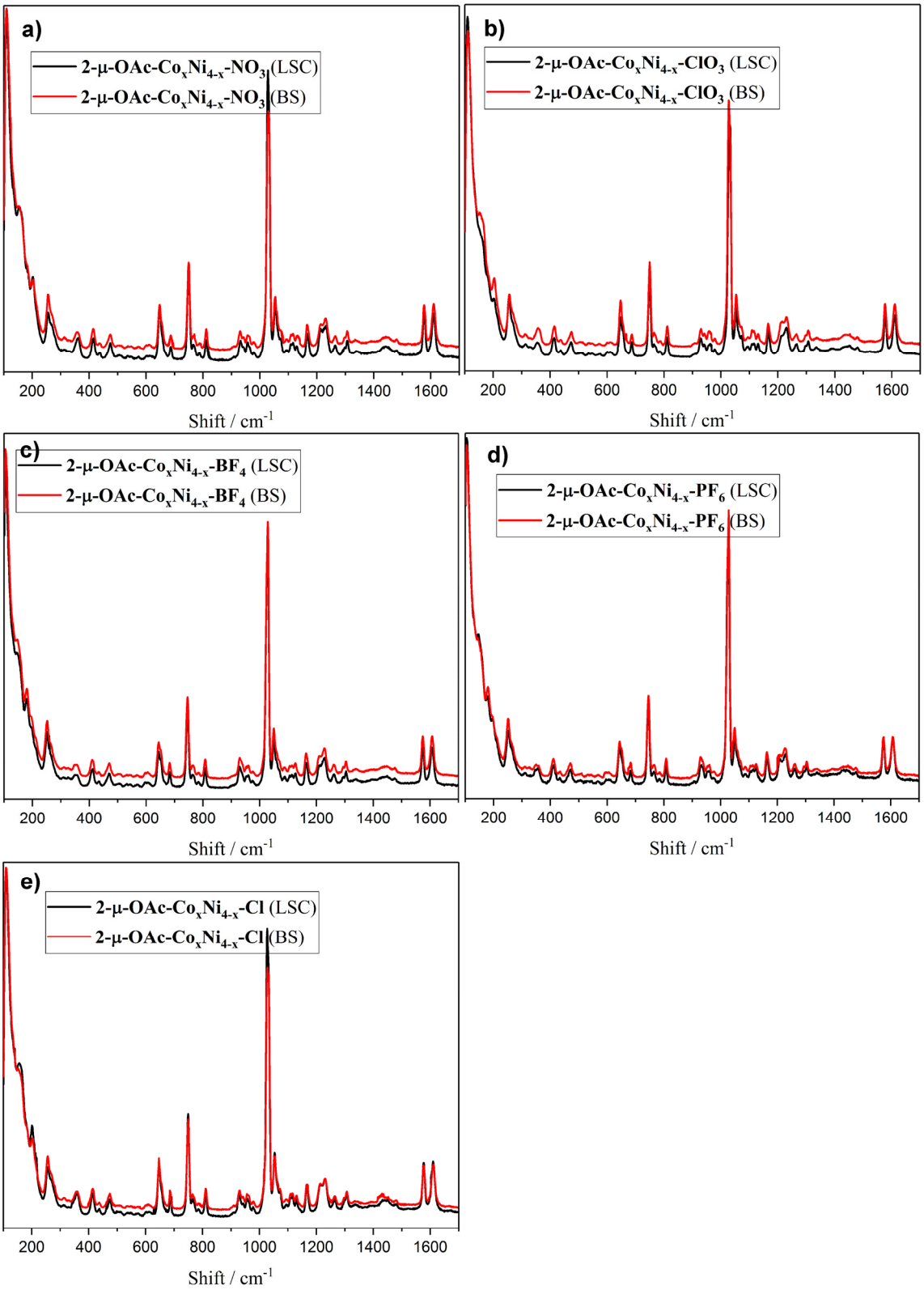

Figure S54. Raman spectra of large single crystals (LSC) and bulk sample (BS) of **2-Co_xNi_{4-x}-NO_3** (**a**), **-ClO_3** (**b**), **-BF_4** (**c**), **-PF_6** (**d**), and **–Cl** (**e**), respectively.

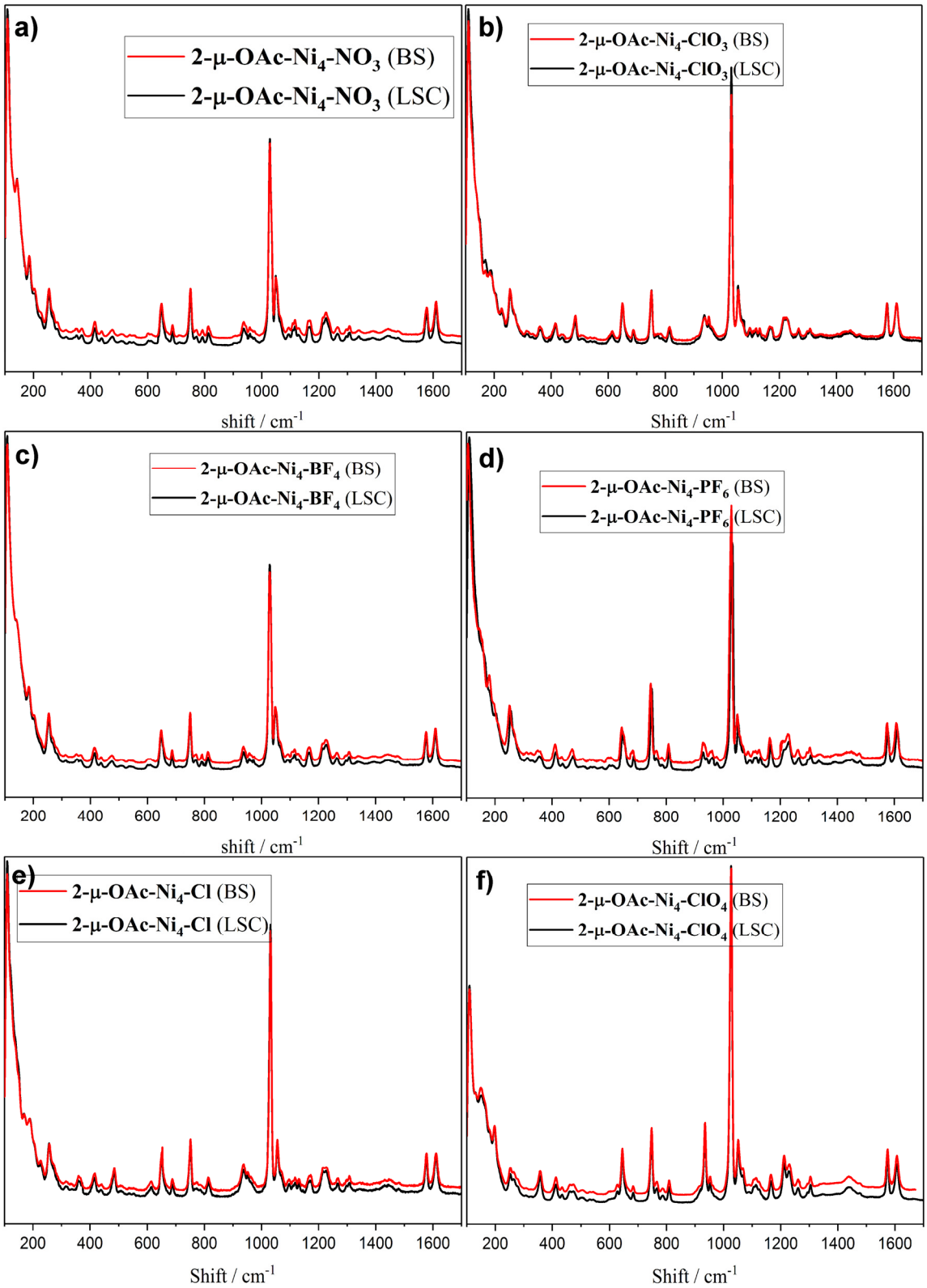

Figure S55. Raman spectra of large single crystals (LSC) and bulk sample (BS) of **2-μ-OAc-Ni$_4$-NO$_3$** (**a**), **-ClO$_3$** (**b**), **-BF$_4$** (**c**), **-PF$_6$** (**d**), and **–Cl** (**e**), respectively.

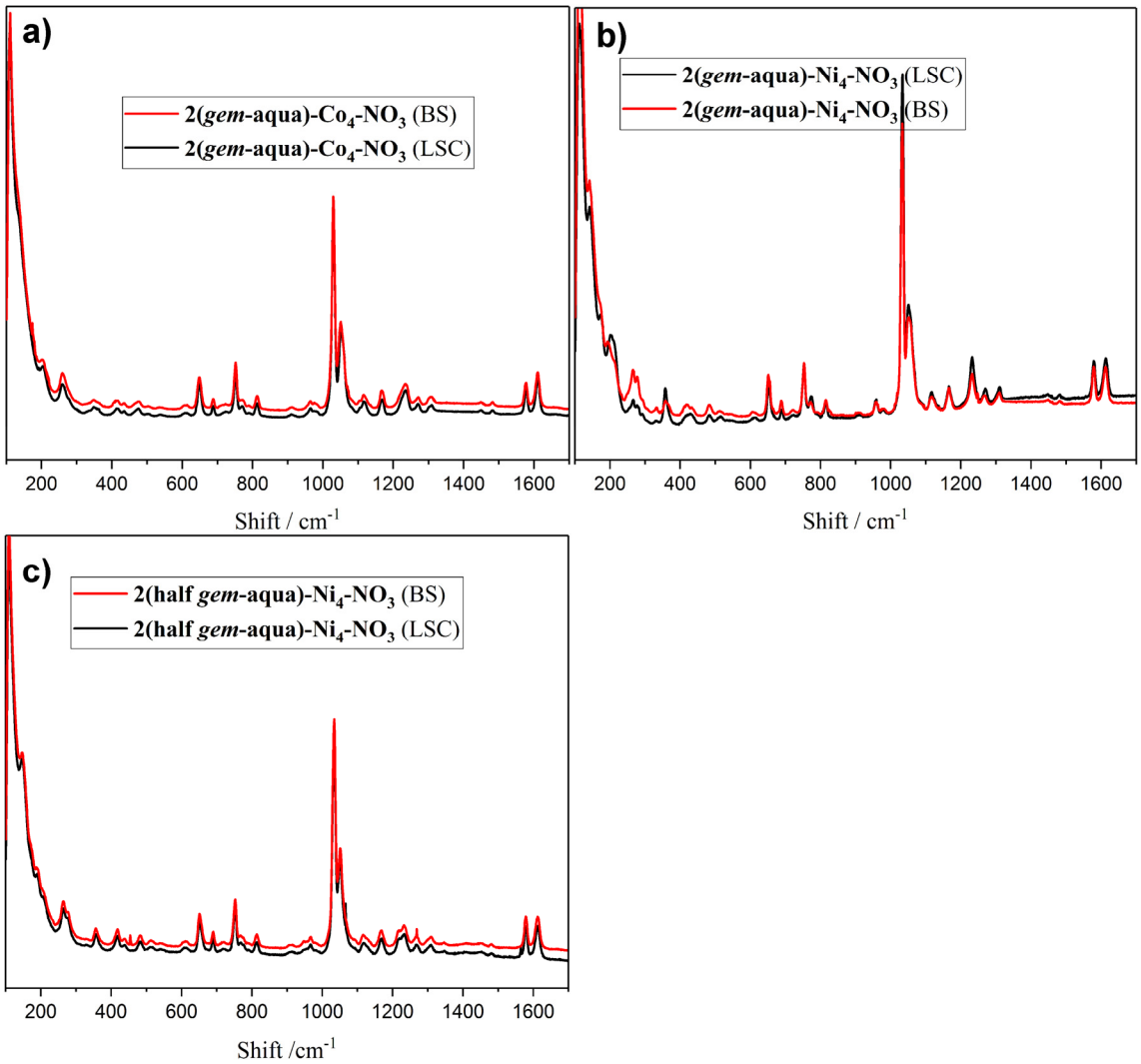

Figure S56. Raman spectra of large single crystals (LSC) and bulk sample (BS) of **2-(*gem*-aqua)-M_4-NO_3** (**a** and **b**) and **2-(half *gem*-aqua)-Ni_4-NO_3** (**c**), respectively.

Table S17. ICP-MS measurements of **2-Co_xNi_{4-x}-ClO_4**, **-BF_4**, **-ClO_3**, and **-PF_6**. The stoichiometric relation of (Co + Ni) was normalized to 4.

Starting ratio of Co:Ni	**2-$Co_xNi_{4-x}O_4$-ClO_4**	**2-$Co_xNi_{4-x}O_4$-BF_4**	**2-$Co_xNi_{4-x}O_4$-ClO_3**	**2-$Co_xNi_{4-x}O_4$-PF_6**
Co:Ni = 3:1	**$Co_{2.51}Ni_{1.49}O_4$**	**$Co_{2.28}Ni_{1.72}O_4$**	**$Co_{2.32}Ni_{1.68}O_4$**	
Co:Ni = 2:2	**$Co_{1.92}Ni_{2.08}O_4$**	**$Co_{1.53}Ni_{2.47}O_4$**	**$Co_{1.56}Ni_{2.44}O_4$**	**$Co_{1.64}Ni_{2.36}O_4$**
Co:Ni = 1:3	**$Co_{1.16}Ni_{2.84}O_4$**	**$Co_{0.84}Ni_{3.16}O_4$**	**$Co_{0.83}Ni_{3.17}O_4$**	

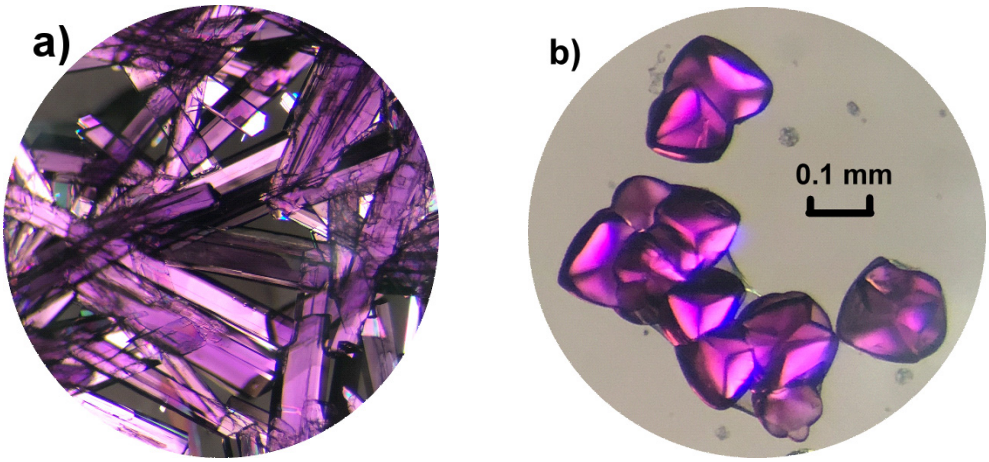

Figure S57. Photographs of the bulk products synthesized by applying 4 mmol NaCl (**a**) and 7 mmol NaCl (**b**). Both syntheses started from a mixture of 0.6 mmol $Co(OAc)_2$ + 0.2 mmol $Ni(OAc)_2$ as metal ion source ((**a**) and (**b**) were photographed with the same magnification).

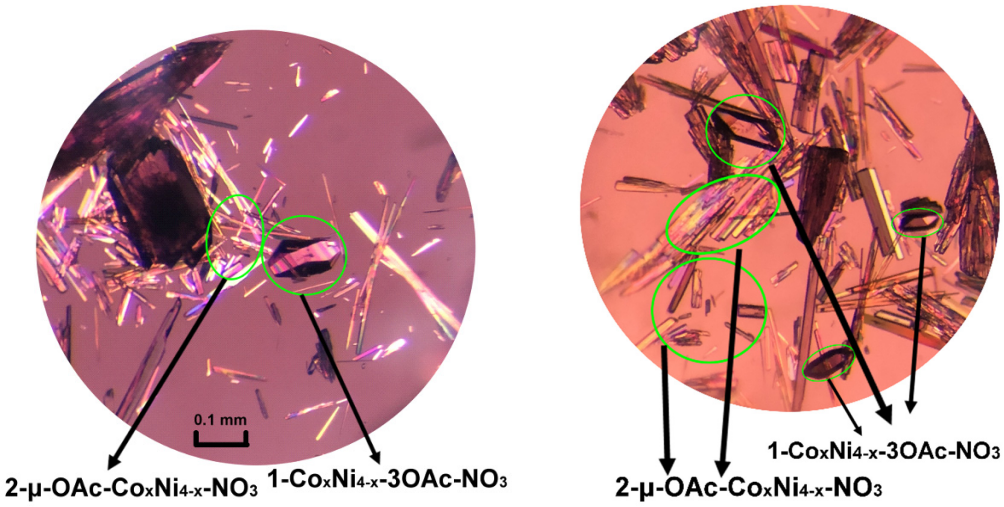

Figure S58. Photographic representations of the bulk products synthesized using 0.6 mmol $Co(OAc)_2$ + 0.2 mmol $Ni(OAc)_2$, 0.4 mmol dpk, and 7 mmol $NaNO_3$ (photos were taken with same magnification).

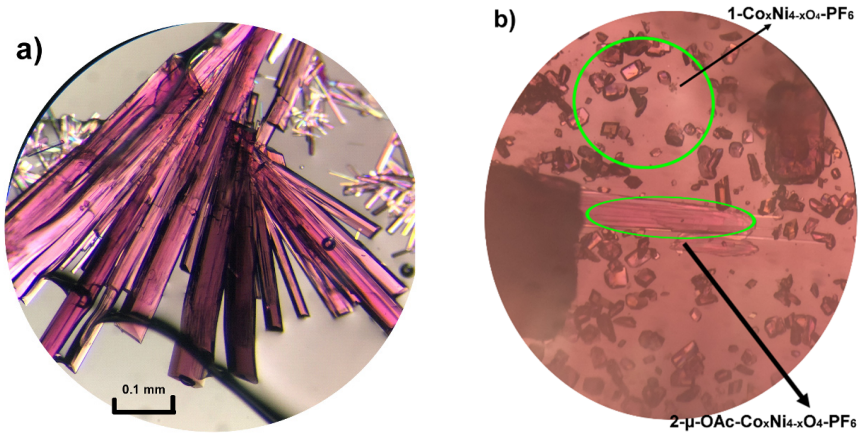

Figure S59. Photographic representations of the bulk products synthesized by applying (**a**) 0.05 mmol $NaPF_6$ and (**b**) 0.2 mmol $NaPF_6$. Both syntheses started from a mixture of 0.6 mmol $Co(OAc)_2$ + 0.2 mmol $Ni(OAc)_2$ as metal ion source ((**a**) and (**b**) = same magnification).

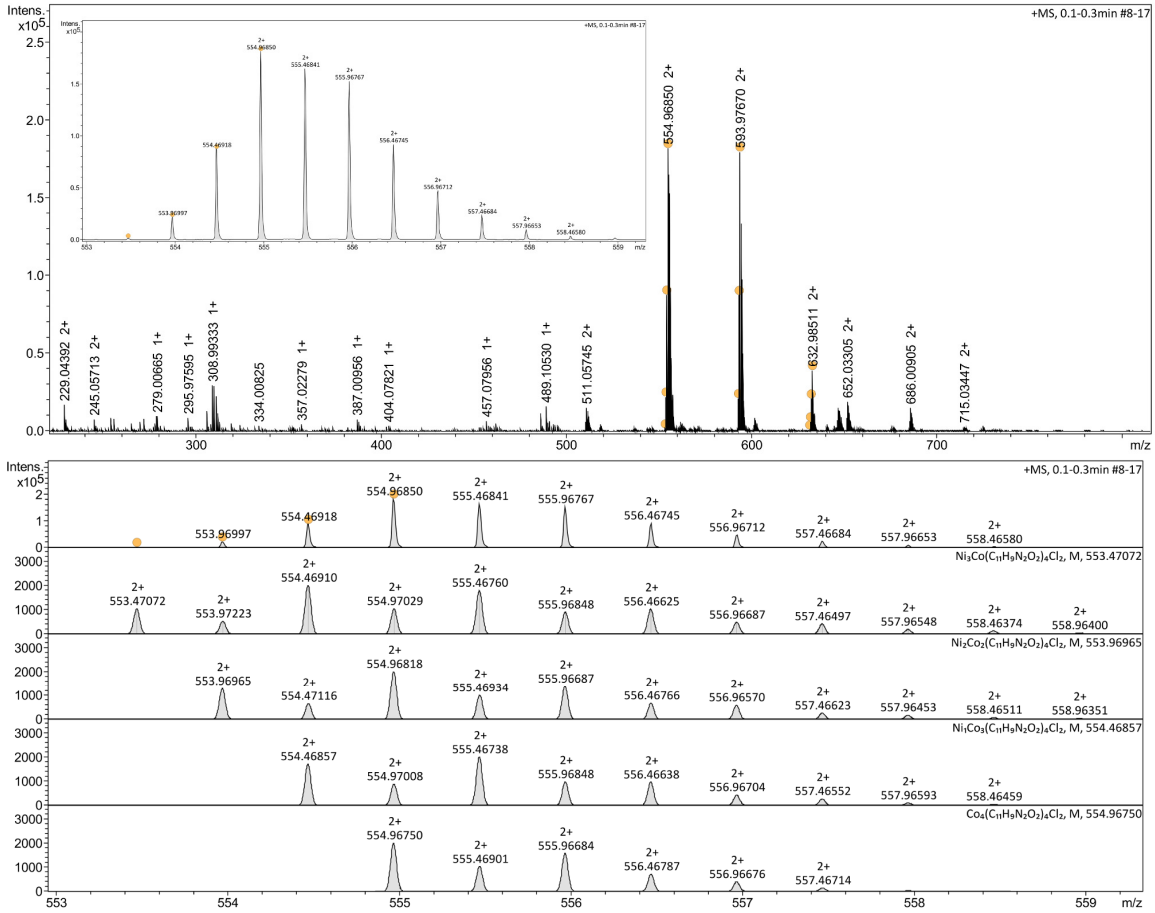

Figure S60. Full HR-ESI-MS spectrum of **1-Co$_{3.31}$Ni$_{0.69}$-4Cl** (top) and isotope patterns of **1-Co$_{3.31}$Ni$_{0.69}$-4Cl** vs. its calculated analogues in the *m/z* range of 553-559^{2+} (bottom).

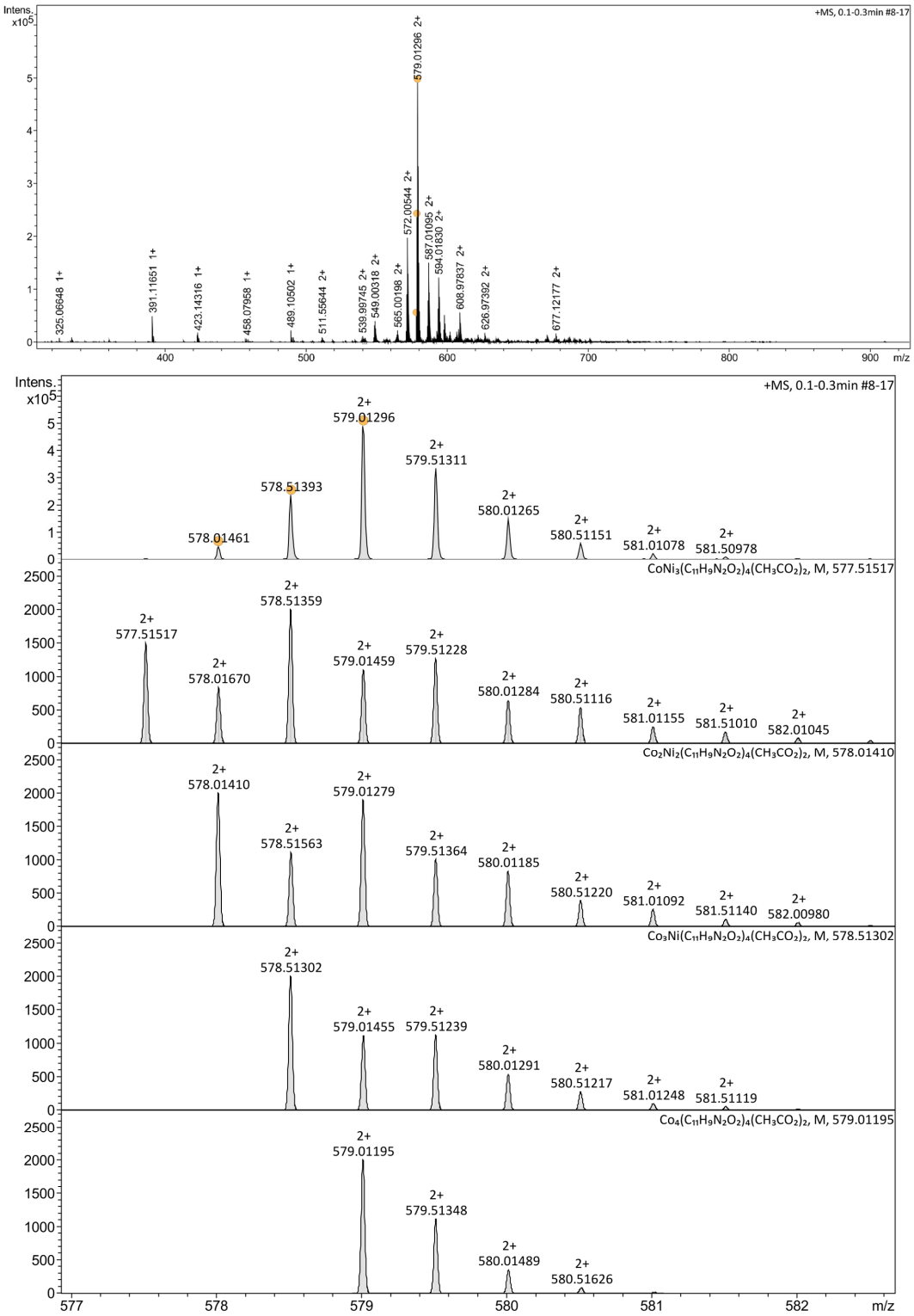

Figure S61. Full HR-ESI-MS spectrum of **1-Co_xNi_{4-x}-3OAc-NO_3** (top) and isotope patterns of **1-Co_xNi_{4-x}-3OAc-NO_3** vs. its calculated analogues in the *m/z* range of 577-583^{2+} (bottom).

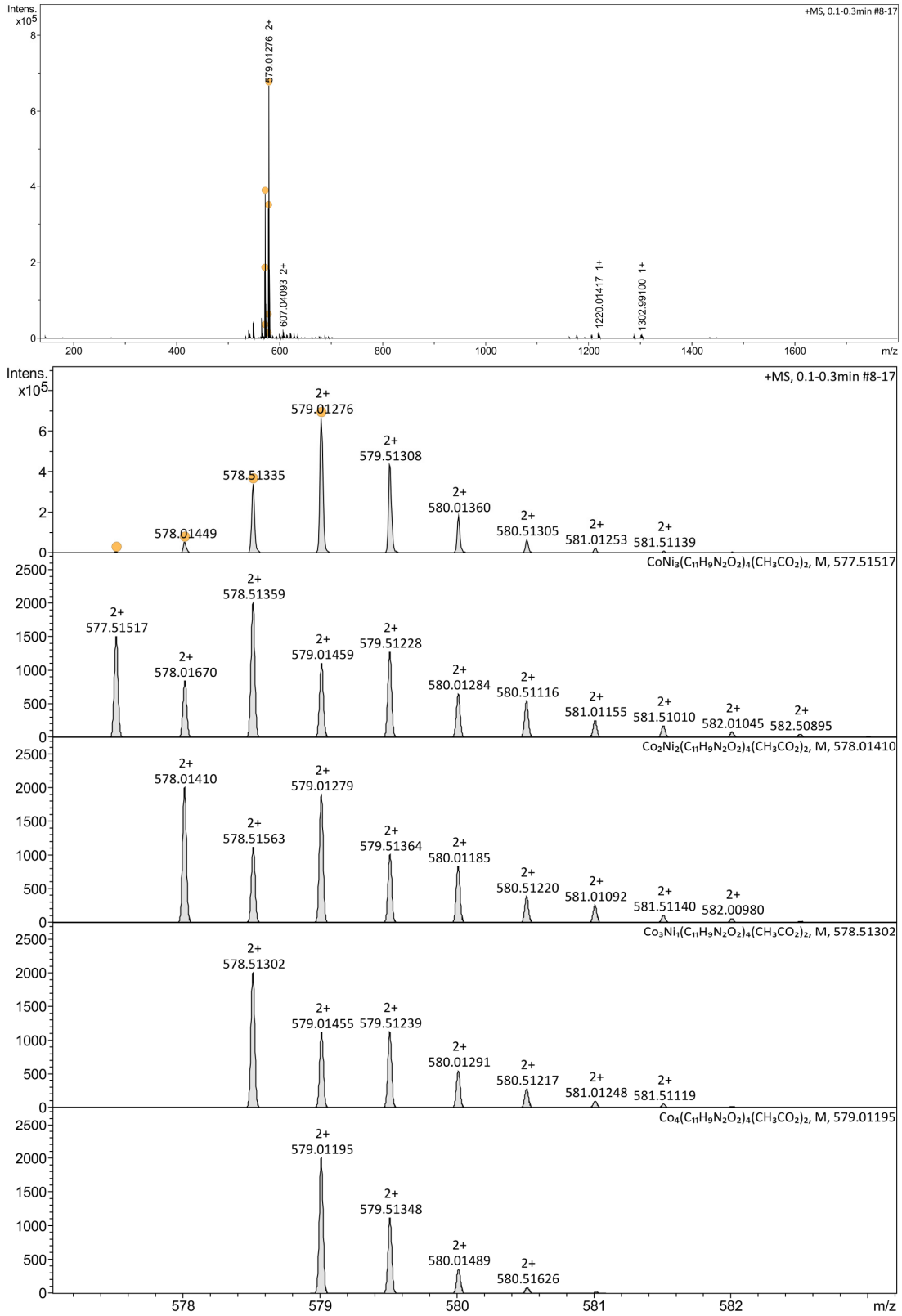

Figure S62. Full HR-ESI-MS spectrum of **1- $Co_{3.28}Ni_{0.72}$-PF_6** (top) and isotope patterns of **1-$Co_{3.28}Ni_{0.72}$-PF_6** vs. its calculated analogues in the *m/z* range of 577-583^{2+} (bottom).

Table S18. Visible-light-driven water oxidation performance of the cubane catalysts.

Catalyst (100 μM)	O_2 / μmol	[a]O_2 yield	[b]TON	[c]TOF / s^{-1}
1-3OAc-ClO_4	13.4	67.0%	16.8	0.20
2-Co_4-ClO_4	15.5	77.5%	19.4	0.24
2(*gem*-aqua)-Co_4-NO_3	16.6	83.0%	20.8	0.27
[d]**2-[Co_5]-NO_3**	9.2	46%	11.5	0.10

[a]O_2 yield = 2*n* (O_2 (GC))/*n* ($Na_2S_2O_8$). [b]TON = *n* (O_2 (GC))/ *n* (**CAT**). [c]$TOF_{initial}$ = *c* (Clark electrode kinetics in 60 s)/60 s/*c* (**CAT**). Conditions: 470 nm LED light; pH 8.5 80 mM, borate buffer; 1 mM $[Ru(bpy)_3]Cl_2$; and 5 mM $Na_2S_2O_8$. [d]**[Co_5]** = $[Co_5(dpy\text{-}C\{OH\}O)_5(dpy\text{-}C\{O\}_2)](NO_3)_3$ (Fig. S11).

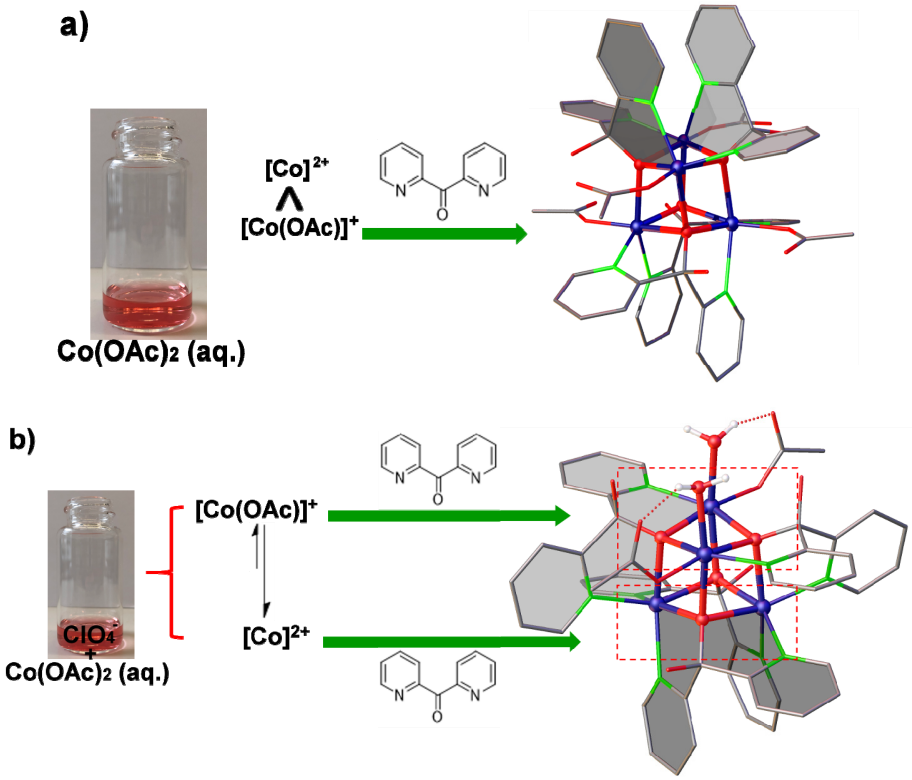

Figure S63. Hypothetical assembly pathways of **type 1** (**a**) and **2** (**b**) cubanes directed by proposed perchlorate-controlled $Co(OAc)_2$ dissociation.

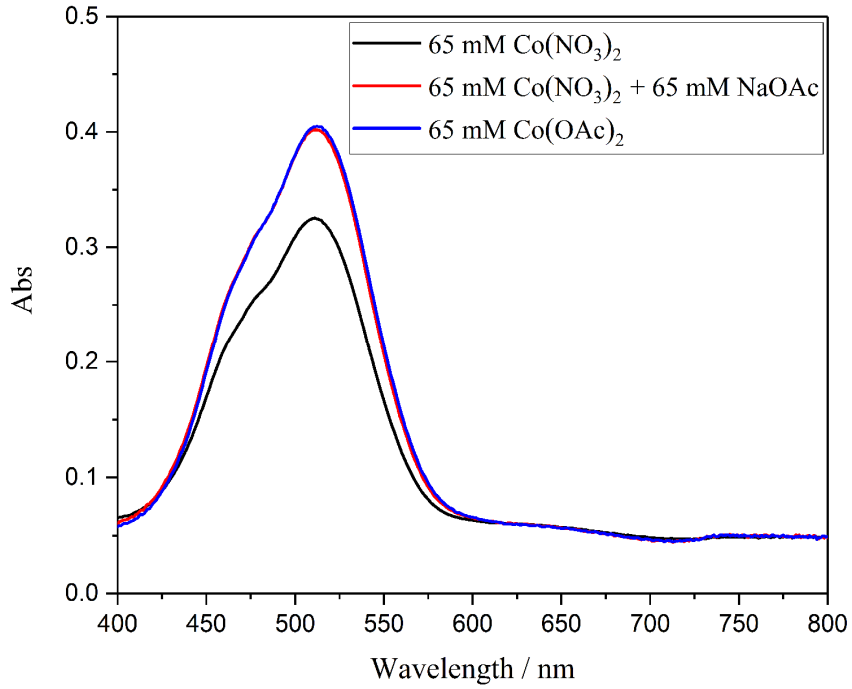

Figure S64. UV/vis spectra of 65 mM $Co(NO_3)_2$ (aq., black) and after adding 1 eq. NaOAc (red) vs. 65 mM $Co(OAc)_2$ (aq., blue).

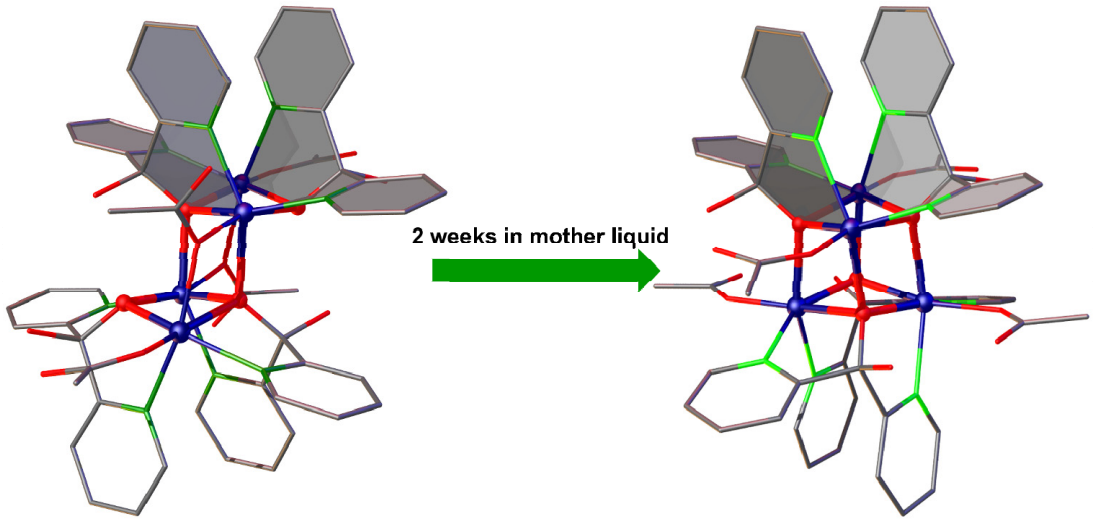

Figure S65. Conversion of the defect cubane $[Co_4(dpy\text{-}C\{OH\}O)_4(OAc)_4]$ into the corresponding **type 1** cubane.

Table S19. Novelty levels of the cubane compounds characterized in this study.

Compound	Novelty level
1-4OAc	**DU**[7]
1-4Cl	**LP**
1-2OAc-2BF$_4$	**LP**
1-3OAc series	**AD**[6]
2-Co$_x$Ni$_{4-x}$ series (0<x≤4)	**AD**[5]
2-μ-OAc-Ni$_4$ series	**AD**[4]
2-μ-OAc-Co$_x$Ni$_{4-x}$ series (0<x<4)	**LP**
2-(*gem*-aqua)-Co$_4$-NO$_3$	**LP**
2-(*gem*-aqua)-Ni$_4$-NO$_3$	**AD**[8]
[Co$_5$(dpy-C{OH}O)$_5$(dpy-C{O}$_2$)](NO$_3$)$_3$	**LP**
2-(half *gem*-aqua)-Ni$_4$-NO$_3$	**LP**

DU = Reported cubane compound found here in a **d**ifferent **u**nit cell.
AD = **A**nionic **d**erivative of a reported cubane.
LP = New **l**igand **p**attern on {M$_4$O$_4$} core.

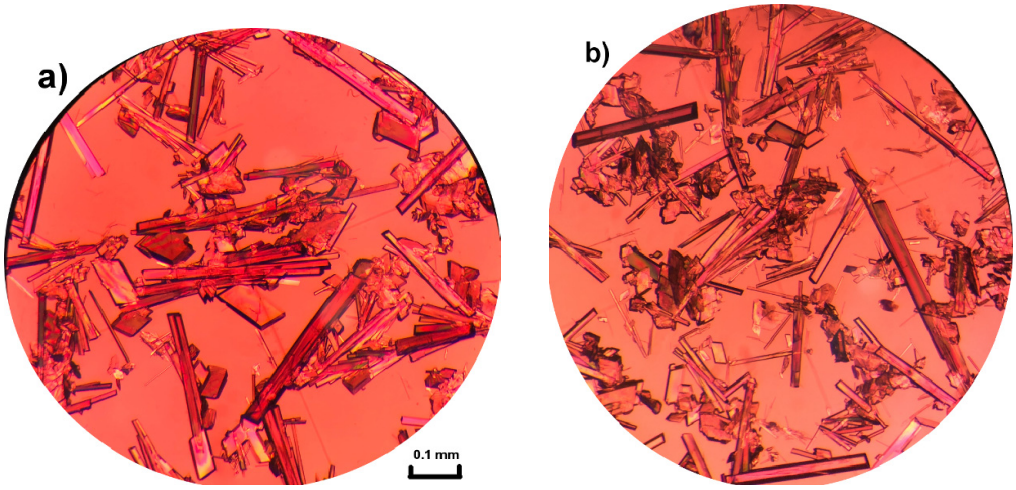

Figure S66. Photographs of **type 1** (quasi-rhombohedral crystals) and **2-μ-OAc** (prismatic crystals) compounds coexisting in the bulk-scale product synthesized by addition of 0.4 mmol dpk to 0.7 mmol Co(OAc)$_2$ + 0.1 mmol Ni(OAc)$_2$ containing 3 mmol NaBF$_4$ (**a**) and NaClO$_3$ (**b**), respectively ((**a**) and (**b**) were photographed with the same magnification).

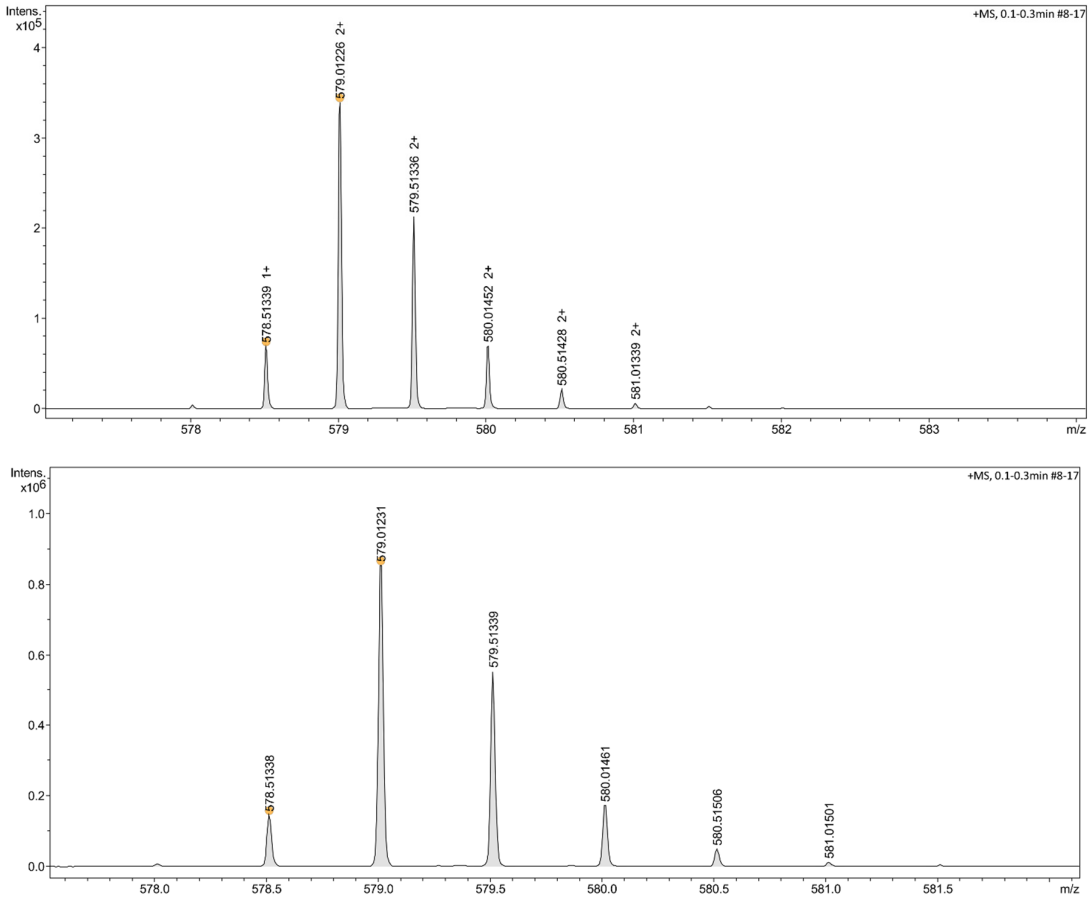

Figure S67. HR-ESI-MS isotope patterns related to the fragmentation of $[Co_xNi_{4-x}(dpy\text{-}C\{OH\}O)_4(OAc)_2]^{2+}$ obtained from measuring **1-Co_xNi_{4-x}-3OAc-BF_4** (top) and **-ClO_3** (bottom), respectively.

Table S20. Reaction electronic energy differences of monomeric and dimeric Co building blocks referenced to [Co_4(dpy-C{OH}O)$_4$(OAc)$_4$] (B3LYP/def2-TZVP/COSMO; cf. Figures 11, S68 and S69 for the respective structural details).

Reactions	Energies / eV	Energies / kcal · mol^{-1}
[Co_4(dpy-C{OH}O)$_4$(OAc)$_4$] (**1-4OAc**) → 2 [Co_2(dpy-C{OH}O)$_2$(μ-OAc)$_2$] (**D1**)	2.35	54.08
1-4OAc → 2 [Co_2(dpy-C{OH}O)$_2$(OAc)$_2$] (**D2**)	2.15	49.50
1-4OAc → 2 [Co_2(dpy-C{OH}O)$_2$(μ-OAc)$_4$] (**D3**)	1.93	44.33
1-4OAc + 4 H_2O → 2 [Co_2(dpy-C{OH}O)$_2$(OAc)$_2$(H_2O)$_2$] (**D4**)	0.76	17.49
1-4OAc + 4 H_2O → 4 OAc + 4 [Co(dpy-C{OH}O)(H_2O)] (**M1**)	12.53	288.08
1-4OAc + 4 H_2O → 4 [Co(dpy-C{OH}O)(OAc)(H_2O)] (**M2**)	5.35	123.01
1-4OAc + 12 H_2O → 4 OAc + 4 [Co(dpy-C{OH}O)(H_2O)$_3$] (**M3**)	5.33	122.63
1-4OAc + 16 H_2O → 4 OAc + 4 [Co(dpy-C{OH}O)(H_2O)$_4$] (**M4**)	4.35	100.01
1-4OAc + 8 H_2O → 4 [Co(dpy-C{OH}O)(OAc)(H_2O)$_2$] (**M5**; OAc^-, O^- *trans*)	4.05	93.16
1-4OAc + 4 H_2O + 4 OAc^- → 4 [Co(dpy-C{OH}O)(OAc)$_2$(H_2O)] (**M6**; H_2O, O^- *trans*)	3.72	85.51
1-4OAc + 8 H_2O → 4 [Co(dpy-C{OH}O)(OAc)(H_2O)$_2$] (**M7**; OAc^-, O^- *cis*)	3.45	79.32
1-4OAc + 8 H_2O → 4 [Co(dpy-C{OH}O)(μ-OAc) *cis*-(H_2O)$_2$] (**M8**)	3.32	76.35
1-4OAc + 8 H_2O → 4 [Co(dpy-C{OH}O)(μ-OAc) *trans*-(H_2O)$_2$] (**M9**)	3.26	75.04
1-4OAc + 4 H_2O + 4 OAc^- → 4 [Co(dpy-C{OH}O)(OAc)$_2$(H_2O)] (**M10**; H_2O, O^- *cis*)	3.02	69.47
1-4OAc + 12 H_2O → 4 [Co(dpy-C{OH}O)(OAc)(H_2O)$_3$] (**M11**; OAc^-, O^- *cis*)	1.87	42.99
1-4OAc + 12 H_2O → 4 [Co(dpy-C{OH}O)(OAc)(H_2O)$_3$] (**M12**; OAc^-, O^- *trans*)	1.83	42.11
1-4OAc + 24 H_2O → 4 [Co(H_2O)$_6$] + 4 dpy-C{OH}O^- + 4 OAc^- (**M'1**)	10.61	244.01
1-4OAc + 16 H_2O → 4 [Co(μ-OAc)(H_2O)$_4$] + 4 dpy-C{OH}O^- (**M'2**)	9.32	214.45
1-4OAc + 20 H_2O → 4 [Co(OAc)(H_2O)$_5$] + 4 dpy-C{OH}O^- (**M'3**)	7.87	180.93
1-4OAc + 8 H_2O → 4 [Co(μ-OAc)$_2$(H_2O)$_2$] + 4 dpy-C{OH}O^- (**M'4**)	7.41	170.44
1-4OAc + 16 H_2O + 4 OAc^- → 4 [Co *trans*-(OAc)$_2$(H_2O)$_4$] + 4 dpy-C{OH}O^- (**M'5**)	4.81	110.69
1-4OAc + 16 H_2O + 4 OAc^- → 4 [Co *cis*-(OAc)$_2$(H_2O)$_4$] + 4 dpy-C{OH}O^- (**M'6**)	4.35	100.16

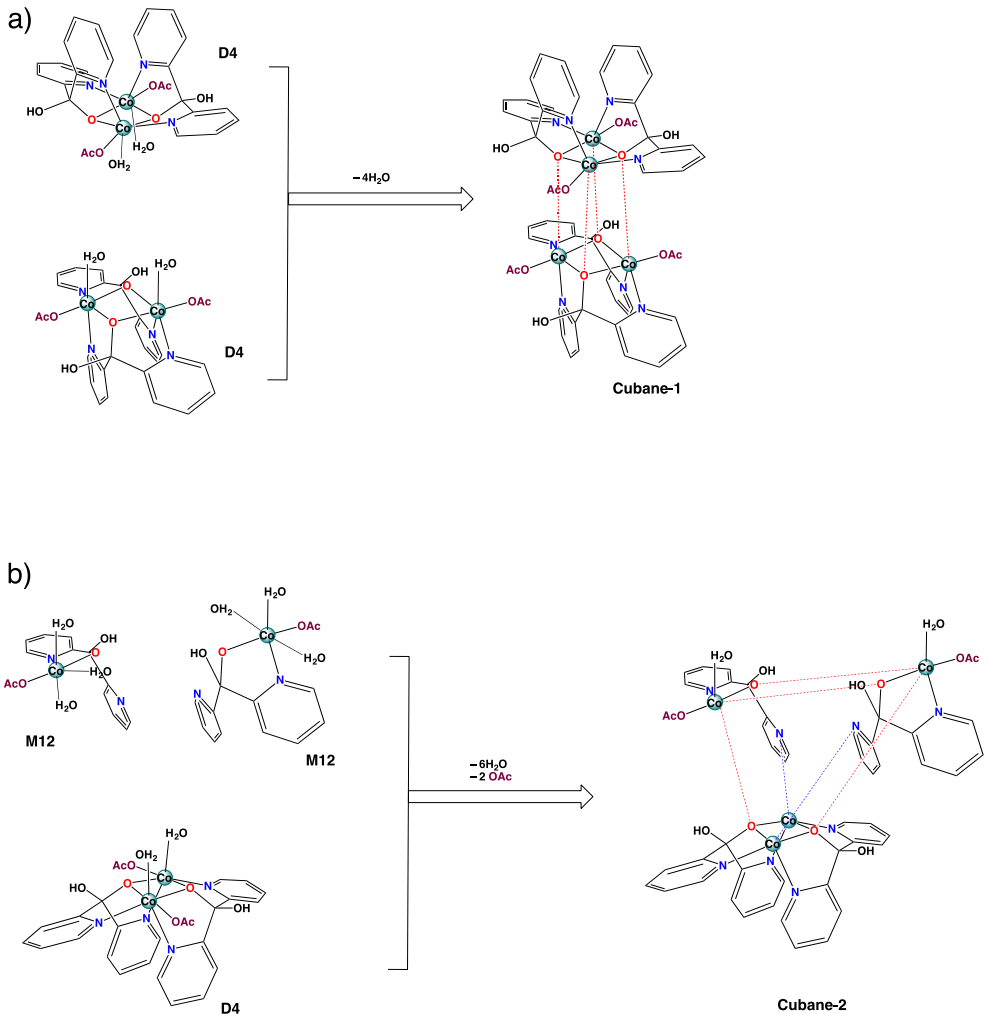

Figure S68. Possible assembly pathways of **type 1** (**a**) and **type 2** (**b**) $\{Co_4O_4\}$ cubanes.

All geometries were optimized using unrestricted Kohn-Sham density functional theory with the BP86[9,10] functional as implemented in Turbomole 7.0.1 package.[11] Single point calculations were performed at the optimized geometries with the hybrid B3LYP[12,13] functional and COSMO as continuum solvent model for water ($\epsilon = 78$). All the above-mentioned functionals were combined with Grimme's D3-type dispersion correction.[14] We have employed triple-zeta valence polarized (def2-TZVP) basis sets[15,16] and the resolution of identity (RI) approach with corresponding auxiliary basis sets[17,18].

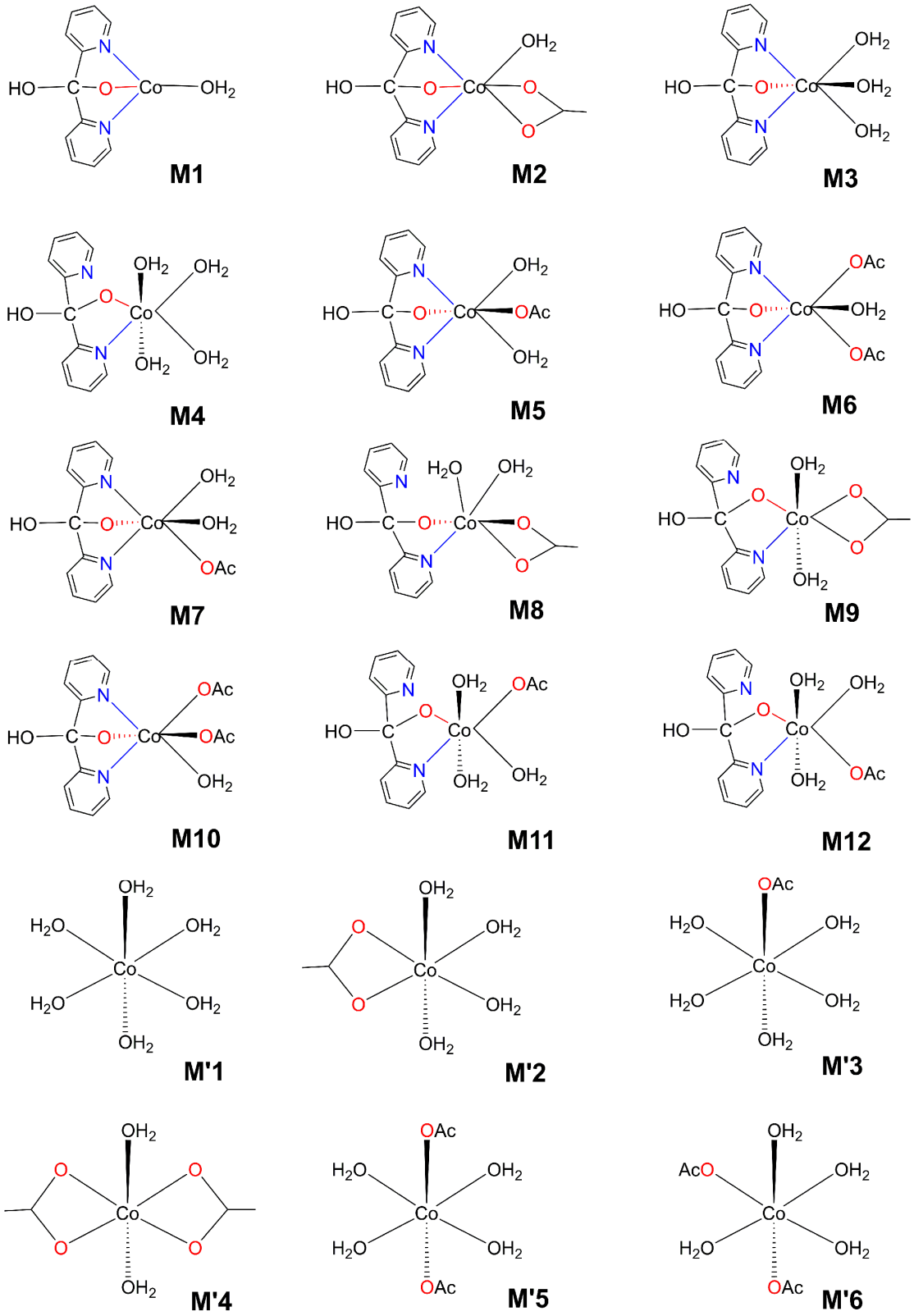

Figure S69. Schematic representations of the computed monomers.

References

(1) Dolomanov, V.; Bourhis, L. J.; Gildea, R. J.; Howard, J. A. K.; Puschmann, H. *J. Appl. Cryst.* **2009**, *42*, 339–341.
(2) Sheldrick, G. M. *Acta Cryst*. **2015**, *A71*, 3-8.
(3) Sheldrick, G. M. *Acta Cryst*. **2015**, *C71*, 3-8.
(4) Efthymiou, C. G.; Raptopoulou, C. P.; Terzis, A.; Boča, R.; Korabic, M.; Mrozinski, J.; Perlepes, S. P.; Bakalbassis, E, G. *Eur. J. Inorg. Chem.* **2006**, *2006*, 2236-2252.
(5) Song, F.; Moré, R.; Schilling, M.; Smolentsev, G.; Azzaroli, N.; Fox, T.; Luber, S.; Patzke, G. R. *J. Am. Soc. Chem.* **2017**, *139*, 14198-14208.
(6) Tong, M.; Zheng, S.; Shi, J.; Tong, Y.; Lee, H. K.; Chen, X. *J. Chem. Soc., Dalton Trans.* **2002**, 1727-1734.
(7) Tsohos, A.; Dionyssopoulou, S.; Raptopoulou, C. P.; Terzis, A.; Bakalbassis, E. G.; Perlepes, S. P. *Angew. Chem. Int. Ed.* **1999**, *38*, 983-985.
(8) Li, Y. -M.; Zhang, J. -J.; Fu, R. -B.; Xiang, S. -C.; Sheng, T. -L.; Yuan, D. -Q.; Huang, X. -H.; Wu, X. -T. *Polyhedron* **2006**, *25*, 1618-1624.
(9) Becke, A. D. *Phys. Rev. A* **1988**, *38*, 3098-3100.
(10) Perdew, J. P. *Phys. Rev. B* **1986**, *33*, 8822-8825.
(11) Ahlrichs, R.; Bär, M.; Häser, M.; Horn, H.; Kölmel, C. *Chem. Phys. Lett*. **1989**, *62*, 165-169.
(12) Becke, A. D. *J. Chem. Phys*. **1993**, *98*, 5648-5652.
(13) Lee, C.; Yang, W.; Parr, R. G. *Phys. Rev. B* **1988**, *37*, 785-789.
(14) Grimme, S.; Anthony, J.; Ehrlich, S.; Krieg, H. *J. Chem. Phys.* **2010**, *132*, 154104.
(15) Schäfer, A.; Huber, C.; Ahlrichs, R. *J. Chem. Phys.* **1994**, *100*, 5829-5835.
(16) Weigend, F.; Ahlrichs, R. *Phys. Chem. Chem. Phys.* **2005**, *7*, 3297-3305.
(17) Eichkorn, K.; Treutler, O.; Ohm, H.; Häser, M.; Ahlrichs, R. *Chem. Phys. Lett*. **1995**, *240*, 283-290.
(18) Weigend, F. *Phys. Chem. Chem. Phys.* **2002**, *4*, 4285-4291.